Rho-associated kinase 1 in health and disease: Vital roles in apoptotic blebbing, efferocytosis, and cancer

Grant Raymond Wickman

Submitted in fulfilment of the requirements for the Degree of Doctor of Philosophy

The Beatson Institute for Cancer Research

College of Medical, Veterinary & Life Sciences

University of Glasgow

November, 2011

Abstract

Rho-associated kinase 1 (ROCK1) is a serine/threonine kinase important for the regulation of the cellular cytoskeleton through the induction of actin stress fibres and acto-myosin contractility. The cleavage and subsequent activation of ROCK1 by caspase 3 during apoptosis is believed to cause many morphological phenomena associated with programmed cell death such as dynamic membrane blebbing. I now formally prove the necessity of ROCK1 cleavage for apoptotic blebbing by knocking-in a caspase cleavage resistant mutant of ROCK1 in a genetically modified model. In addition, animals homozygous for non-cleavable ROCK1 demonstrate a phenotype consistent with auto-immune disease suggesting that apoptotic blebbing is important to mediate rapid efferocytosis, which is a rapid phagocytic clearance of the cellular corpse, and thus maintain self-tolerance. Furthermore, apoptotic blebbing is important for the clearance of apoptotic cells and I demonstrate a novel mechanism for ROCK to mediate the release of factors participating in macrophage migration to dying cells. ROCK induced apoptotic blebs and bodies lose membrane integrity prior to secondary necrosis and leak intracellular material. Using quantitative mass spectrometry I identified numerous proteins that were previously unrecognized to be released during apoptosis. The release of protein was found to be impaired following ROCK antagonism with Y27632 which underscores the importance of ROCK activity in apoptotic protein release. One of these proteins, gelsolin, was released following caspase cleavage and encourages macrophage motility towards apoptotic cells. Finally, I now demonstrate that the three nonsynonymous somatic mutations in the ROCK1 gene identified in the Cancer Genome Project lead to elevated kinase activity and drive actin cytoskeleton rearrangements that promote increased motility and decreased adhesion, characteristics of cancer progression. Mapping of the kinase-interacting regions of the carboxy-terminus combined with structural modeling provides insight into how these mutations likely affect the regulation of ROCK1. Consistent with the frequency of ROCK1 mutations in human cancer, these results support the conclusion that there is selective pressure for the ROCK1 gene to acquire ‘driver’ mutations that result in kinase activation.

Table of Contents

List of Tables

List of Figures

Abbreviations

ACAMP	Apoptotic cell-associated molecular patterns
AC-CM	Apoptotic cell conditioned medium
AIHA	Auto-immune haemolytic anaemia
ANA	Anti-nuclear antibodies
ANOVA	Analysis of variance
Arg	Arginine
CHX	Cycloheximide
DAPI	4',6-diamidino-2-phenylindole
DAPK	Death-associated protein kinase
DC	Dendritic cell
DIC	Differential interference contrast
DNA	Deoxyribonucleic acid
ΔROCK1	Cleaved ROCK1
dRP S19	Dimer of ribosomal protein S19
ECM	Extracellular matrix
EOB	Eyelids open at birth
FACS	Fluorescence activated cell sorting
FBS	Foetal bovine serum
GAP	GTPase activating protein
GDP	Guanosine diphosphate
GEF	Guanine nucleotide exchange factors
GFP	Green fluorescent
GlcNAc	n-acetylglucosamine
GSN	Gelsolin
GST	Glutathione S-transferase
GTP	Guanosine-5'-triphosphate
H&E	Haematoxylin and eosin
HMGB-1	High-mobility group box
LC-MS	Liquid chromatography and mass spectrometry
LDH	Lactate dehydrogenase
LIMK	LIM kinase
LPC	Lysophosphatidylcholine
Lys	Lysine
MCV	Mean corpuscular volume
MEF	Mouse embryonic fibroblasts
mES	Mouse embryonic stem cell
MFG-E8	Milk fat globule epidermal growth factor 8
MLC	Myosin light chain
MLCK	Myosin light chain kinase
PAF	Platelet activating factor
PARP	Poly (ADP-ribose) polymerase
PCR	Polymerase chain reaction
PH	Pleckstrin homology domain
PI	Propidium iodide
PIP2	Phosphatidylinositol (4,5)-bisphosphate (PIP_2),

PIP3	Phosphatidylinositol (3,4,5)-trisphosphate
pMLC	Phosphorylation of MLC
PS	Phosphatidyl serine
RBC	Red blood cell
RBD	Rho binding domain
RNA	Ribonucleic acid
RNAi	RNA interference
ROCK	Rho-assocaited kinase
ROCK1nc	ROCK1 non-cleavable
RP	Splenic red pulp
S1P	Sphingosine-1-phosphate
SDS-PAGE	Sodium dodecyl sulfate polyacrylamide gel electrophoresis
SEM	Standard error of the mean
SILAC	Stable isotope labeling with amino acids in cell culture
SLE	Systemic lupus erythematosus
TGF-b	Transforming growth factor
TNFa	Tumor necrosis factor
TyrRS	Tyrosyl tRNA synthetase
WP	Splenic white pulp
WT	Wild type
ZIPK	Zipper-interacting protein kinase
Z-VAD-FMK	N-benzyloxycarbonyl-Val-Ala-Asp-fluoromethylketone

Acknowledgment

I owe everything to Mike, all his ideas are always right (at least most of the time). Also, he’s a decent sort of guy. Thanks to everyone at The Beatson Institute and especially CRUK for funding my laboratory play time. I would like to thank Debs and my weans, Finlay and Esme, for supporting me during the last 4 years and helping to make this a success.

Author’s Declaration

I am the sole author of this thesis. The work presented in this thesis is entirely my own unless otherwise stated.

1. Rho-associated protein kinase (ROCK): regulation and function in apoptosis and cancer

(Text extracted from Wickman, G., Samuel, P., Lochhead, P., Olson M.F. The Rho-Regulated ROCK kinases in cancer. In: K. van Golen (ed.) The Rho GTPases in Cancer. Springer Press. (2010) pp. 163-192. and Wickman, G. and Olson M.F. A review of ROCK induced blebbing in apoptotic cell clearance and auto-immune disease. In review at Cell Death and Differentiation)

Rho-associated protein kinases (ROCK) are central and prominent downstream effectors of the RhoA, RhoB and RhoC GTP-binding proteins. The predominant function of ROCK is the regulation and modulation of the cytoskeleton. Specifically, ROCK promotes the stabilization and bundling of actin filaments (F-actin) and the generation of acto-myosin contractility via the phosphorylation of downstream substrates. As a result, ROCK proteins are indispensable for many cellular processes dependent upon the cytoskeleton including, but not limited to: cell motility, adhesion, apoptosis and phagocytosis. Given the critical role of ROCK1 and 2 in these diverse physiological processes, it is unsurprising that these kinases are involved in the development and progression of multiple diseases including cancer [1]. While ROCKs are also implicated in diabetic nephropathy and a diverse array of cardiovascular diseases, the involvement of ROCK in the pathology of these disorders is outside the scope of this thesis [2,3].

1.1 ROCK: structure, and regulation

There are two isoforms of the ROCK serine/threonine kinases, ROCK1 (ROKβ) and ROCK2 (Rho kinase or ROKα), which share 64% overall homology with 89% homology within the kinase domain [4] (Figure 1.1a). ROCK is most closely related to the myotonic dystrophy kinase (DMPK, 48% identity in kinase domain with ROCK1) and the DMPK-related Cdc42-binding kinases MRCKα and MRCKβ (each with 53% kinase domain identity with ROCK1), which appear to share some overlapping functions in the regulation of the cytoskeleton [5]. The ROCK kinases contain an amino-terminal kinase domain, a central coiled-coil domain (55% identity), followed by a split pleckstrin homology domain containing a C1 conserved region (80% identity) (Figure 1.1a). A Rho-binding domain (RBD) lies within the coiled-coil region of ROCK, structural studies have revealed that the RBD forms a coiled-coil that interacts with the switch I and II regions of GTP-bound RhoA [6,7]. Several lines of investigation have revealed that ROCK1 and

ROCK2 form homo- and heterodimers that influence kinase activity, inhibitor sensitivity and normal function *in vivo* [8-10]. Experiments using either wild-type RhoA loaded with non-hydrolyzable GTP-γS or GTPase-deficient RhoAG14V, revealed that Rho-GTP can increase ROCK specific activity in kinase assays and the formation of ROCK-dependent actin stress fibres and focal adhesions in cultured cells [11]. Studies examining the mechanism of ROCK activation by Rho-GTP revealed that expression of ROCK RBD and PH fragments attenuate activation which suggests that the carboxyl terminal domain of ROCK negatively regulates kinase activity [11,12]. While it is clear from these data that Rho-GTP binding to the RBD within the carboxyl terminus of ROCK relieves this negative regulation leading to increased kinase activity, the precise mechanistic details of this auto-inhibition remained elusive (Figure 1.1b).

The association of additional proteins to ROCK, including other small GTP-binding proteins, appears to regulate kinase activity. RhoE, Gem, and Rad have each been shown to bind ROCK at sites distinct from the RBD[13,14]. The binding of Gem to ROCK1 was found to attenuate phosphorylation of the MYPT1 regulatory subunit of the PP1M phosphatase complex but not LIM kinase, suggesting that Gem induces a shift in ROCK substrate specificity [14]. In addition, the overexpression of Gem and Rad in endothelial cells result in reduced stress fibres and focal adhesions, consistent with inhibition of ROCK activity [14]. Similar effects on stress fibres are reported for RhoE overexpression [15], which was found to bind within the amino terminal kinase domain and may sterically interfere with kinase-substrate interactions [13]. Alternatively, RhoE and RhoA appear to be competitive for ROCK binding, despite their binding at distinct sites, thus RhoE may antagonize ROCK function by inhibiting RhoA-mediated activation [13]. In further support of a role for RhoE in ROCK regulation, the protein kinase PDK 1 has been shown to enhance ROCK1 activity, not through phosphorylation, but by blocking the association of RhoE [16]. RhoE, Rad/Gem display discrete subcellular distributions, being located at the Golgi apparatus and the cytoskeleton respectively, and it has been suggested that the distribution of these negative regulators is important for the modulation of ROCK activity at specific intracellular sites [17].

The lipid second messengers arachadonic acid (AA) and sphingophosphocholine (SPC) appear to be highly efficacious ROCK activators. ROCK purified from

chicken gizzard was activated 5-6 fold following exposure to AA, independent of RhoA [18]. In addition, SPC enhanced contractility of vascular smooth muscle in a ROCK inhibitor sensitive, but GTP-independent, manner [19]. Together these observations suggest that lipid activation is sufficient to stimulate ROCK and catalyze acto-myosin contractility. However, the relevance of these two lipid signaling pathways in the regulation of ROCK in non-smooth muscle cell types remains to be demonstrated. A role for phosphatidyl inositides in ROCK activation has also been observed. Purified ROCK2, but not ROCK1, binds phosphatidylinositol (3,4,5)-trisphosphate (PIP_3) and phosphatidylinositol (4,5)-bisphosphate (PIP_2), which activate kinase activity independent of Rho-GTP [20]. It has been suggested that the differential binding properties of ROCK1 and ROCK2 towards PIP_3 and PIP_2 may be important for subcellular regulation allowing ROCK to initiate discrete spatial functions.

Phosphorylation of ROCK2 at several sites by polo like kinase 1 appears to promote RhoA dependent activation [21]. Although additional serine/threonine and tyrosine phosphorylation sites have been identified (http://www.phosphosite.org), which may be involved in ROCK regulation, the prevalence and function of these phosphorylations remain to be determined. Interestingly, structural studies revealed that phosphorylation within the kinase domain was not necessary for the formation of a catalytically competent conformation [9].

1.2 ROCK: expression, substrates, and cellular contractility

Both ROCK isoforms are ubiquitously expressed in normal tissue and appear to have enhanced expression in brain, liver, and skeletal muscle [22]. Examination of intracellular localization revealed a predominantly cytosolic distribution pattern [23,24]. However, more detailed analysis has revealed ROCK localized to: plasma membranes [23,25], acto-myosin filaments [23,26], nucleus [27], mitotic cleavage furrow [28,29] and centrosomes [30]. These observations are consistent with a role for ROCK as a mediator of the actin cytoskeleton, and suggest that proper subcellular localization likely plays a key regulatory role.

More than 20 ROCK substrates have been identified, and while many have only been tested with one isoform, it seems likely that most substrates would be

phosphorylated *in vitro* by either kinase given the 89% identity between ROCK1 and ROCK2. If there were differences in substrate phosphorylation by each isoform, this would probably result from more subtle differences in subcellular localization and/or protein-protein interactions. ROCK regulates the cytoskeleton via phosphorylation of numerous downstream target proteins (Figure 1.2). ROCK phosphorylates LIM kinases-1 and –2 (LIMK1 and LIMK2) at Threonine-508 and-505 in their respective activation loops, which result in increased LIMK catalytic activity and the subsequent phosphorylation and inactivation of the actin-severing protein cofilin, thereby stabilizing filamentous actin [31-34]. Cofilin induced actin severing and the generation of barbed ends appear to be an important component of intracellular actin cycling which in-turn dictates cytoskeletal structure. The LIM kinases can also be phosphorylated and regulated by p21 activated protein kinases (PAK) 1 and 4 suggesting that multiple signaling networks converge on LIMK to modify the cellular cytoskeleton and subsequent cellular function [35,36]. In addition, ROCK participates in the phosphorylation of the myosin II light chains (MLC), a key mechanism for regulation of acto-myosin contractility [37]. MLC phosphorylation promotes the release of the myosin heavy chain tail allowing for assembly into filaments, and facilitates the association of the myosin head with F-actin. The myosin head uses ATP to 'walk' towards the barbed end, when multimeric myosin is associated with more than one actin filament to provide traction, this process then allows for sliding of actin filaments in the opposite direction, thereby generating contractile force. While ROCK has been shown to phosphorylate recombinant MLC at the same site (Ser 19) as the Ca^{2+} dependent myosin light chain kinase (MLCK) [38], experiments with GTPγS in airway smooth muscle failed to demonstrate significant MLC phosphorylation or cell contraction in Ca^{2+} depleted and therefore MLCK inactive conditions [39]. These observations suggest that ROCK-mediated phosphorylation of MLC at Ser19 may not be a physiologically significant pathway to regulate cell contractility, at least in some cell types. Instead, the regulation of MLC phosphorylation, and thus cellular contraction, by ROCK may be mediated by inhibition of the myosin light chain phosphatase PP1M. This protein complex is made up of a PP1Cδ catalytic subunit, a myosin light chain binding subunit (MBS) and a smaller M20 subunit of unknown function [40]. ROCK has been found to phosphorylate the ubiquitously expressed MYPT1 myosin binding subunit at two sites (Thr 696 and Thr 853 in the human form), which inhibits MLC dephosphorylation [41-43]. As a result, a net gain in

MLC phosphorylation would actually require less activity by kinases such as MLCK directed towards MLC than under conditions in which PP1M was not inhibited, leading to an increase in MLC phosphorylation and greater cellular contractility [39,44]. In addition, many ROCK effects may be amplified by direct phosphorylation and activation of the Zipper-interacting protein kinase (ZIPK), which phosphorylates many of the same substrates as ROCK [45]. Taken together, ROCK activation leads to a concerted series of events that promote acto-myosin mediated force generation and subsequent morphological changes (Figure 1.2).

1.3 Cellular consequences of ROCK activation

The increase in cellular contractility stimulated by ROCK leads to the prominent formation of actin stress fibres. These are bundles of contractile actin and myosin II filaments found along the length of the cell body of cultured cells and terminate at discreet points at the membrane known as focal adhesions. In fact, stress fibre formation was one of the first cellular activities identified for the Rho-associated kinases and either ROCK antagonists or dominant negative expression can impair their formation [11,22,46]. In addition, the formation of focal adhesion complexes and the subsequent aggregation of integrins also appears to be dependent upon Rho-ROCK contractility [46,47]. The formation of these structures can be induced by multiple factors including, but not limited to: platelet-derived growth factor, and lysophosphatidic acid [48-50]. While ROCK is clearly involved in the generation of stress fibres, it should be noted that expression of ROCK alone generates “stellate” fibres with an architecture distinctively different from those stimulated by Rho [22]. Expression of ROCK with another Rho binding protein, the Diaphanous-related formin mDia1, gave rise to stress fibres similar to those seen induced by Rho [51], indicating that although ROCK plays a central and critical role, Rho induction of stress fibre formation requires the input of additional signaling pathways. Nonetheless, ROCKs are clearly vital enzymes for cytoskeletal modification which in turn is responsible for many important biological processes such as cell migration, apoptosis, and embryonic development.

1.4 ROCK1 and cell motility

The dynamic reorganization of the cytoskeleton has long been understood as the underlying mechanism allowing cell migration and invasion [52]. Given the

importance of ROCK in cytoskeletal remodeling and acto-myosin contractility, it is not surprising that the enzyme has been implicated in cell migration. Expression of constitutively active ROCK in MM1 hepatoma cells significantly enhanced invasion and dissemination of tumour cells in an *in vivo* model [53]. This enhanced migration was also observed with MM1 cells expressing RhoAG14V and was reversed with the ROCK antagonist Y27632 [53]. These observations are supported by a significant body of evidence implicating a role for ROCK in two dimensional *in vitro* migration experiments [17]. However, significant morphological differences are observed in cells grown in monolayer culture versus a more physiological 3D matrix [54]. These differences call into question the relevance of 2D models of cellular migration for studying *in vivo* cell movement. Instead, three dimensional migration studies are required to recapitulate a more realistic environment as a model for physiological migration and invasion.

Single cell migration within a 3D matrix can be categorized into two distinct modes, mesenchymal and amoeboid [55]. Mesenchymal migration is characterized by: a fibroblast/spindle like morphology; dependence upon focal adhesions; integrin binding; and matrix proteolysis. The amoeboid form is marked by: a rounded cell body; limited dependence upon matrix adhesions; and limited requirement for proteolytic matrix remodeling. Mesenchymal migration appears to have limited dependence upon ROCK; in contrast, amoeboid migration is heavily dependent upon ROCK. In evidence, Y27632 was found to significantly inhibit the matrigel invasion of several amoeboid cell lines, while it failed to inhibit mesenchymal-like invasion [56]. Consistent with these observations, the amoeboid migration of DMS79 cells in collagen gels was associated with membrane blebbing, a cellular feature of ROCK activation [57,58]. Membrane blebbing appears to be a general characteristic of cells undergoing amoeboid migration, and is likely important for cell movement within three dimensional matrices without necessitating proteolytic remodeling [56,59]. Furthermore, several cell lines have demonstrated plasticity in migration strategies and, in the presence of protease inhibitors, can be shifted from Y27632 insensitive mesenchymal migration to amoeboid, whereupon cell movement is sensitive to Y27632 treatment [56]. These observations clearly suggest a significant role for ROCK in cellular migration; however, a precise mechanism of control remains to be demonstrated. Nonetheless, ROCK has been proposed to regulate contraction of cortical actin rings which initiate membrane blebbing and deformation of the extracellular matrix [55,56,60].

1.5 Programmed cell death and ROCK1

Programmed cell death, or apoptosis, is a vital process mediating the removal of aged, damaged, or developmentally unnecessary cells in multicellular organisms [61,62]. ROCK appears to play a vital role in several processes of programmed cell death. First defined in 1972, apoptosis is an active process involving 4 well defined stages; initiation, effector, execution, and clearance [63].

1.5.1 Apoptotic Initiation and effector stages

Apoptosis is now recognized to be initiated by multiple stimulatory cues that can be divided into extracellular (extrinsic) or intracellular (intrinsic) signals which are not mutually exclusive. Viable cells can be induced to execute programmed cell death following the activation of death receptors by various extracellular (extrinsic) ligands such as Fas ligand, and tumour necrosis factor alpha (TNFα) [64]. The activation of death receptors initiates a caspase cleavage cascade culminating in caspase-3 activation. Caspases are cysteine-dependent aspartate-directed proteases that are expressed as inactive proforms and their function is vital to the execution of apoptosis. Caspases are activated in complex proteolytic cascades involving initiator caspases, such as caspase 8/9, which cleave and activate executioner caspases, such as caspase 3, that are necessary and sufficient to execute the apoptotic programme. Alternatively, cell death can be initiated in the absence of extrinsic factors. This intrinsic pathway can be activated by cellular stress or DNA damage and is dependent upon the pro-apoptotic activity of proteins, such as the Bcl family, that permeabilize the outer mitochondrial membrane causing the release of proteins normally contained only within the mitochondria. These proteins, such as cytochrome c, Smac, and Omi, upon release trigger the activation of caspase 9 which in turn cleaves and activates caspase 3 [65]. Regardless of the induction mechanism the activation of caspase 3 is a critical effector protease leading to the execution of programmed cell death. Once activated caspase 3 proteolytically cleaves over 100 intracellular proteins at a specific Asp-x-x-Asp motif [66]. Caspase cleavage of target proteins can cause either a gain- or loss-of-function which dramatically alters their regulation and function [66]. The altered activity of these proteins is collectively responsible for the execution of the apoptotic programme. The importance of caspase cleavage in apoptosis is underscored in experiments using caspase inhibitors, such as N-

benzyloxycarbonyl-Val-Ala-Asp-fluoromethylketone (Z-VAD-fmk). These compounds, which bind to the catalytic site and inhibit the further cleavage of cellular substrates, consistently allow cells to escape programmed cell death induced by both intrinsic and extrinsic signals [67]. Thus the activation of executioner caspases is a key switch triggering a multitude of independent cellular cascades resulting in the characteristic rapid compartmentalization and fragmentation of the cell associated with apoptotic cell death.

1.5.2 ROCK and the execution of apoptosis

Apoptotic cells can be easily discriminated from viable counterparts based on several morphological hallmarks. Not only do apoptotic cells have a very conspicuous nuclear condensation and fragmentation, but they also have very characteristic plasma membrane blebs. These are balloon-like protrusive blisters of the cellular plasma membrane that can be retracted and reformed in a dynamic cycling process which can cover the entire cellular surface of apoptotic cells (Figure 1.3a). The formation of apoptotic blebs is more of a physical, rather than a biochemical, process and they are believed to form as a result of increased hydrostatic pressure following acto-myosin dependent cellular contraction [68,69]. During their formation, the plasma membrane tears away from the underlying cytoskeletal cortex and rapidly forms an enveloped area filled with cytoplasm (Figure 1.3b). When newly formed, the bleb is devoid of polymerized actin and other cytoskeletal proteins into which an actin cortex will rapidly polymerize followed by the recruitment of cytoskeletal bundling proteins and myosin, which then power bleb retraction [70]. In apoptotic cells this cyclic process of bleb formation and retraction can occur over several hours and as programmed cell death progresses blebs become packed with cellular organelles and condensed chromatin and form the basis of sub-cellular membrane clad apoptotic bodies [71]. However, it must be noted that apoptotic blebbing is not a universal feature of programmed cell death; some cell types do not appear to generate membrane blebs nor undergo fragmentation [72]. Nonetheless, blebbing remains a very common feature of apoptotic cells and is considered a major morphological hallmark of programmed cell death.

In 2001 it was discovered that apoptotic blebbing is dependent upon ROCK activity [73,74]. Moreover it was apparent that apoptotic ROCK activation, which is

vital to drive blebbing, is independent of its canonical activator Rho. This non-classical activation of ROCK was associated with cleavage of ROCK1, but not ROCK2, by caspase 3 at a conserved site near the C-terminus (1110DETD1113)(Figure 1.4). Further investigation revealed that caspase cleaved ROCK1 yields a highly active kinase fragment that is sufficient to induce membrane blebbing identical to that seen in apoptotic cells. In addition, the cleaved ROCK1 fragment appears to be important for disruption of nuclear integrity and the packaging of fragmented DNA into membrane blebs and apoptotic bodies [73,75]. Thus the generation of constitutively active ROCK kinase fragments appears to be a *bona fide* regulatory mechanism for the complete execution of cellular apoptosis. When cell death has been triggered by extrinsic factors such as TNFα, ceramide or Fas-receptor ligation, ROCK1 activation is a relatively late event [57,76] and ROCK inhibition does not halt the apoptotic process [57]. However, in some contexts chronic or high intensity ROCK activity may contribute to the initiation of apoptosis. Data from ROCK1 knockout mice revealed that cardiac pressure overload was less effective at inducing cardiomyocyte apoptosis in relative to controls, suggesting a potential role for ROCK1 in myocardial failure [77]. While ROCK cleavage is tightly associated with the formation of apoptotic blebs, formal proof for the necessity of cleavage remains to be provided. Although ROCK2 is not cleaved by caspase 3 and is therefore unlikely to be involved in apoptotic blebbing induced by conventional intrinsic and extrinsic stimulus, it is cleaved by granzyme B [78]. Granzyme B is a serine protease injected into target cells by cytotoxic T-cells and natural killer cells to induce cell death by mitochondrial disruption and direct caspase 3 cleavage. Interestingly granzyme B cleaves ROCK2 at a homologous site to caspase 3 cleavage of ROCK1; cleavage of ROCK2 at D1131 liberates the C-terminal regulatory domain causing constitutive activation capable of inducing membrane blebs (Figure 1.4). Due to the activation of caspase 3 granzyme B induced apoptosis also leads to the cleavage of ROCK1 and thus the importance of ROCK2 cleavage towards the formation of apoptotic blebs remains unclear. Furthermore, as ROCK2 is not cleaved during apoptosis induced with conventional signals, the post-translational modification to produce a constitutively active ROCK2 appears to be unnecessary for apoptotic blebbing.

While the cleavage of ROCK1 is clearly vital to blebbing, it seems dispensable for many other apoptotic phenomena including caspase activation and

phosphatidylserine externalization. This leaves open the question of precisely what the biological significance of ROCK1 cleavage, and by extension apoptotic membrane blebbing, might be. One tantalizing possibility for the importance of ROCK1 activation during apoptosis is to aid phagocytosis of cellular remains.

1.5.3 Apoptotic cell clearance and auto-immune disease

The apoptotic programme is ultimately responsible for the final act of cellular disposal, or efferocytosis. As a testament to the efficiency and rapidity of efferocytosis it is surprisingly difficult to histologically detect apoptosis despite $>10^9$ cells executing apoptotic programmes per day in adult tissues [79-81]. There are several broadly defined phases of phagocytic clearance of apoptotic cells which include 1) Find-me, characterized by the release of soluble signals which attract macrophages to the dying cell; 2) Eat-me, in which a phagocyte becomes stimulated by engaging with signals expressed on the apoptotic cell membrane; 3) Engulfment, a series of cytoskeletal modifications in the phagocyte to take up the dead cell; and finally 4) Processing, digestion of the cellular remains through lysosomal degradation [82-84].

Importantly, the apoptotic cells are active participants in these processes and display significant modifications to their membranes that aid recognition and uptake. This material can include lipid, protein, and modified carbohydrates. The best characterised of these externalized factors is phosphatidyl serine (PS), which is normally restrained to the inner leaflet of the plasma membrane [85]. During early apoptosis membrane asymmetry is lost; PS becomes externalized and serves as a major factor for apoptotic cell recognition. Externalized PS can be recognized by the protein milk fat globule epidermal growth factor 8 (MFG-E8), which tethers the phospholipid to integrin $\alpha_v\beta_3$ expressed on macrophages and monocytes [86] (Figure 1.5). Alternatively PS can be recognized directly by one or more receptors expressed on macrophages, including; Bai1, Tim5, and Stabilin2 [62]. Curiously, PS externalization has also been demonstrated in viable cells suggesting that PS serine exposure alone may be insufficient to mediate phagocytosis and that other signals are necessary [87,88]. Thus, it has been proposed that the ‘eat-me’ signal received by phagocytes must be sufficiently strong to initiate efferocytosis [89]. The strength of such a signal could be augmented by the binding of additional ‘eat-me’ molecules, such as MFG-E8. Alternatively, the spatial concentration of PS on

apoptotic cell membranes may also serve as a phagocytosis signal which will be discussed in greater detail below [89]. In addition to PS externalization, apoptotic cells have numerous modifications of their membrane contents. The generation of apoptotic bodies causes the cell to lose membrane which is replaced from intracellular organelles such as the Golgi and endoplasmic reticulum [90]. This scavenging of intracellular membranes results in the externalization of protein and glycan groups, including n-acetylglucosamine (GlcNAc), which are normally expressed only on intracellular membranes [91]. Externalization of GlcNAc is recognized as a determinant of apoptotic thymocyte phagocytosis [92]. Moreover, many of the newly externalized proteins are modified by cleavage, likely by activated caspases, which might easily affect their function and/or recognition [66,93]. The abnormal externalization of intracellular material is believed to collectively serve as apoptotic cell-associated molecular patterns (ACAMPs), which either alone or in conjunction with plasma proteins such as MFG-E8, complement C1q, mannose-binding lectin, and surfactant protein A are then recognized by macrophages to mediate clearance (Figure 1.5)[89,94-96]. The binding of a macrophage to a target apoptotic cell creates an engulfment synapse and the diverse molecular interactions between ACAMP and macrophage mediate important components of efferocytosis such as, binding, and engulfment [97-99].

The proper execution of apoptosis and subsequent corpse clearance provides powerful anti-inflammatory signals to the engulfing cells and, importantly, remains immunologically silent [100-102]. Furthermore, the engulfment of early apoptotic cells is regarded to induce a tolerogenic response and proteins will be appropriately recognized as ‘self’, thus avoiding the activation of adaptive immunity towards apoptotic material [103]. Collectively, it is the combination of rapid apoptotic cell clearance linked to suppression of immune activation that allow apoptosis to proceed rapidly and efficiently with a minimum of tissue disturbance consequently maintaining tissue homeostasis. One of the key features of apoptotic cells that assist in the rapid silent removal of the cellular fragments is a stable intact membrane, generally detected by the exclusion of impermeable dyes (such as propidium iodide) that prevents the release of intracellular proteins and subsequent immunological activation [104]. This is in contrast to necrotic cell death, wherein cells inappropriately lyse and spill their intracellular contents leading to a rapid pro-inflammatory response (Figure 1.5) [101,105]. For this reason defects in efferocytosis are believed to cause inappropriate pathological inflammation leading

to the generation of auto-immune disease. Indeed, numerous genetically modified mouse models removing vital elements of cell recognition and clearance machinery including, but not limited to: complement C1q, and MFG-E8 display an auto-immune phenotype characteristic of systemic lupus erythematosus (SLE). SLE is a chronic systemic auto-immune disease which affects nearly 5 million people globally, 90% of which are female [106]. The disease is characterized by: the generation of auto reactive antibodies, particularly against nuclear antigens; the formation of antibody-immune complexes; and pro-inflammatory cytokine production [107,108]. Animal models with defective efferocytosis develop a similar age and female dominant pathology associated with increased anti-nuclear antibodies (ANA), splenomegaly (enlarged spleen), and glomerulonephritis (kidney immune-complex deposition) [109,110]. Given the systemic nature of the disease it is not surprising that SLE affects multiple organ systems including joints, skin, lymph and kidneys. While the pathophysiology of SLE is multifactorial, the best defined abnormality associated with the disease is a failure in apoptotic cell clearance. Not only are macrophages from SLE patients deficient in autologous efferocytosis *in vitro*, but the number of tingible body macrophages, which are responsible for the ingestion of apoptotic corpses in lymphoid tissue germinal centres, are frequently reduced in SLE sufferers [111,112]. Consistent with these observations, SLE is associated with greater numbers of circulating apoptotic bodies and an accumulation of apoptotic cells in the germinal centres of lymph nodes [113,114]. Furthermore, complement C1q deficiency, which is associated with increased undigested apoptotic debris, is a potent trigger for SLE [115]. The increase in free un-phagocytised apoptotic debris in SLE is a likely cause of SLE's classic diagnostic feature, ANA. As mentioned previously, the failure to timely clear apoptotic cells can result in immune activation towards intracellular material, including nuclear proteins and DNA. Supporting this possibility, SLE associated ANA can be specific for novel antigens revealed only after apoptotic enzymatic modification, such as cleavage [93]. Furthermore, these autoreactive antibodies are somatically mutated IgG isotypes suggesting that they are the products of B-cell affinity maturation and thus the result of an antigen driven immune response [116,117]. Collectively these observations underscore the importance of apoptotic cell clearance in the maintenance of self-tolerance.

However, it is important to note that apoptotic clearance failure in itself may be insufficient to promote auto-immune disease; in fact, mannose-binding lectin-

deficient mice have demonstrated apoptotic clearance defects without autoimmunity [118]. This suggests that additional determinants, apart from clearance, participate in the immunological processing of apoptotic cell debris. It has been proposed that immunosuppressive TGF-β release stimulated by binding of apoptotic cells to macrophages may be sufficient to avoid potentially problematic auto-antibody generation, even in the absence of clearance [119]. Nonetheless, defective cell clearance, as evidenced by mutation or elimination of the myriad components of efferocytosis, are undoubtedly linked to autoimmune disease as well as several other disorders in human and mice, including; atherosclerosis, neuropathy, arthritis, and anaemia [62,120].

1.5.4 ROCK1 blebbing and auto-immune disease

Numerous studies have attempted to define the importance of blebbing towards apoptotic clearance and found several, potentially contradictory, roles for blebs and apoptotic bodies. There have been several key *in vitro* studies demonstrating that inhibition of apoptotic blebbing can significantly impair corpse clearance by monocytes and macrophages [91,121,122]. Further investigation revealed that impaired corpse clearance following defective blebbing could be rescued by the PS bridging protein, MFG-E8. The implication of these studies is twofold: firstly, apoptotic blebbing directly mediates efferocytosis; and secondly, PS externalization may be a mechanism linking blebbing and phagocytosis. While the apoptotic externalisation of PS appears to be independent of ROCK activity, the sub-cellular localization of the phospholipid might be [57,122]. In fact, microscopic analysis reveals that apoptotic blebs become highly enriched for the externalized phospholipid [123]. Thus it appears that apoptotic blebs are serving as focal points for externalized PS to accumulate, which is then recognized by macrophages to trigger engulfment. The possibility that apoptotic blebs provide context for macrophage recognition are consistent with data demonstrating PS exposure on viable cells is insufficient to trigger phagocytosis. Surprisingly, MFG-E8 failed to further enhance the *in vitro* phagocytic uptake of normal blebbing apoptotic cells, as might be expected. This suggests that apoptotic blebbing itself is sufficient to mediate corpse clearance, alternatively, in the instance of defective blebbing, efferocytosis can be achieved with the aid of bridging molecules like MFG-E8; thus there appears to be a significant redundancy in clearance mechanisms. These redundant compensating mechanisms may explain why many genetically modified mice with defective

clearance mechanisms are neither developmentally lethal nor display severe auto-immune phenotypes (if displayed at all), as measured by survival and overall health.

One of the most striking examples highlighting the potential importance of apoptotic blebs is the demonstration of their robust opsonization with C1q in human endothelial cells [123-125]. Complement fixation in these cells was restricted entirely to the surface of blebs while the remainder of the cell surface remained clear of C1q binding [124]. This high density opsonization on the surface of apoptotic blebs likely binds multiple macrophage receptors which efficiently trigger efferocytosis. The importance of this mechanism is underscored by the autoimmune disorders observed in C1q deficient mice [110]. Collectively, ROCK dependent blebbing and the subsequent release of 'come-find-me' and/or the sub-cellular accumulation of 'eat-me' factors would be expected to facilitate rapid efferocytosis and thus maintain self-tolerance.

Apoptotic blebs are also intimately associated with the generation of auto-reactive antibodies. In fact, many of the newly externalised bleb-associated proteins are frequent auto-antigens in SLE including: nucleosomes, Ro, and La (Figure 1.5 [126,127] [89,125]. This outcome is in opposition to the typical physiological response and cannot be explained by macrophage phagocytosis. Other than macrophages, apoptotic blebs may also be cleared by professional antigen presenting dendritic cells (DC)(Figure 1.5)[128,129]. The uptake of apoptotic cells by dendritic cells or macrophages appears to have opposing consequences. As previously mentioned, macrophage phagocytosis is anti-inflammatory while DC uptake leads to secretion of pro-inflammatory cytokines and the presentation of self-antigens for auto-antibody generation [128-131].

Collectively, all of these studies demonstrate that apoptotic blebbing, as a mechanism to mediate cell clearance, is a double edged sword. While blebs appear to be important for rapid uptake and clearance they also are simultaneously sources of auto-antigens. It appears that the same material that is recognized by macrophages to mediate clearance is also recognized by other cell types, such as dendritic cells, to generate auto-immune antibodies. The mechanisms leading to these opposing outcomes is currently unclear, however, defects in macrophage uptake or increases in apoptosis appear to be important

determinants. Hypothetically, the accumulation of apoptotic debris would likely lead to an increased probability of DC activation and, over time, this inappropriate activation overcomes self-tolerance and generates auto-reactive antibodies characteristic of SLE. While the linkage between apoptotic blebbing and autoimmune disease is broadly recognized, definitive proof of the importance of apoptotic blebbing has not been forthcoming. The studies investigating apoptotic blebbing in the context of clearance and auto-immune disease are largely limited to *in vitro* experimentation that cannot recapitulate the complexity of interactions between apoptotic cells and their environment. Furthermore, they also typically suffer from their dependence on chemical inhibitors to interfere with apoptotic blebbing. The removal of these agents prior to analysis of macrophage phagocytosis is vital and, unfortunately, can never be guaranteed. In addition, the apoptotic cells have to be subjected to extensive additional washing steps which may alter the stability and structure of the apoptotic cells and thus affect outcome in subsequent assays. As a result, many of the observations regarding the importance of blebbing towards autoimmune disease are severely limited. Thus the current investigational methods are incapable of providing physiologically relevant insight into the role of ROCK induced apoptotic blebbing in the clearance of corpses and generation of autoimmune disease. Ultimately proof that apoptotic blebs are important for cell clearance and/or the generation of autoimmune disease requires a biological model of defective blebbing. Of note, a ROCK1 knockout mouse has been generated, however no evidence of either defective apoptotic blebbing *in vitro* or auto-immune disease *in vivo* has been reported.

1.6 ROCK functions in embryonic development

Targeted deletion in mice has revealed distinct roles for ROCK1 and ROCK2 in embryonic development. Knock-out mice generated by targeted deletion of exons 3-4 of the ROCK1 gene (in the C57Bl/6 strain background) were born at the expected Mendelian ratio, but were not viable and consequently were cannibalized by the mother [132]. Developmental abnormalities of ROCK1$^{-/-}$ mice included failure in the closure of eyelids (eyelids open at birth phenotype – EOB) and of the ventral body wall. The latter phenomenon results in the protrusion of the abdominal contents into an omphalocele. Closer scrutiny revealed that polymerization of filamentous actin at the umbilical ring was reduced, resulting in incomplete closure of the abdominal wall and herniation of abdominal organs, particularly the liver and

intestine. Furthermore, actin cable structures within the leading edge of cells composing the eyelid epithelial sheets were disorganized, accounting for EOB. In both cases, phosphorylation of MLC was not observed. Two further versions of ROCK1 knockout mice have been generated either by targeted deletion of exon 5 (and studied in the FVB strain of mice)[133] or exon 1 (and studied in the C57Bl/6 strain)[134]. In neither case were EOB or omphalocele phenotypes observed, which might be explained by strain-specific genetic differences. However, in each case under-representation of homozygous ROCK1 knock-out mice in litters was observed. In addition, ROCK1-deficient animals were resistant to reactive cardiac fibrosis resulting from physical stress on the cardiac muscle, which may be mediated by reduced ROCK1-mediated expression of fibrogenic cytokines and extracellular matrix protein production by cardiac fibroblasts [133,134].

Genetic deletion of ROCK2 on the C57Bl/6 background also exhibited EOB and omphaloceles [135], suggesting that either there is a requirement for each individual ROCK protein, or for a minimum level of total ROCK activity, in the actin driven movement of epithelial sheets required for these developmental processes. This second possibility is supported by the observation that ROCK1/ROCK2 double heterozygous mice also exhibited EOB and omphaloceles [135], although at a lower frequency than ROCK1$^{-/-}$ or ROCK2$^{-/-}$ mice. The lack of effect in phenotype in other tissues suggests that ROCK1 and ROCK2 are able to functionally compensate for each other, or that the requirement for total ROCK activity is lower. Interestingly, approximately 90% of ROCK2 knock-out mice on the mixed C57Bl/6-129/Sv strain background died *in utero* at around 13.5 days postcoitum from coagulation of blood within the placental labyrinth layer [136].Surviving ROCK2$^{-/-}$ mice were runted, suggesting nutritional deficiency resulting from placental impairment, with hemorrhages observed in hind limbs supporting the conclusion that there were defects in blood coagulation. Actin structures within the placental labyrinth layer of ROCK2$^{-/-}$ mice were apparently normal, suggesting an actin-independent role for ROCK2 in the placenta. Interestingly, there may be a role for ROCK1 within the placenta where it robustly associates with caveolin1 within lipid rafts of syncitial trophoblasts [137]. The strain-specific differences in the effects of ROCK deletion strongly suggest the influence of modifier genes or strain-specific differences in ROCK activity.

1.7 ROCK inhibitor specificity

Many studies that have aimed to identify the biological activities of ROCK have made use of the potent small molecule inhibitors that are commercially available. The most commonly used inhibitor is Y27632 [138]; others include Y-32885 [138], H-89 [139], HA-1077 (fasudil)[140], HA-1100 (hydroxyfasudil)[141], H-7 and H-8 [142], H-1152 [143], Rockout [144] and [N-(4-Pyridyl)-N'-(2,4,6-trichlorophenyl)urea][145]. There are always questions about the specificity and selectivity of small molecule inhibitors, given that the majority act as ATP-competitors and the 3-dimensional structure of protein kinases, including the ATP-binding regions, are highly related [146]. Recently, a panel of ROCK inhibitors (Y27632, H-7, H-8, HA-1077, H-89, H-1152) was tested against a panel of 70 protein kinases [147]. These experiments revealed that none of the ROCK inhibitors is absolutely specific, with the Rho-regulated PRK2 being inhibited to the same extent by all tested ROCK inhibitors and both MSK1 and RSK1 being at least 50% inhibited by all the tested compounds at concentrations that inhibited ROCK2 by at least 90%. These studies indicate that although ROCK inhibitors are useful tools, they should not be relied upon to be conclusive.

Therefore, a greater confidence would be engendered in studies that make use of ROCK inhibitors if a number of additional conditions were satisfied including:

1. Structurally unrelated inhibitors should produce the same biological endpoints at concentrations that produce equivalent kinase inhibition. The lowest effective doses should be used to reduce off-target effects.

2. Dose-response experiments to establish rank order of potency for a set of inhibitors, *i.e.* the most potent ROCK inhibitors should be the most effective if a biological response is mediated by ROCK.

3. Examination of the relationship between ROCK inhibitor dose, substrate phosphorylation and biological endpoint.

4. Where possible additional methods should be used to inhibit ROCK function, such as RNAi-mediated knockdown.

Although care should be taken in interpreting the results of inhibitor studies, they are undoubtedly useful and convenient tools. Our understanding of the biological

functions of ROCK has been vastly aided by the ready availability of these inhibitors. However, their utility is most robust in excluding the possible involvement of a particular signaling pathway in specific biological responses when adequate positive controls are in place.

1.8 ROCK and cancer

Given the diverse array of cellular functions of ROCK it is unsurprising that the kinases have been significantly implicated in the pathogenesis of cancer. Increased expression of Rho GTP-binding proteins has been reported for a wide variety of cancers [148,149]. Although the mechanisms leading to elevated Rho expression have not been widely investigated, it was recently reported that metastatic breast cancer cells overexpress a microRNA that increases the expression of RhoC [150]. In addition to increased levels of Rho proteins, specific examples of elevated expression or mutation of Rho activating guanine nucleotide exchange factors and downregulation or deletion of Rho inactivating GTPase accelerating proteins have been detected [149]. These findings suggest that there may be increased ROCK activity associated with cancer. Consistent with this possibility, elevated expression of ROCK1 and ROCK2 was observed in bladder [151] testicular cancer [152,153], and squamous-cell carcinoma [154]. In the case of bladder cancer, elevated expression was significantly correlated with poor survival [151]. Finally, recent efforts to identify somatic mutations in human cancers have identified mutations in both ROCK1 and 2 [155]. Statistical analysis of the mutation rate of ROCK1 suggests that the mutations are perhaps drivers of the oncogenic process. These mutations will be discussed in greater detail in Chapter 4. The increased expression and activity of ROCK could contribute to cancer initiation and progression in several ways. In the sections below, I summarize the evidence that supports a role for ROCK in promoting proliferation, survival and metastasis.

1.8.1 Proliferation

The ready availability of potent ROCK inhibitors, especially Y27632 [138], has made it possible to examine the role of ROCK in mitogen-induced proliferation in a wide variety of cell types, both in tissue culture and *in vivo* (Table 1.1), albeit with the caveats noted above. In some instances, RNAi-mediated knockdown of ROCK expression has been found to impair proliferation [156]. ROCK inhibitors antagonise

a wide range of mitogenic stimuli including agonists for G-protein-coupled serpentine receptors and tyrosine kinase growth factor receptors to mechanical stretching. The single most common cell type in which ROCK inhibition has an apparent anti-proliferative effect is in vascular smooth muscle, with a number of reports indicating a similar effect in airway and prostatic smooth muscle cells. The prevalence of reports on vascular smooth muscle cells may reflect two factors; the critical role of ROCK in regulating both the contraction and proliferation of smooth muscle cells, and the high level of interest in ROCK inhibitors as agents to treat cardiovascular diseases. The lower occurrence of publications reporting an effect of ROCK inhibitors on proliferation in other tissues may reflect a role for ROCK in a limited number of cell types, or may be a function of lower interest in investigating the contribution of ROCK to proliferation in non-muscle cells

Consistent with the anti-proliferative effect of ROCK inhibitors, expression of active forms of ROCK1 and ROCK2 have been shown to induce proliferation of bovine endothelial cells and mouse fibroblasts respectively [157,158]. In addition, active ROCK1 was found to co-operate with a weakly activated form of Raf1 to promote oncogenic transformation of immortalized mouse fibroblasts. In a recent paper it was discovered that conditional activation of ROCK2 in skin leads to contractility dependent epithelial hyperproliferation and skin thickening [154]. The proliferative effect of ROCK2 in epithelial cells is a result of mechanical paracrine stimulation of β-catenin due to increased extracellular collagen deposition. The activation of ROCK2 in this model was further associated with increased tumour formation following chemical carcinogenesis. This work suggests that ROCK activation and subsequent acto-myosin contractility help create an extracellular environment or ‘niche’ that is permissive for hyperproliferation and the generation of cancerous lesions.

There are a limited number of studies reporting stimulation of proliferation by Y27632, indicating that replication of some cell types may be restrained by ROCK activity. Treatment of rat embryonic kidney cells [159] human primary keratinocytes [160] and human embryonic stem cells [161] induced proliferation, while expression of a conditionally activated ROCK2 in primary keratinocytes led to cell cycle arrest and terminal differentiation upon induction of catalytic activity [160]. Similarly, expression of a constitutively active ROCK2 inhibited the proliferation of endothelial cells while Y27632 partially rescued cells from an inhibition of proliferation induced by TNF-α

[162]. Taken together, the literature supports the conclusion of a general role for ROCK as a promoter of cell replication, with anti-proliferative functions in selected cell types. What is missing from consideration are studies in which activation or inhibition of ROCK had no effect on proliferation, with a few exceptions (*e.g.* references [163-165]), lack-of-effect results are generally left unpublished.

Table 1.1. Anti-proliferative effects of ROCK antagonism

Cell type	ROCK Inhibitor	Mitogen	References
Glioma cell lines	Y-27632	Lysophosphatidic acid	166
Astrocytes	Y-27632	PAR-1 agonists	167
Mouse Embryo Fibroblasts	Y-27632	Macrophage migration inhibitory	168
Tenon's Capsule Fibroblasts	H-1152P	Wound healing	169
Oral squamous carcinoma cells	Y-27632	Sonic hedgehog	170
Gastric epithelial cells	Y-27632	Glycine-extended gastrin	171
Umbilical vein endothelial cells	Y-27632	Oxidized LDL	172
Vascular smooth muscle cells	Y-27632	PDGF-BB	173
Airway smooth muscle cells	Y-27632	Serum	174
Prostatic smooth muscle cells	Y-27632		175
Cardiac myocytes	Y-27632	Serum	176
Atrial myofibroblast cells	Y-27632	Serum	177
Myoblasts	Y-27632	Serum	178
T cells	Y-27632	Concanavalin A	179
$CD34^+$ hematopoietic progenitor stem cells	Y-27632	CXCL12	180
Chondrocytes	Y-27632	Serum	181
Hepatic stellate cells	Y-27632	Serum	182
Pancreatic stellate cells	Y-27632 Fasudil	Serum, PDGF-BB	183
Adrenal Zona glomerulosa cells	Y-27632	Serum	184

1.8.2 ROCK and cell survival

There also appears to be a role for ROCK in cell survival. Inhibition of ROCK activity induces cell death in corneal epithelial cells [185], airway epithelial cells [186],

neointimal smooth muscle cells [187-189], vascular smooth muscle cells [190,191], endothelial cells [192] hepatic stellate cells [193], spinal cord motor neurons [194], rheumatoid synovial cells [195] and in H_20_2 treated intestinal epithelial cells [196]. These effects were not limited to non-transformed cells as ROCK inhibition also induced cell death in anaplastic thyroid cancer cells [197] glioma cells [198] $CD34^+$ chronic myeloid leukemia progenitor cells [199] and H_20_2 or camptothecin treated neuroblastoma cells [200].

Whether ROCK activation is pro-apoptotic or pro-survival is likely context specific and dependent upon cell type and death stimulus. Although there are some examples of ROCK inhibitors resulting in tumour regression *in vivo* (*e.g.*[198,201]), it remains to be determined whether this resulted from the inhibition of ROCK-mediated protection in the tumour cells. It is also remains to be determined whether a pro-survival activity of ROCK plays a significant role in human cancers. The precise molecular mechanisms through which ROCK might mediate its effects on cell survival remain to be elucidated.

1.8.3 ROCK in tumour cell invasion and metastasis

Tumour cells are recognized to utilize the complete array of migration strategies, from the migration of multicellular sheets to individual cell motility [55]. As previously discussed ROCK activity is particularly vital for the amoeboid migration of cancer cells [56,60]. Treatment of morphologically round cancer cell types (A375, WM266.4, LS174T) with the ROCK inhibitor Y27632 was found to significantly impair cell motility, while in contrast migration of cancer cells with an elongated morphology (BE and SW962) was highly resistant to Y27632 [56]. Furthermore, amoeboid tumour cell migration and invasion are dependent upon matrix deformation rather than proteolytic remodeling [60]. Interestingly, cancer cells display a remarkable plasticity in migration strategy and can switch between mesenchymal and blebbing strategies to maintain motility. This strategy switching involves a complex signaling interplay between competitive Rho and Rac signals [56,202]. Although cancer cells can use several different migration strategies, the amoeboid ROCK-dependent motility appears to favor metastatic disease. In fact, overexpression of RhoC, an effector of ROCK, is not only correlated but is essential for metastatic disease in several *in vivo* models [203-205]. This increased metastatic phenotype is associated with increased membrane blebs suggesting an important role for ROCK induced

amoeboid motility [203]. These observations are further supported by numerous studies that directly implicate ROCK in tumour cell invasion by examining *in vivo* metastasis in the presence of ROCK inhibitors. In one study, HA-1077 (fasudil) reduced tumour burden and ascites resulting from peritoneally disseminated MM1 (rat hepatocellular carcinoma) cells in rats by half, decreased lung nodule formation in mice by HT1080 (human fibrosarcoma) cells by 40% and limited breast cancer formation in mice by MDA-MB-231 (human breast carcinoma) cells three-fold [206]. ROCK inhibitors also were found to reduce the *in vivo* invasiveness of human hepatocellular carcinoma [207,208], human prostate cancer [209] and mouse lung cancer cells [210]. A positive role for ROCK in cancer cell invasiveness *in vivo* was further demonstrated with human colorectal cancer cell lines expressing a conditionally active version of ROCK2 [211]. These cells formed highly vascularized tumours in mouse xenografts that aggressively and individually invaded into the surrounding stroma upon ROCK activation. These results suggest that ROCK2 activity is not only sufficient for tumour invasion, but is also sufficient for the induction of angiogenesis possibly by increasing the plasticity of tumour tissue thereby facilitating invasion by endothelial cells, potentially aiding tumour growth and dissemination. This possibility is supported in a recent paper demonstrating that ROCK driven actomyosin contractility encourages the loss of tumour cell cohesion and the switch from collective to individual migration [212]. Collectively, these studies are consistent with ROCK as a central mediator of tumour cell invasiveness and metastasis through blebbing motility.

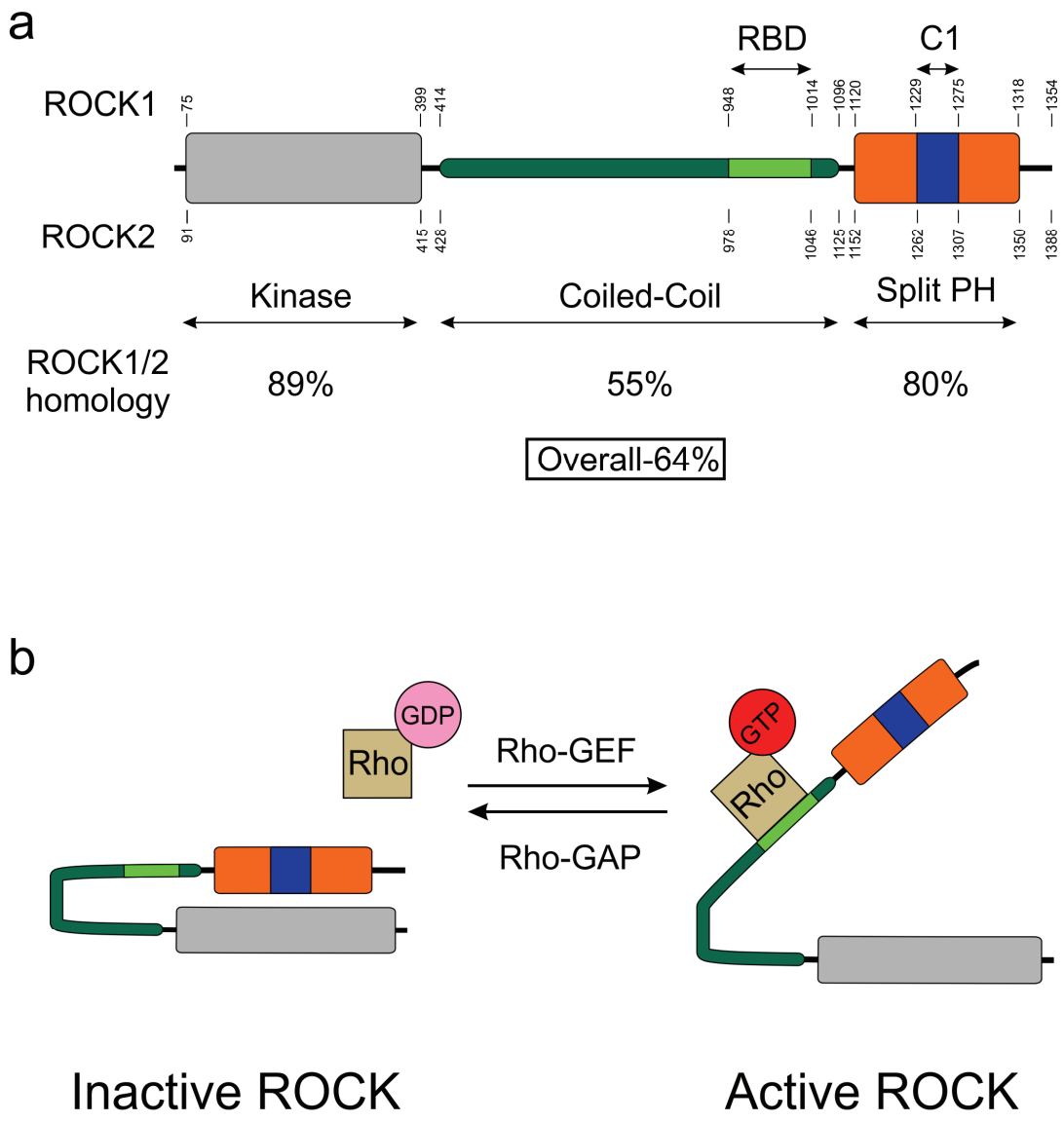

Figure 1.1. Rho associated kinase structure, homology, and regulation
(a) Line diagram of ROCK1 and 2 protein domains and homology. Domain location from N-terminus indicated above and below diagram for ROCK1/2 respectively. Kinase domain is in grey; Coiled-coil in dark green; Rho-binding domain (RBD) in light green; Split pleckstrin homology (PH) in orange; and cysteine-rich (C1) domain in blue. Percent sequence homology for ROCK1 and 2 shown below line diagram. (b) Line diagram illustrating activation of ROCK following Rho GDP-GTP exchange by Rho. Rho-GDP (guanosine diphosphate) is exchanged for GTP (guanosine triphosphate) with the aid of a Rho-guanine nucleotide exchange factor (GEF). Rho-GTP then binds to the Rho binding domain (light green) and induced a conformational change which relives kinase auto-inhibition. The kinase is then returned to an inactive state by hydrolysis of GTP to GDP after binding of a Rho- GTPase activating protein (GAP) to the Rho protein.

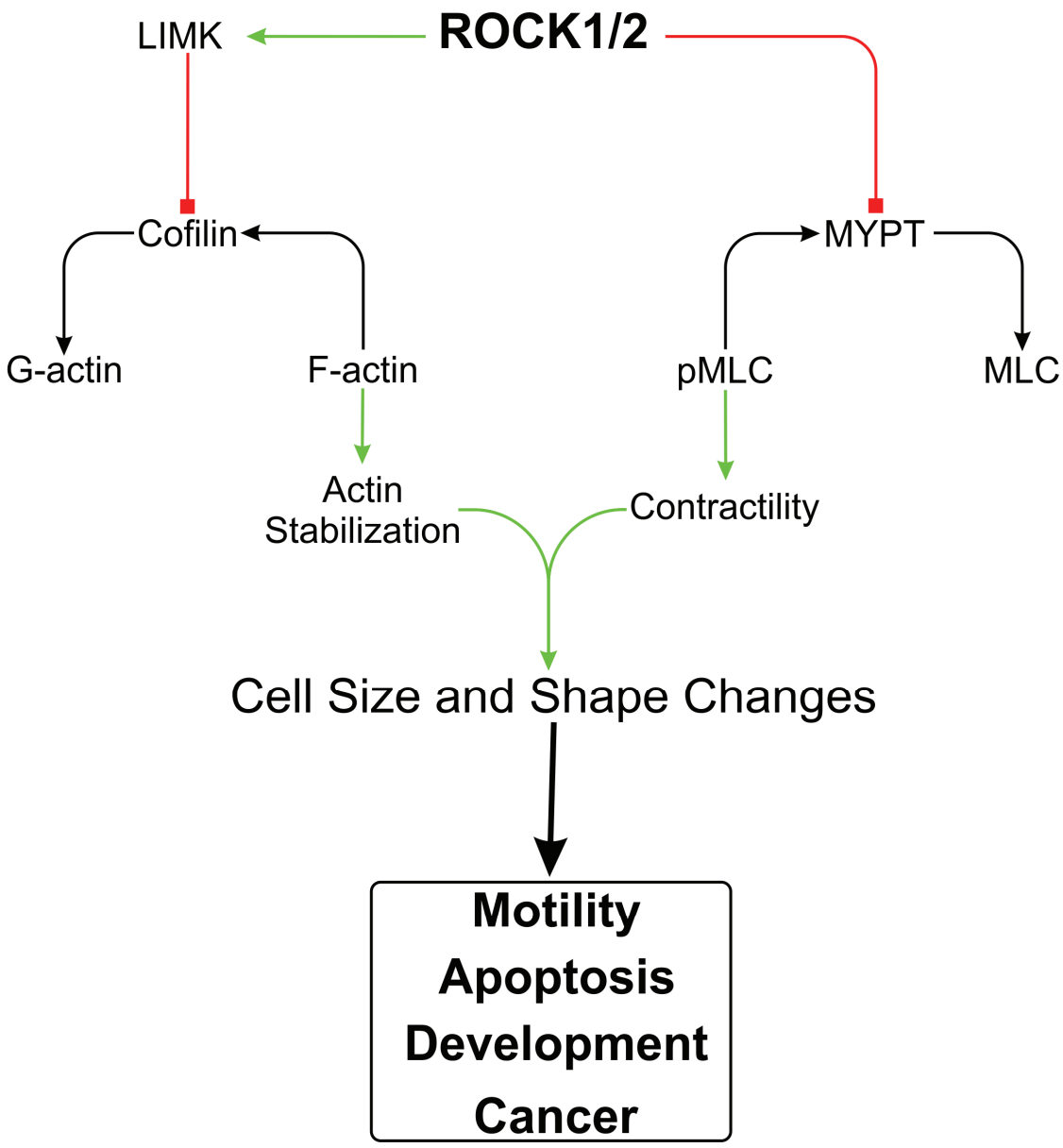

Figure 1.2. Diagram of intracellular ROCK signalling
Stimulatory inputs are indicated by green arrows and inhibitory in red. LIMK, LIM kinase; MYPT, myosin phosphatase target subunit; MLC, myosin light chain. The net activity of ROCK activation is to stabilize actin filaments and increase acto-myosin contractility, the outcome is profound changes to cell size and shape.

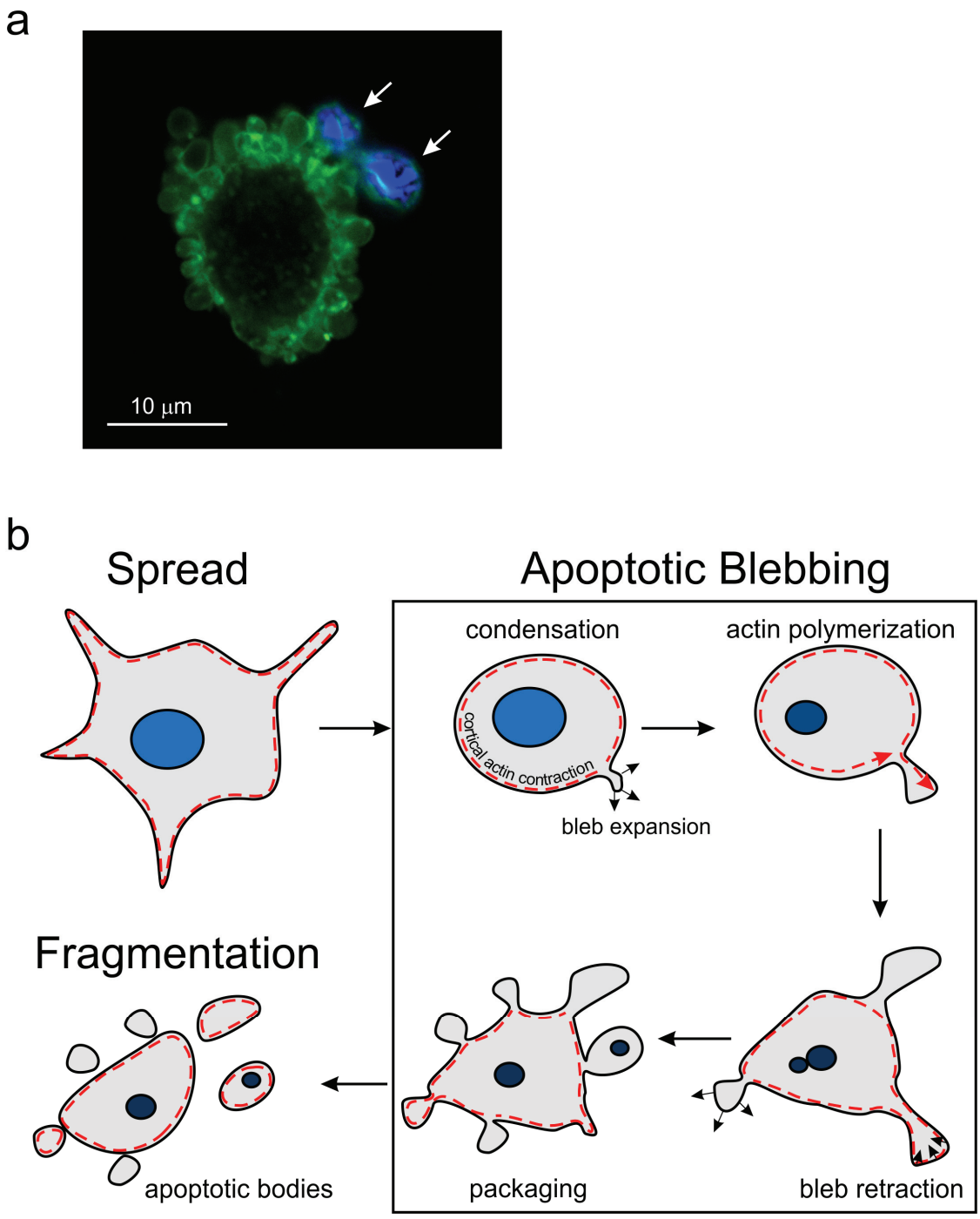

Figure 1.3. The generation of apoptotic blebs
(a) Representative immunofluorescence micrograph of an apoptotic mouse embryonic fibroblast. Apoptosis was induced with TNFα (50 ng/ml) and cycloheximide (10 μg/ml). After 2 hours the cells were fixed with paraformaldehyde and plasma membrane stained with fluorescent lipid dye DiO (green) and nucleus is stained with DAPI (blue). The cell has many apoptotic blebs some of which contain nuclear fragments (white arrows). Image acquired at 63X oil immersion objective with a laser scanning confocal microscope. (b) Diagram illustrating the mechanism of bleb generation and retraction in apoptotic cells. Black lines indicate cellular membrane and dotted red line underneath is the cytoskeletal cortex. As a result of cortical contraction intracellular pressure builds and blebs spontaneously form and expand. Actin rapidly polymerizes into the newly formed blebs and then acto-myosin contractility retracts the protrusion. Cellular components become packaged in the bleb which can eventually fragment into apoptotic bodies.

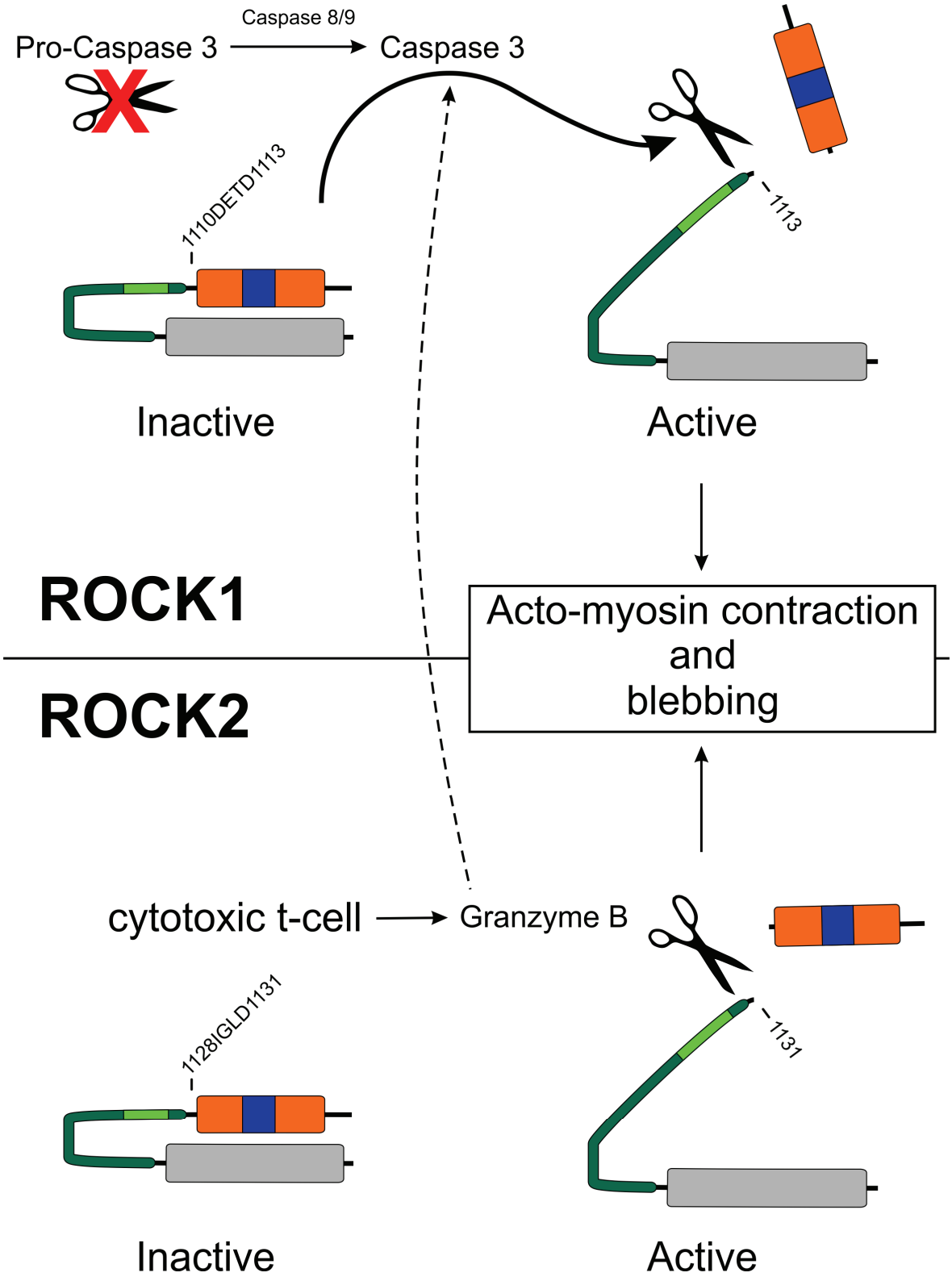

Figure 1.4. Non-canonical activation of ROCK1/2
Schematic illustration of cleavage of ROCK1 and ROCK2 induced by caspase 3 and granzyme B respectively. Cleavage generates constitutively active kinases that induce contractility and blebbing.

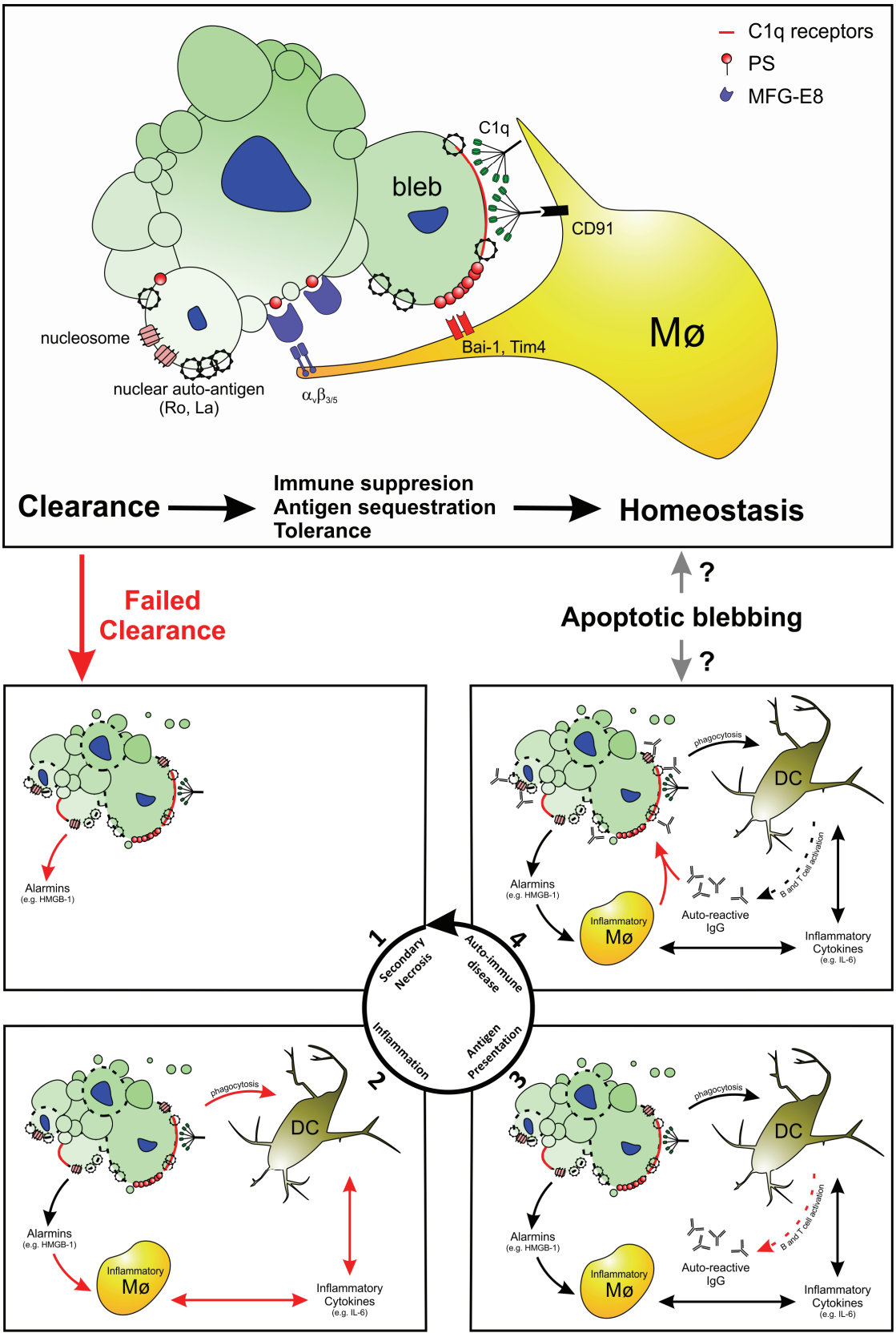

Figure 1.5. Apoptotic blebbing in efferocytosis and auto-immune disease
Schematic illustration of apoptotic cell blebs in concentrating eat-me factors and aiding clearance. Alternatively blebs concentrate nuclear antigens and participate in auto-immune disease. MØ, macrophage; DC, dendritic cell, PS, phosphatidyl serine.

2. Consequences of apoptotic blebbing: ROCK1 cleavage and auto-immune disease

2.1 Introduction

During apoptosis ROCK cleavage and activation appears to be not only vital for the formation of blebs but may be involved in the clearance of the cellular corpse [72-74,122]. As previously discussed, many of the studies investigating the importance of apoptotic ROCK cleavage and its numerous biological consequences have been limited to in vitro studies often using pharmacological inhibitors. While undoubtedly valuable, these reports do not provide proof that ROCK cleavage is necessary for apoptotic bleb formation or yield understanding of the biological function of blebbing. Therefore, the conclusions derived from these studies are at best speculative.

In order to answer these fundamental questions about the role of ROCK1 cleavage and activation in apoptosis, I made a genetically modified (GM) knock-in mouse expressing non-cleavable ROCK1 (ROCK1nc) that renders the protein insensitive to caspase-cleavage. The generation of this model will provide definitive evidence whether the cleavage of ROCK1 is essential for apoptotic blebbing, which could then prove to be an ideal model to assess the *in vivo* biological impact of blebbing in homeostasis. These studies could be fundamentally important in our understanding of auto-immune disease and either provide validation for the current understanding of the role of apoptotic blebbing or necessitate a re-analysis of current thinking.

2.2 Results

2.2.1 Generation of ROCK1 non-cleavable (ROCK1nc) knock-in mouse

A targeting vector bearing two mutations in exon 27 (3338A>C and 3339T>A) of the mouse ROCK1 gene was generated with a floxed neomycin selection cassette in the preceding intron (Figure 2.1). The targeting vector was generated with 3.1 kb 5' and 5.1 kb 3' homology arms respectively. When translated, the mutant ROCK1 bears a single missense substitution (D1113A), thus modifying the caspase cleavage site from DETD to DETA. This modification renders the kinase

insensitive to caspase cleavage [57]. Following transfection of the targeting vector in 129 mouse embryonic stem cells (mES) the cells were selected for stable insertion by neomycin resistance and then surviving clones were screened for properly targeted homologous recombination. I performed the primary screen by polymerase chain reaction (PCR) of genomic DNA purified from neomycin resistant clones with the 5' primer within the neomycin cassette and 3' outside the homology arm (Figure 2.2a). This reaction was predicted to generate a 3.5 kb product from homogonously recombined mES cells and no product from the wt ROCK1 locus (Figure 2.2a). A positive product of the expected size was detected in 3 out of 200 clones (6b, 7h, and 4g) indicating homologous recombination at the 3' arm of the mutant ROCK1 allele (Figure 2.2b). The preliminary hits were re-confirmed and found to be positive; however, the 4g had far less reaction product compared to 6b and 7h (Figure 2.2c). Clones 6b, 7h, and 4g were further examined for 5' homology using PCR with 5' primer outside the homology arm and the 3' primer within the neomycin cassette. This reaction was predicted to generate a 5.5 kb product from homologously recombined mES cells and no product from the wt ROCK1 locus (Figure 2.3a). Only 6b and 7h generated products of the expected size, indicating that these clones had a correct homologous knock-in of the mutant ROCK1 gene (Figure 2.3b). Clone 6b was used to generate animals and 7h was held in reserve. The mES 6b clones were injected into fertilized mouse blastocysts and then implanted into pseudopregnant mice. The resulting male mosaic offspring were then bred onto a wildtype female C57 black 6 (C57BL/6). Offspring were routinely genotyped using Transnetyx genotyping service to detect the mutant ROCK1nc allele for germline transmission. This genotyping uses a quantitative PCR reaction coupled with a specific fluorescent probe to determine hetero- and homozygosity (Figure 2.4). The construct generation, transfection and embryo manipulation was performed by The Beatson Institute Transgenic Technology core facility.

2.2.2 Breeding strategy for ROCK1nc

Mice heterozygous for the mutant ROCK1nc gene retained the neomycin selection cassette within the intron sequence which needed to be removed to avoid any interference in ROCK1 expression. As previously mentioned, the neomycin cassette was flanked by LoxP sequences and the cassette was removed by crossing female ROCK1nc$^{+/-}$, neomycin$^{+/-}$ to male C57BL/6 expressing ubiquitous

Cre recombinase leaving a residual LoxP site (Figure 2.5a). The resulting animals verified as ROCK1nc$^{+/-}$, neomycin$^{-/-}$, Cre$^{+/-}$ were bred onto wild type C57BL/6 to remove Cre (Figure 2.5a). Deletion of neomycin and removal of Cre was confirmed by genotyping from Transnetyx. The resulting heterozygous ROCK1nc (neo and Cre null) animals were interbred to generate animals for experimentation. ROCK1nc mice generated from heterozygous breeding were born in the expected Mendelian ratios (Figure 2.5b) without gross abnormalities. ROCK1nc homozygous mice were also bred to generate experimental animals and found to be viable and thrive (data not shown).

2.2.3 ROCK1nc mutation does not alter kinase function

The substitution mutation that was introduced in the ROCK1 caspase cleavage site is not anticipated to affect kinase activity or activation. The location of the caspase cleavage site is outside of both the N-terminal kinase and C-terminal regulatory domains. Given the nature of the ROCK1nc mutation, a change in kinase function should only be observed following induction of apoptosis and caspase cleavage, under non-apoptotic conditions the kinase is expected to behave identically to wt ROCK1. Nonetheless, verification that ROCK activity is unaffected by the introduction of the D1113A mutation was necessary. To address this, I immunoprecipitated myc tagged ROCK1wt and ROCK1nc constructs expressed in HEK293 cells and analysed activity of approximately 200 ng of kinase in a fluorescence polarization assay (Figure 2.6a). Both ROCK1 and ROCK1nc induced an identical level of substrate phosphorylation (Figure 2.6b), thus the introduction of the D1113A mutation does not affect ROCK1 activity. Moreover, kinase activity in untransfected cells was similar to background, suggesting that no contaminating kinases were co-immunoprecipited. This work was performed in collaboration with Dr. Nicola Rath. I next sought to confirm that ROCK1nc cellular expression does not alter cellular phenotype compared to wt. In order to validate the in vitro biology of ROCK1nc expression I generated mouse embryonic fibroblasts (MEFs) from E13.5 pups in homozygous wild-type (wt) and ROCK1nc mice. The MEFs generated in either strain were morphologically identical and had similar proliferation rates (Figure 2.7a and data not shown). I determined the cell based activity of ROCK1nc or wt MEFs by examining the formation of actin stress fibres and phosphorylation of MLC (pMLC), two hallmarks of cellular ROCK activity, following a 5 min stimulation with 10% FBS. As can be

seen in Figure 2.7a, the formation of stress fibres and pMLC is identical in either cell line. Furthermore, introduction of the ROCK antagonist, Y27632, similarly suppressed both responses in each cell line (Figure 2.7a). The effect of FBS on pMLC in wt and ROCK1nc MEFs was quantified using a 96 well plate in-cell western blot approach. Following treatment MEFs were fixed, permeabilized and stained for pMLC with a fluorescent secondary antibody. The fluorescence of pMLC in each well was quantified using a LiCOR Odyssey scanner. Cell numbers were normalized to total nuclear fluorescence detected by DRAQ5 (Figure 2.7b). Consistent with microscopic observations, MEFs expressing either wt or non-cleavable ROCK1 behaved identically to one another following treatment with FBS +/- Y27632 (Figure 2.7c). These observations suggest that under growth conditions ROCK1nc mutation affects neither *in vitro* kinase activation nor its sensitivity to chemical inhibitors.

2.2.4 ROCK1nc is resistant to apoptotic cleavage

I next sought to ascertain if the ROCK1-D1113A mutant was indeed resistant to caspase cleavage during apoptosis. Lysates of wt and ROCK1nc MEFs treated +/- TNFα and cycloheximide (CHX) for 4 hours were western blotted for ROCK1. In non-apoptotic cells ROCK1 expression in wt or ROCK1nc MEFs was identical, which I expected from a 'knock-in' at the endogenous locus (Figure 2.8). Following TNFα treatment ROCK1 cleavage is apparent in ROCK1wt MEFs while in ROCK1nc cells no ROCK1 cleavage product was observed, indicating that the mutant ROCK protein is indeed caspase cleavage resistant (Figure 2.8). Verification that MEFs were apoptotic was confirmed by appearance of cleaved poly (ADP-ribose) polymerase (PARP), a classic marker of apoptosis (Figure 2.8). In addition, I observed that apoptosis in wt MEFs was associated with increased MLC phosphorylation, a hallmark of ROCK activation; however, no such increase was observed in the mutant cells (Figure 2.8). This work was performed in collaboration with Dr. Nicola Rath. As ROCK1nc MEFs express a fully functional kinase, the lack of apoptotic MLC phosphorylation is best explained by defective cleavage associated with decreasing levels of ROCK activating RhoA-GTP which are insufficient to activate the kinase. A clear implication of these observations is that, due to decreasing ROCK1 activation signals, apoptotic cells must constitutively activate ROCK1 (by caspase cleavage) to induce and maintain MLC phosphorylation. The phosphorylation of MLC would be expected to induce acto-

myosin contractility which, in turn, likely causes blebbing. These observations are consistent with the suspected role of cleaved ROCK1 as a potent inducer of apoptotic blebbing.

2.2.5 ROCK1nc expression abolishes apoptotic blebbing

Having established that ROCK1nc is resistant to caspase cleavage, I then asked if its expression disturbs apoptotic blebbing. Microscopic time-lapse images captured on 30 second intervals clearly demonstrate a profoundly defective apoptotic morphology in ROCK1nc MEFs compared to wt (Figure 2.9). This defect is characterized by a failure to retract, condense, and bleb. In addition, the cellular processes which fail to retract appear to fragment and remain adhered (Figure 2.9, lower panel, red arrows). This fragmentation seen in ROCK1nc MEFs is in contrast to the highly ordered formation of free floating subcellular apoptotic bodies (Figure 2.9, upper panel, white arrows).

2.2.6 ROCK1nc expression does not affect phosphatidyl serine (PS) externalization

As the externalization of PS during apoptosis is reported to be independent of ROCK activity [57,122] I wanted to verify if this observation is consistent in non-blebbing ROCK1nc MEFs. Both wt and ROCK1nc MEFs were either left in starve medium (control) or treated with TNFα for 24 hours prior to staining with fluorescently labeled annexin V for FACS analysis. As can be seen in Figure 2.10 over 80% of MEFs bind annexin V, and thus externalize PS, following 24 hour treatment with TNFα, indicating that the cells are highly apoptotic. Consistent with the previous reports no difference in annexin V binding was observed between MEFs expressing wt and non-cleavable ROCK1 (Figure 2.10)[73]. Therefore the failure to cleave ROCK1 appears to affect only the morphological features of apoptosis and other components of the apoptotic programme progress independently.

2.2.7 Homozygous ROCK1 mice are viable and thrive

As previously mentioned homozygous ROCK1nc mice were born in expected ratios and had no gross phenotype. In addition, homozygous animals were interbred to generate experimental animals which produced viable thriving

offspring (data not shown). Furthermore, homozygous females could give birth to multiple litters with no apparent difficulties (data not shown).

2.2.8 Homozygous ROCK1nc mice have apoptotic cell accumulation

Having established that expression of non-cleavable ROCK1 abolishes apoptotic blebbing, I sought to identify if there was a subsequent defect in efferocytosis. Consequently I analysed the appearance of cleaved caspase 3, a hallmark of programmed cell death, in the splenic lymphoid follicles of 35 week old male animals. Maturing lymphocytes have an extraordinarily high level of apoptosis, 95% of which are eliminated by apoptosis. In fact, Bak and Bax knockout mice, whose cells cannot execute the apoptotic programme, develop massive splenomegaly and the organ size increases more than 30-fold due to the progressive accumulation of lymphocytes that fail to apoptose [213]. Thus the physiologically high level of apoptosis in the spleen makes it an ideal organ to assess the clearance of apoptotic cells in ROCK1nc mice. In wild type animals numerous apoptotic corpse fragments (black arrows), staining for cleaved caspase 3, were scattered throughout the lymphoid follicle (surrounded by black dashed line) and very few large intact apoptotic cells were seen (red arrow) (Figure 2.11a). This fragmented staining pattern is consistent with the phagocytic uptake of apoptotic debris by surveilling macrophages. In contrast, active caspase 3 stain in ROCK1nc splenic follicles is associated with numerous large intact cells (red arrows) in addition to some fragmented staining (black arrows)(Figure 2.11a). Further analysis shows that ROCK1nc mice have far more unfragmented apoptotic cells than wild-type (Figure 2.11b). While preliminary, the accumulation of apoptotic cells in ROCK1nc mice is very interesting and could be caused by either a failure of efferocytosis and/or increased follicular apoptosis. However, further studies are required to conclusively determine if lack of apoptotic blebbing impairs corpse clearance.

2.2.9 Homozygous ROCK1nc mice display an inflammatory/auto-immune phenotype

As previously discussed, mice with defective apoptotic clearance can develop an auto-immune phenotype characterized by: splenic enlargement (splenomegaly), generation of ANAs, and deposition of immune complex in the kidney. I initially examined formalin fixed kidney sections of 15 week old male ROCK1nc

homozygous mice for IgG and found that some animals have a significant deposition of immunoglobulins within the glomerulus (Figure 2.12). Many of the glomeruli in the kidney of this animal were positive for mouse IgG. Physiologically, the kidney glomerulus, which is the basic filtration apparatus of the organ, is not associated with the deposition of immune complex and the detection of IgG on the glomuluar membrane is a characteristic of glomerulonephritis, a chronic kidney condition frequently seen in auto-immune diseases including SLE [214,215]. While the incident rate of auto-reactive antibodies in the kidneys of ROCK1nc mice is unclear, these data are the first indication that failure to cleave ROCK1 during apoptosis, and thus impair blebbing and potentially efferocytosis, leads to auto-immune disease. Currently a large cohort of animals is ageing for further investigation.

In collaboration with a clinical veterinary pathology lab, the haematology of wt and ROCK1nc animals was analysed. On pathological review the mutant ROCK1nc mouse erythrocytes displayed aniscytosis, which is a high variability in erythrocyte size. Individual red blood cells (RBC) from mutant animals can be abnormally small compared to the uniform erythrocyte size seen in wild-type animals (Figure 2.13a). This observation is further supported by additional clinical haematology data indicating that 6 week old ROCK1nc mice have significantly reduced RBC numbers (haematocrit) and mean corpuscular volume (MCV), an indication of erythrocyte size (Figure 2.13 and c). In addition, female mutant mice have a further significant reduction in MCV compared to their male littermates (Figure 2.13c). While the reduction in haematocrit was significant the magnitude of the reduction would not be considered clinically anaemic. Nonetheless, homozygous ROCK1nc mice have a significant defect in either erythrocyte generation or destruction. While a reduced erythrocyte production cannot be ruled out the observed reduction in circulating RBC and MCV is consistent with macrophage phagocytosis, suggesting that ROCK1nc may be increasing erythrocyte destruction.

The approximate lifespan of a mouse erythrocyte is 50 days and they are usually removed from circulation by resident macrophages in the spleen [216]. Despite a high level of continuous erythrocyte phagocytosis in the spleen, the removal is hard to detect due to efficiency of disposal. However, increases in the rate of erythrocyte removal lead to an accumulation of iron within the splenic

macrophages, this iron is then stored in the phagocytes' cytoplasm in an iron-strorage complex called haemosiderin. The deposition of haemosiderin is associated with numerous pathologies including haemorrage and haemolytic anaemieas, and is detected with the histochemical stain Perls Prussian Blue [217]. To this end I examined splenic haemosiderin deposits in 10 week old wt and ROCK1nc male and female mice to determine if the mutant mice had an increased rate of RBC destruction. As expected, no haemosiderin could be detected in the spleens of wild-type animals, while homozygous ROCK1nc mice had significant accumulation of haemosiderin in the splenic red pulp (RP), the physiological compartment for erythrocyte removal (Figure 2.14a). Quantitation of the splenic haemosiderin deposition revealed significantly more staining in female animals than in male littermates (Figure 2.14b). I next analysed whether the appearance of haemosiderin in the ROCK1nc spleen is associated with age. As can be seen in Figure 2.15 (top panels) 4 week old female ROCK1nc mice display no accumulation of iron in the spleen while at 25 weeks haemosiderin is not only visible in the red pulp but positive cells are also visible within the white pulp (WP) (Figure 2.15, black arrows). The appearance of haemosiderin in the WP indicates the presence of highly invasive phagocyte that is engulfing large numbers of erythrocytes in the splenic red pulp before migrating into the white pulp. This is possibly the result of an on-going inflammatory response in which erythrocytes are inappropriately phagocytosed by inflammatory macrophages activated by secondarily necrotic cells. To ascertain the identity of these cells I stained fixed splenic sections with antibodies against F4/80, a transmembrane protein expressed on mouse macrophages. Given the importance of macrophages in erythrocyte phagocytosis they are known to be abundant in the splenic red pulp, this was confirmed in both wt and ROCK1nc animals (data not shown and Figure 2.15, middle panels). However, by 25 weeks ROCK1nc spleens show an accumulation of invasive macrophages in the white pulp that is not seen in younger or wild-type animals (Figure 2.15, middle panel, black arrows). This invasive population of macrophages appears to co-localize with WP haemosiderin. Preliminary observations also suggest that these invasive macrophages phagocytize nuclear material and thus are engulfing not just erythrocytes, but other nucleated cells as well (data not shown). Finally, heamatoxilyn and eosin staining demonstrates that the WP in 25 week ROCK1nc animals has a reduced cellularity compared to 4 week old animals (Figure 2.15, bottom panels). Collectively these observations are consistent with the haematology data and

suggest that ROCK1nc mice have an increased rate of erythrocyte phagocytosis. Furthermore, this increased phagocytic signature in the spleen is characterized by the presence of an invasive macrophage population that is likely engulfing more than RBCs. Moreover, the enhancement of this phenotype in female animals is highly suggestive of an auto-immune disease. The causes of increased splenic phagocytosis are unclear and may be due to autoimmune disease such as auto-immune haemolytic anaemia (AIHA) or other pro-inflammatory triggers. A large cohort of animals is ageing to investigate these possibilities.

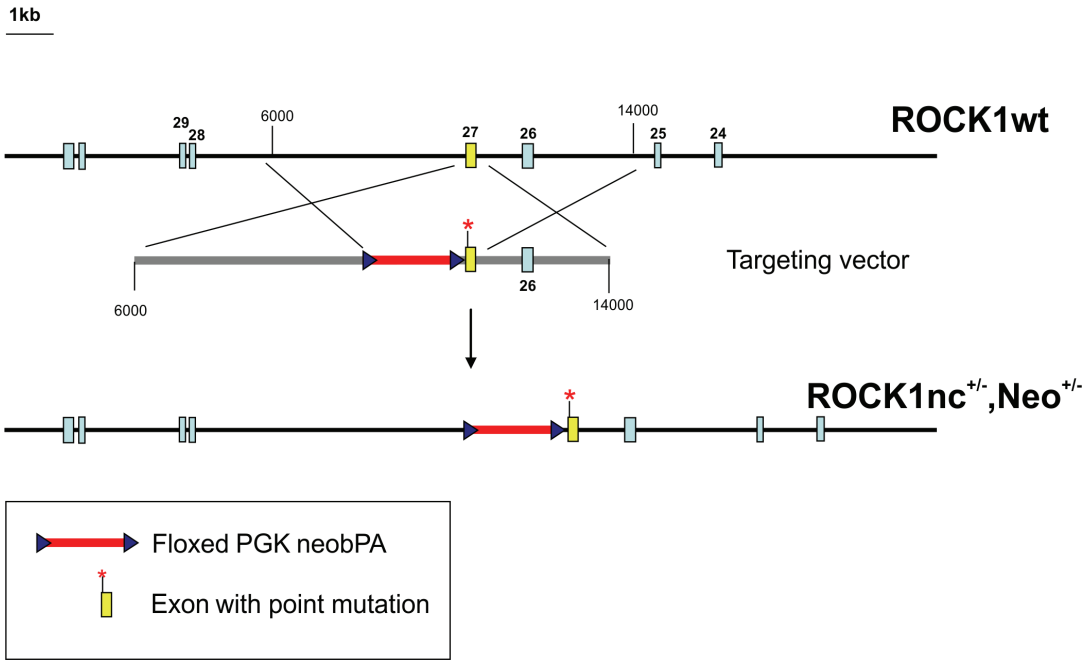

Figure 2.1. Homologous recombination targeting strategy to generate ROCK1 non-cleavable allele

Line diagram of mouse genomic ROCK1 wild type (ROCK1wt) locus with numbered ROCK1 exons indicated by blue boxes (top). Targeting vector homology arms to ROCK1 wildtype locus is indicated by black crosses. Targeting vector contains mutations 3338A>C and 3339T>A in ROCK1 exon 27 (yellow box, indicated by asterisk) and a neomycin (neo) selection cassette in red flanked by LoxP sequences (blue triangles). Targeting vector is transfected into mouse embryonic stem cells that are then selected for stable vector insertion with neomycin. After homologous recombination the expected mutant ROCK1 non-cleavable (ROCK1nc) genomic locus is shown on bottom.

a

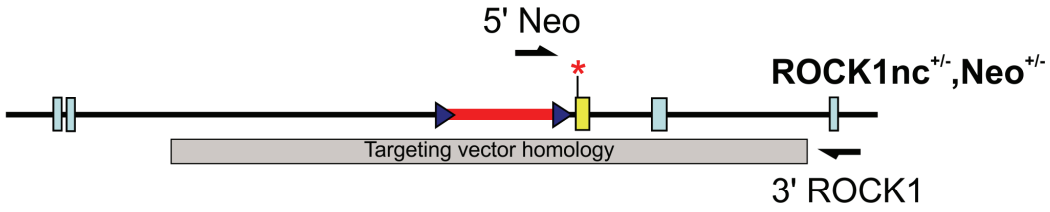

Predicted Screening Products

Screening Primers	ROCK1 wt (kb)	ROCK1 nc (kb)
5' Neo / 3' ROCK1	-	3.5

b

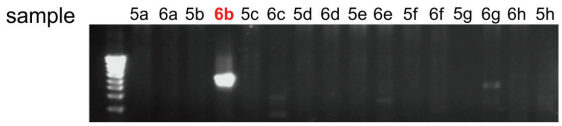

c

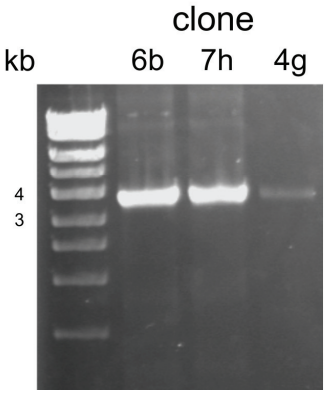

Figure 2.2. 3' homologous recombination screening strategy and results
(a) Line diagram of PCR screening strategy of genomic DNA from neomycin resistant mouse embryonic stem cells (mES). 5' PCR primer is indicated with black arrow and is within the Neo cassette, 3' primer is outwith the targeting vector homology arm. These primers should generate a 3.5 kb PCR reaction product from mES cells with correct 3' recombination, while no product should be evident from wildtype ROCK1 or incorrect targeting vector insertion (in table). (b) Representative agarose gel electrophoresis of PCR products from the genomic screening reactions. Each lane represents a separate reaction from individual neomycin resistant clone. PCR reaction from sample 6b (highlighted in red) yielded an expected reaction product of 3.5 kb suggesting correct 3' homologous recombination while the remainder of samples were negative. (c) Agarose gel electrophoresis of confirmatory PCR reactions from positive samples identified in initial screening reactions. Clones 6b, 7h, and 4g all confirmed positive for 3' ROCK1nc homologous recombination.

a

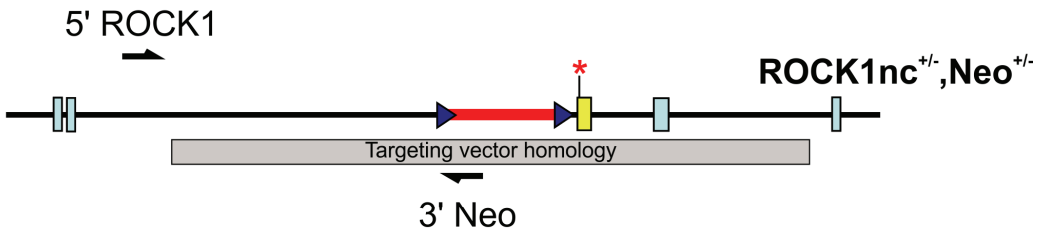

Predicted Screening Products

Screening Primers	ROCK1 wt (kb)	ROCK1 nc (kb)
5' ROCK1 / 3' Neo	-	5.5

b

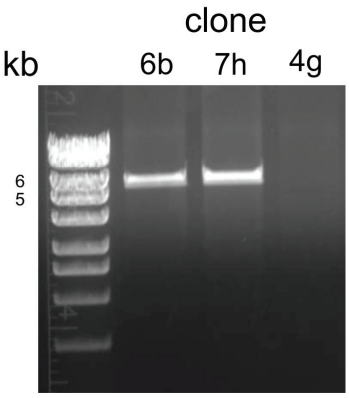

Figure 2.3. 5' homologous recombination screening strategy and results
(a) Line diagram of PCR screening strategy of genomic DNA from neomycin resistant mouse embryonic stem cells (mES). 5' PCR primer (indicated with black arrow) is outwith the targeting vector homology arm, 3' primer is within the neo selection cassette. These primers should generate a 5.5 kb PCR reaction product from mES cells with correct 5' recombination, while no product should be evident from wildtype ROCK1 or incorrect targeting vector insertion (in table). (b) Representative agarose gel electrophoresis of PCR products from samples with correct 3' homologous recombination (6b, 7h, and 4g). Samples 6b and 7h both produced a PCR product of expected size while clone 4g had no reaction product. mEs clones 6b and 7h demonstrate correct homologous recombination of the mutant ROCK1nc targeting vector.

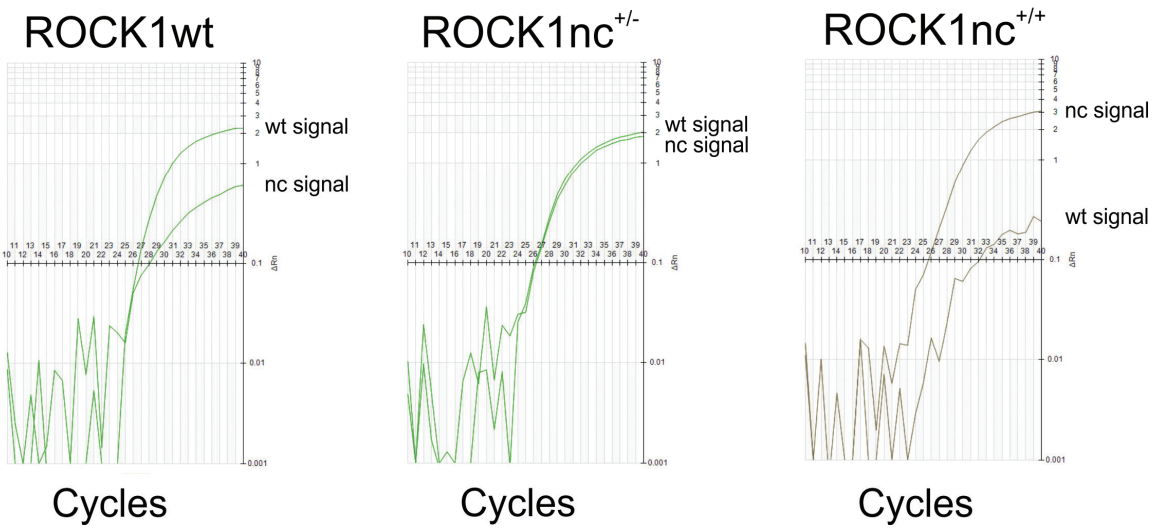

Figure 2.4. Animal genotyping using quantitative PCR
Representative traces of quantitative PCR (qPCR) reactions used to routinely genotype animals potentially bearing the mutant ROCK1 allele. ROCK1 locus spanning the 3338A>C and 3339T>A mutations was amplified in the presence of complimentary fluorescent tracers against wild type and mutant ROCK1. The resulting fluorescent signal over 40 reaction cycles determines individual animal genotype.

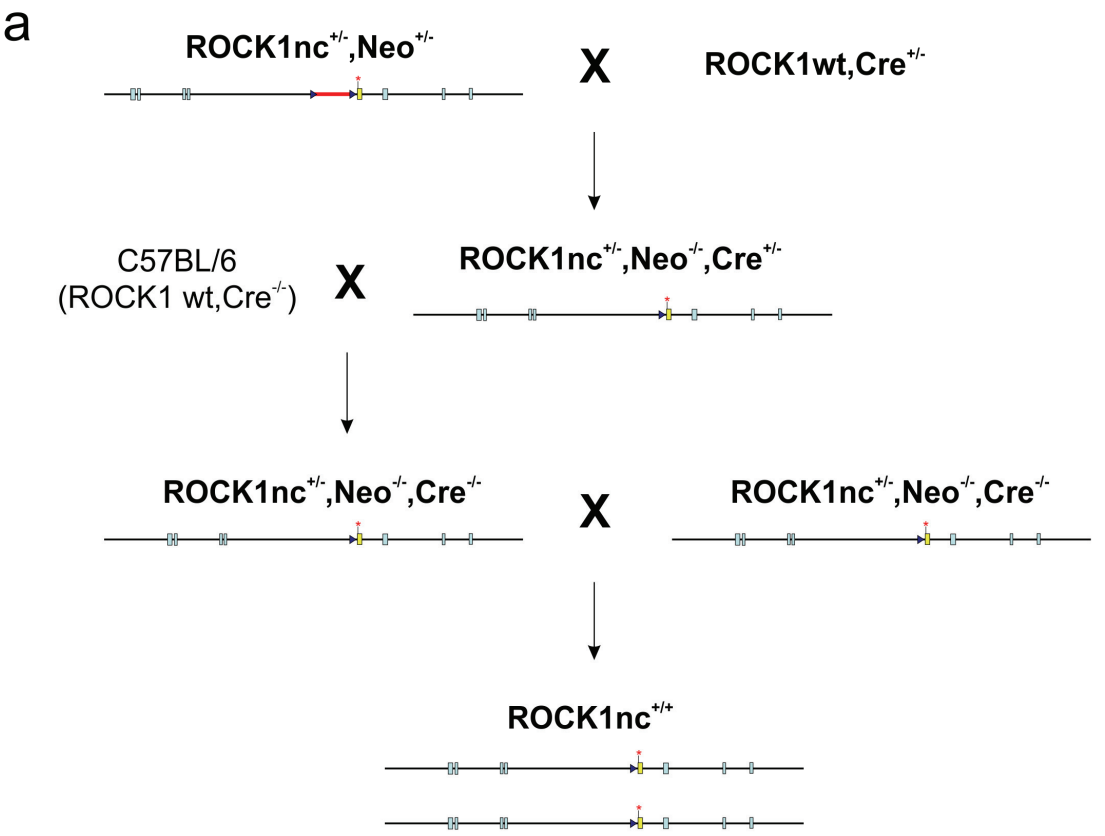

b

Heterozygous ROCK1nc$^{+/-}$ Birth Rates	
Genotype	Number of Offspring
ROCK1nc$^{-/-}$ (wt)	26
ROCK1nc$^{+/-}$	66
ROCK1nc$^{+/+}$	37

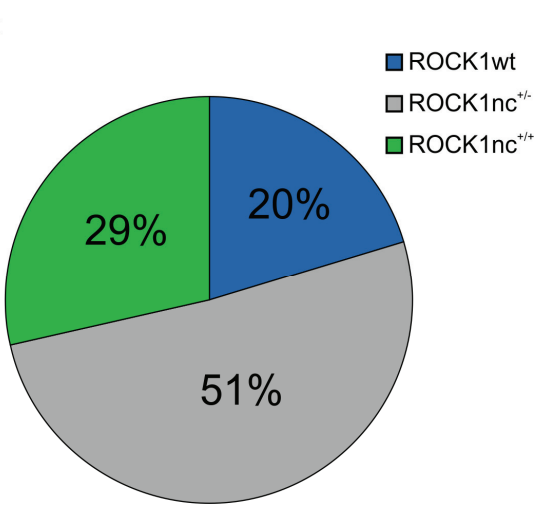

Figure 2.5. ROCK1nc breeding strategy and Mendelian ratios
(a) Genetic line diagrams indicating genetic status and animal breeding. Matings are indicted with an X, and resultant desired offspring with an arrow. (b) Summary of offspring genotypes from ROCK1nc heterozygous matings n=129 animals from 4 mating pairs. (c) Pie chart of offspring genotypes from matings in (b) with indicated percentages.

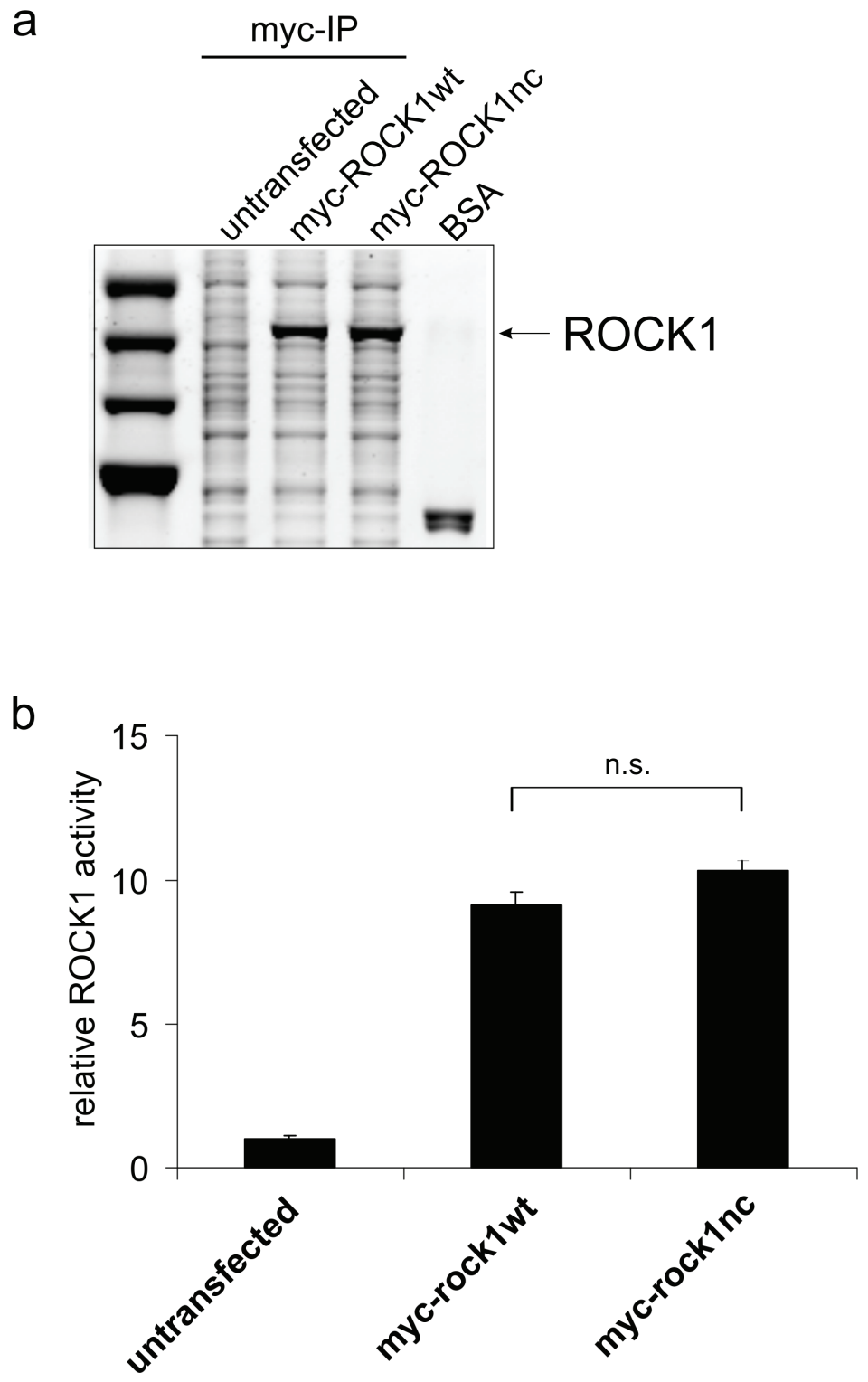

Figure 2.6. ROCK1nc function is identical to wild type kinase
(a) Representative polyacrylamide gel of immunoprecipitated (IP) myc-tagged ROCK1wt and ROCK1nc expressed in HEK-293 cells. 200 ng bovine serum albumin (BSA) ran in indicated lane and is used to estimate kinase mass used in subsequent assay. (b) Fluorescence polarization assay of 200 ng IP myc-tagged constructs. Bars represent mean +/- SEM of ROCK1 activity relative to untransfected. n=4. Figure courtesy of Nicola Rath.

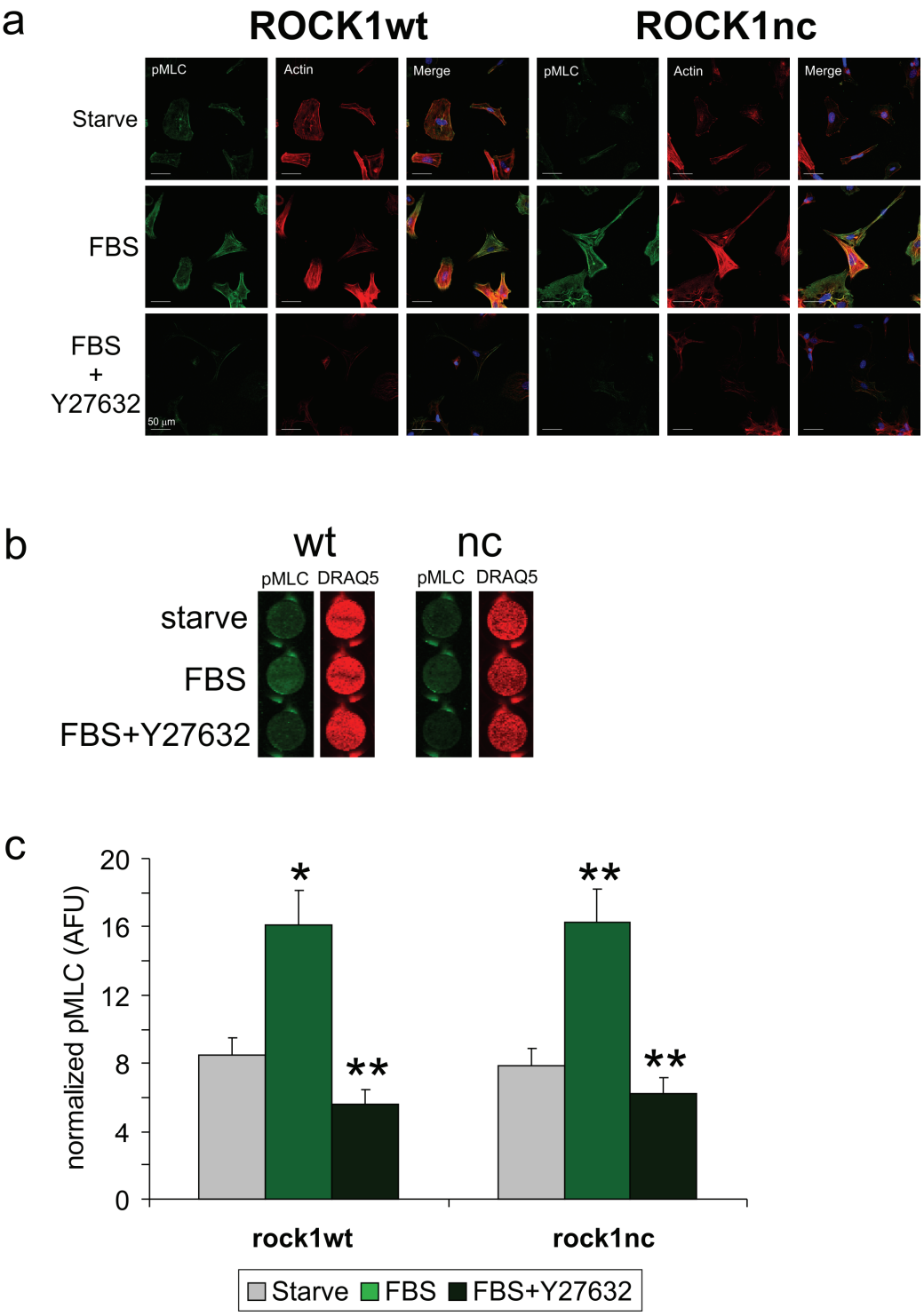

Figure 2.7. Cellular ROCK1 activity is identical in viable homozygous ROCK1wt and ROCK1nc fibroblasts

(a) Representative immunofluorescent confocal micrographs showing thr18/ser19 myosin light chain phosphorylation (pMLC) and f-actin in homozygous ROCK1wt and ROCK1nc mouse embryonic fibroblasts (MEFs). MEFs were starved overnight before treatment with 10% FBS for 5 min +/- 10 µM Y27632 then fixed and stained. Cells were incubated with Y27632 for 30 min prior to serum stimulation were appropriate. Images acquired on 40x oil objective using an Olympus FV1000 laser scanning confocal microscope. (b) Representative images of in-cell-western blot detecting pMLC (green) and cell nuclei (DRAQ5, red). MEFs were plated in 96 well plates and treated identically as in (a). Total cellular fluorescence of pMLC and DRAQ5 was captured on Odyssey scanner using infrared fluorescent secondary antibodies. (c) Quantitation of in-cell-western pMLC fluorescence normalized to cell number (DRAQ5 fluorescence). Bars represent mean ± SEM. Statistical comparison performed by ANOVA followed by Dunnetts multiple comparison test. (n=3)(*, $p<0.05$; **, $p<0.01$).

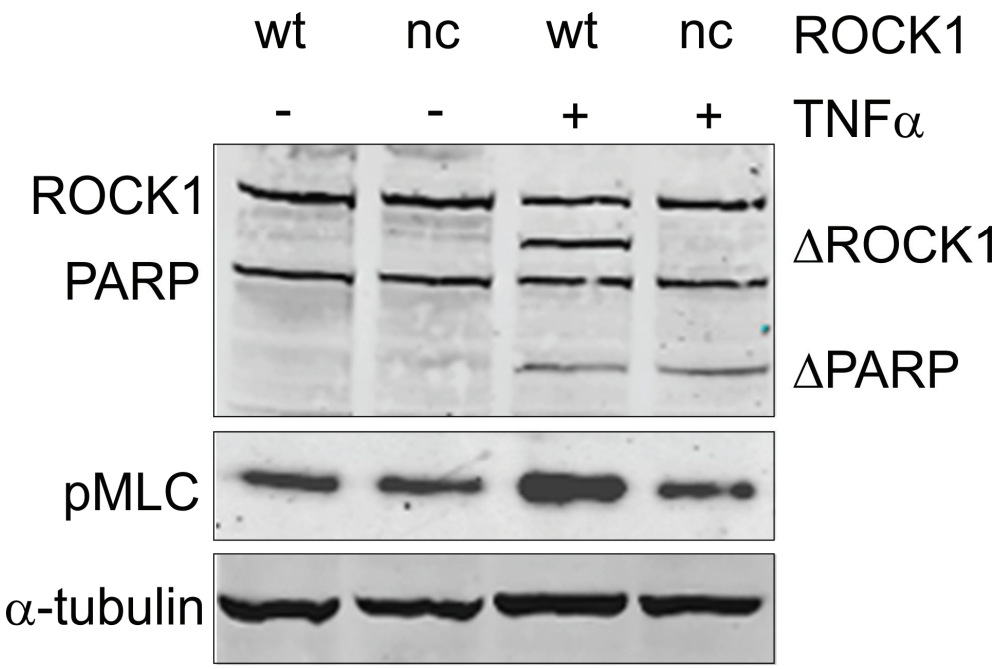

Figure 2.8. ROCK1nc is resistant to apoptotic cleavage
Representative western blot of homozygous wild type and non-cleavable MEF lysates from cells treated with and without TNFα+CHX for 4 hours as indicated. Blotting paper was probed for ROCK1, poly ADP-ribose polymerase (PARP), phosphorylated myosin light chain (pMLC), and α-tubulin. Apoptotically cleaved ROCK1 (ΔROCK1) and PARP (ΔPARP) is detected as immunoreactive lower molecular weight bands as indicated. Figure courtesy of Nicola Rath.

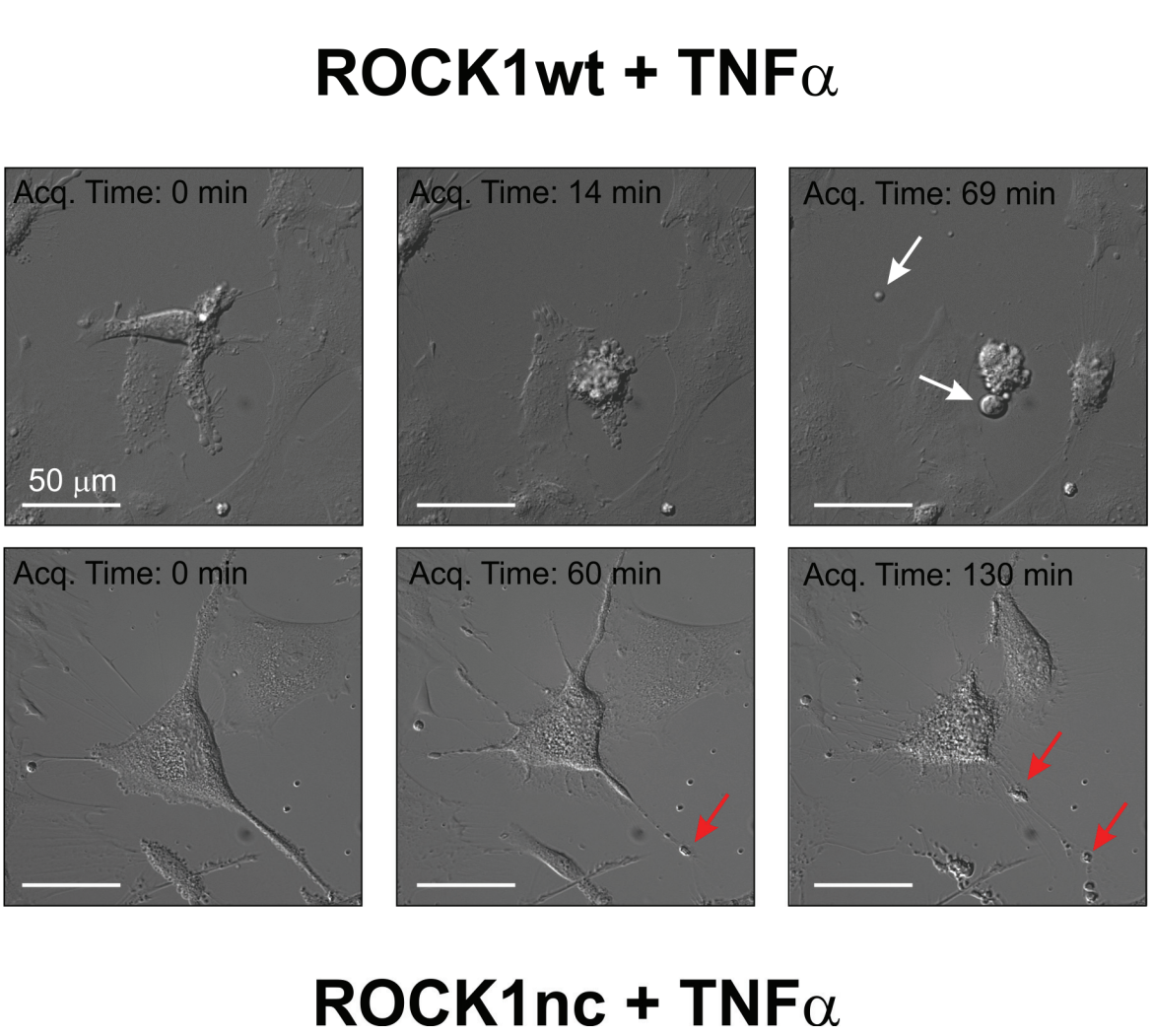

Figure 2.9. Apoptotic ROCK1nc MEFs fail to bleb
Representative time lapse images of apoptotic ROCK1wt and ROCK1nc MEFs. Following overnight starvation MEFs were treated with TNFα+CHX and then differential interference contrast (DIC) images were captured every 30-60 seconds for several hours. Discreet sub-cellular apoptotic bodies are indicated with white arrows. Cellular fragmentation due to failed contraction is indicated with red arrows. Images acquired using a 20x DIC objective lens. During microscopy cells were maintained at 37°C in 5% CO_2 atmosphere.

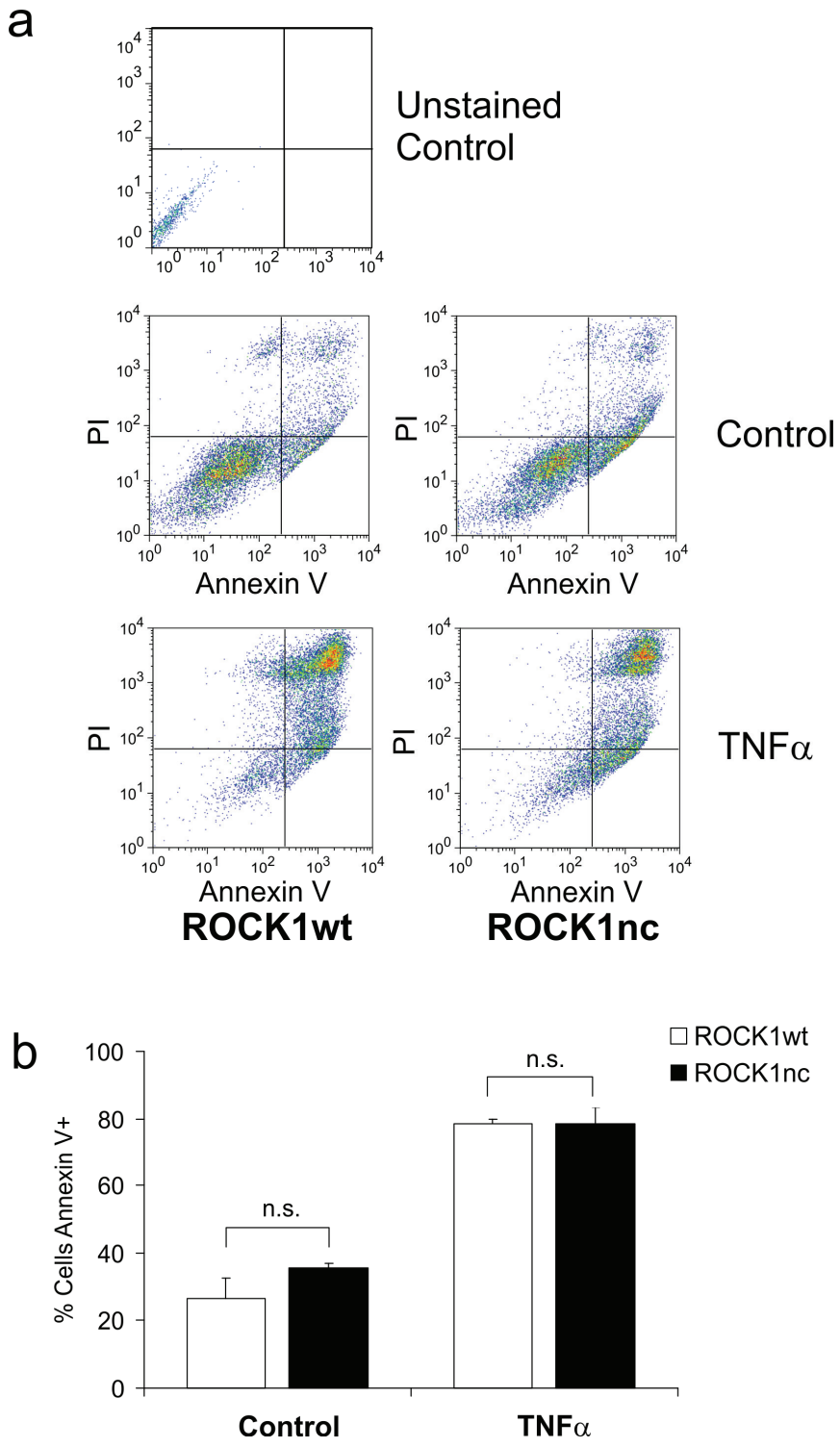

Figure 2.10. Externalization of phosphatidyl serine is not dependent on ROCK1 cleavage
(a) Representative FACS dot plots of ROCK1wt and ROCK1nc MEFs treated ± TNFα for 24 hours. Cells were collected and stained with annexin V, to detect phosphosphatidyl serine (PS) externalization, and PI to determine membrane function. (b) Quantitation of annexin V positive MEFs as in (a). Bars represent mean ± SEM of percentage of cells externalizing PS after treatment (n=3). Statistical comparison performed by t-test.

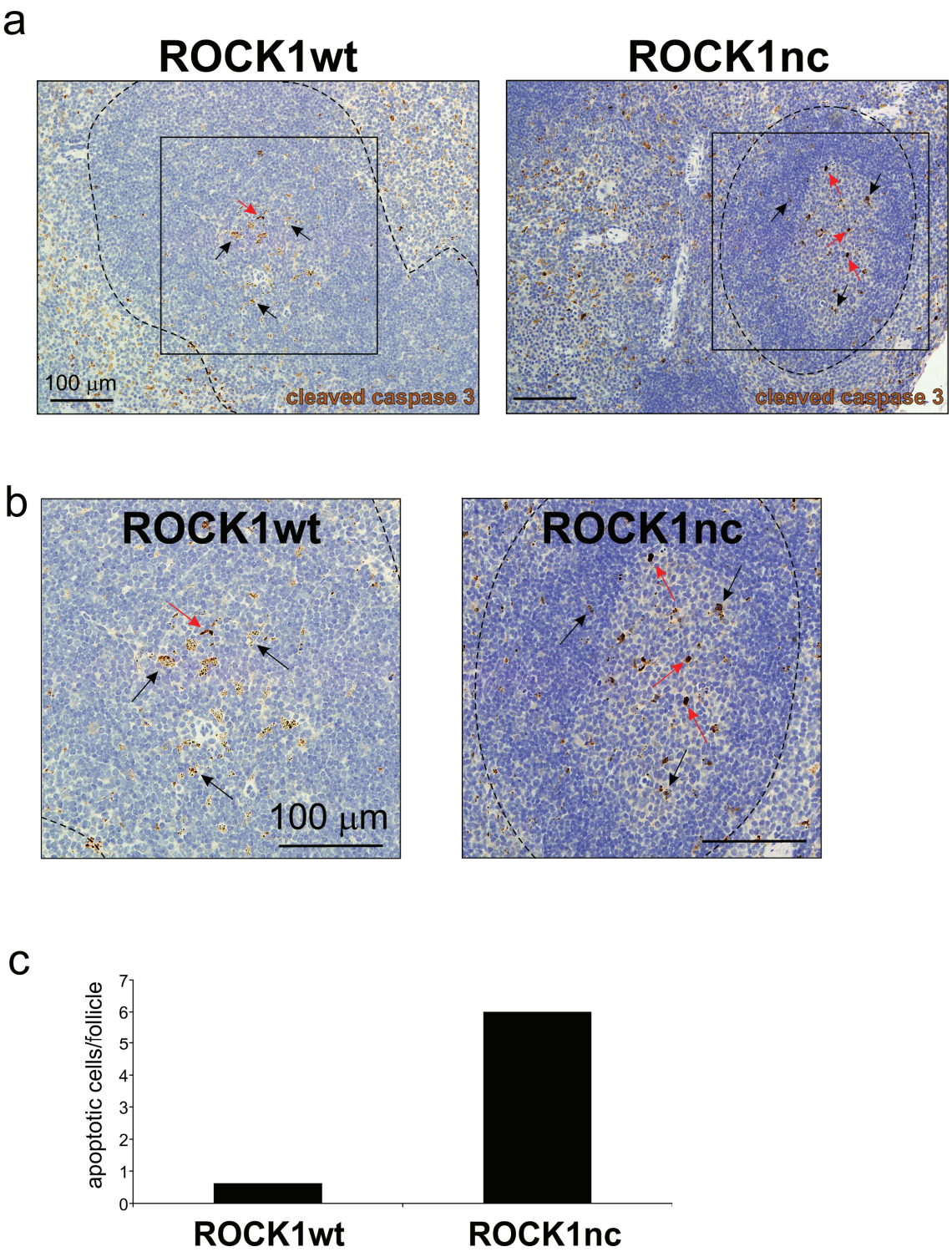

Figure 2.11. Apoptotic cell accumulation in ROCK1nc mice
(a) Representative images of formalin fixed spleens from 35 week old male ROCK1wt and ROCK1nc mice. Tissue is stained for cleaved caspase 3 (brown) and haematoxylin (blue nuclei). Lymphoid follicles outlined by dashed black line. Red arrows indicated non-fragmented apoptotic cells and black arrows indicate fragmented apoptotic cell debris which has been largely phagocytised. Bright field images acquired using a 20x objective lens on Olympus BX51 upright microscope. (b) Zoom of boxed area in (a) (c) Mean number of unfragmented apoptotic cells (cleaved caspase 3 positive) per splenic lymphoid follicle in 35 week old ROCK1wt and ROCK1nc male mice (n=1, 12-13 follicles/spleen).

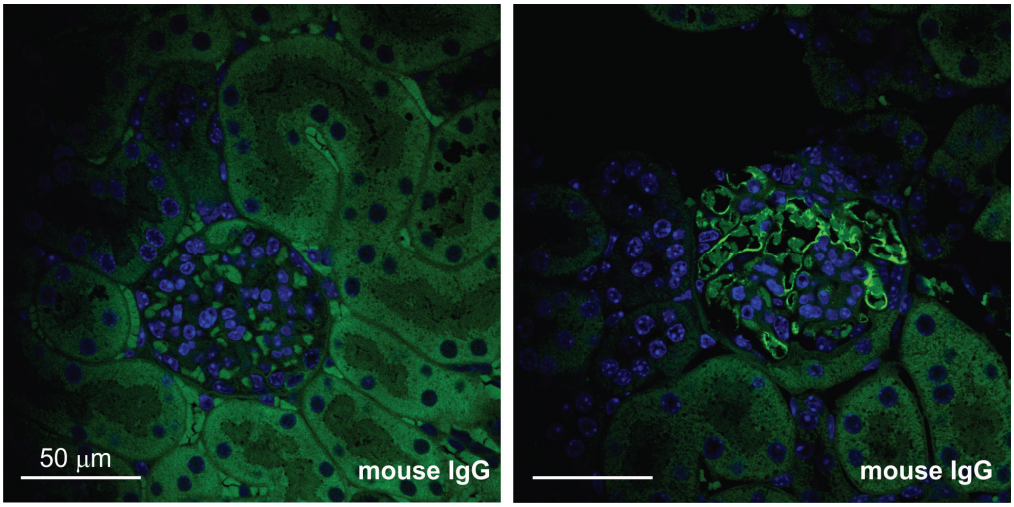

Figure 2.12. ROCK1nc mice have auto-immune kidney IgG deposition
Representative confocal micrographs of formalin fixed kidney sections from two 15 week old male ROCK1nc mice. Tissue is immunofluorescently stained for mouse IgG (green) and cell nuclei (blue). Images captured with 60x oil immersion objective with an Olympus FV1000 laser scanning confocal microscope.

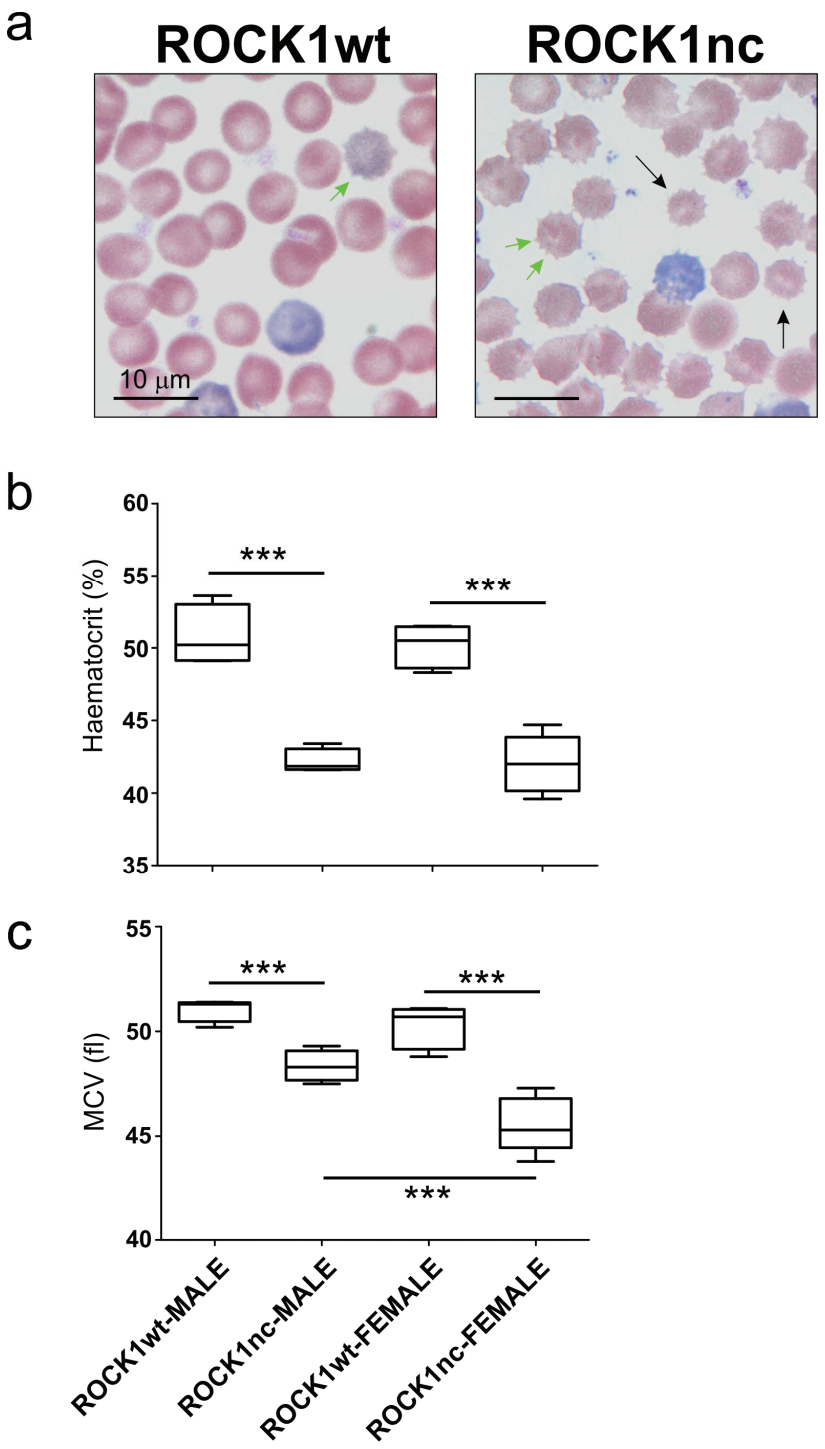

Figure 2.13. ROCK1nc mice have reduced erythrocyte volume and haematocrit
(a) Representative bright field images of giemsa stained peripheral blood smear from ROCK1wt and ROCK1nc mice. Red blood cells are stained red and reticulocytes (immature erythrocytes) blue. Black arrows indicate smaller erythrocytes. Cellular spicules are indicated with green arrows and are artefacts of sample preparation. (b) and (c) Box and whisker plots of clinical haematology results from ROCK1wt and ROCK1nc mice demonstrating reduced haematocrit and mean corpuscular volume (MCV), respectively. Statistical comparison performed by ANOVA followed by Tukey Kramer multiple comparison test (n=4-5)(***, $p<0.001$).

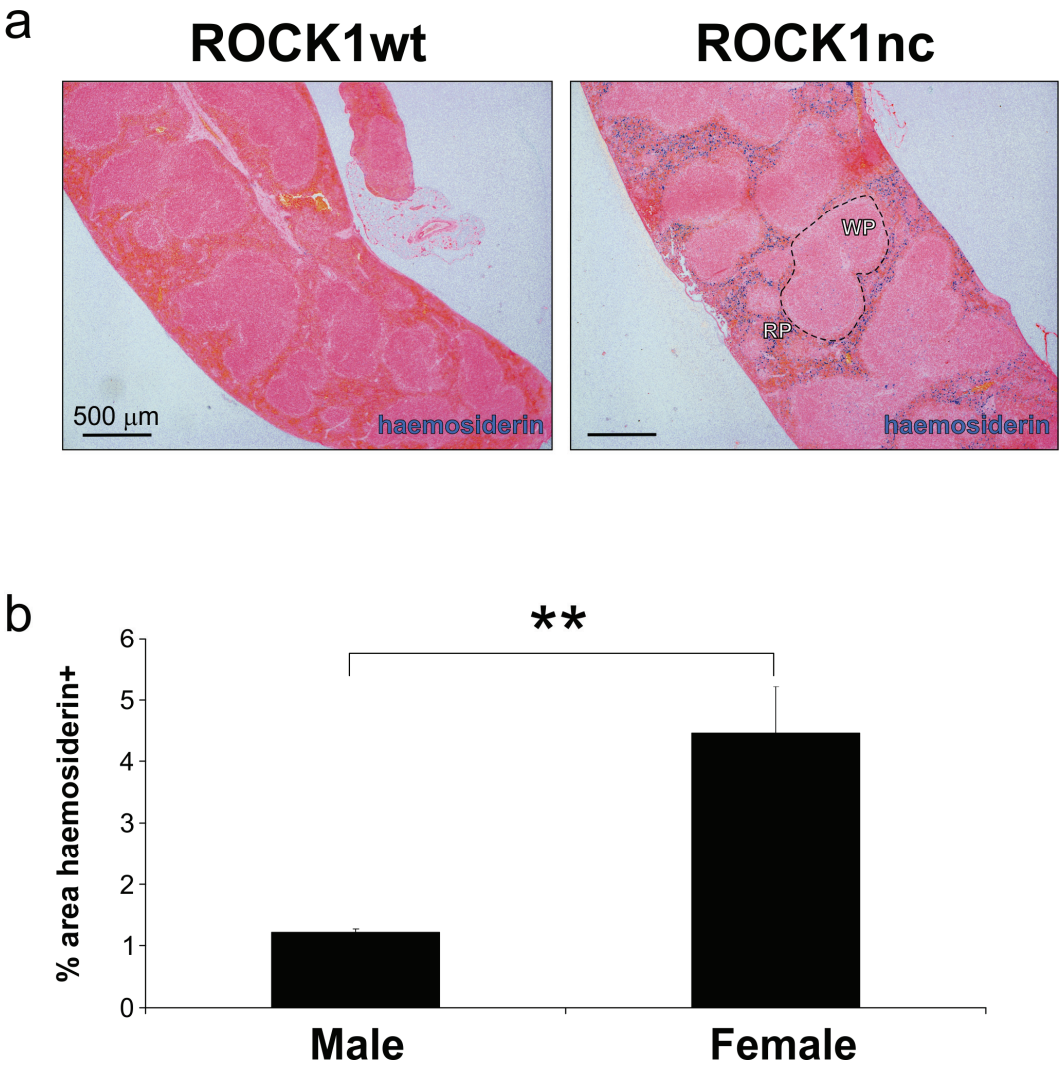

Figure 2.14. ROCK1nc mice have increased erythrocyte phagocytosis
(a) Representative images of formalin fixed spleens from 10 week old male ROCK1wt and ROCK1nc mice. Tissue is stained for haemosiderin (blue) and counter stained with eosin (pink nuclei). Lymphoid follicles outlined by dashed black line. WP indicates white pulp, RP indicates red pulp. Bright field images acquired using a 4x objective lens on Olympus BX51 upright microscope. (b) Quantitation of splenic haemosiderin deposits in spleen expressed as a percentage of splenic area. Bars represent mean $\pm$ SEM and statistical comparison performed by t-test (n=3)(**, $p<0.01$).

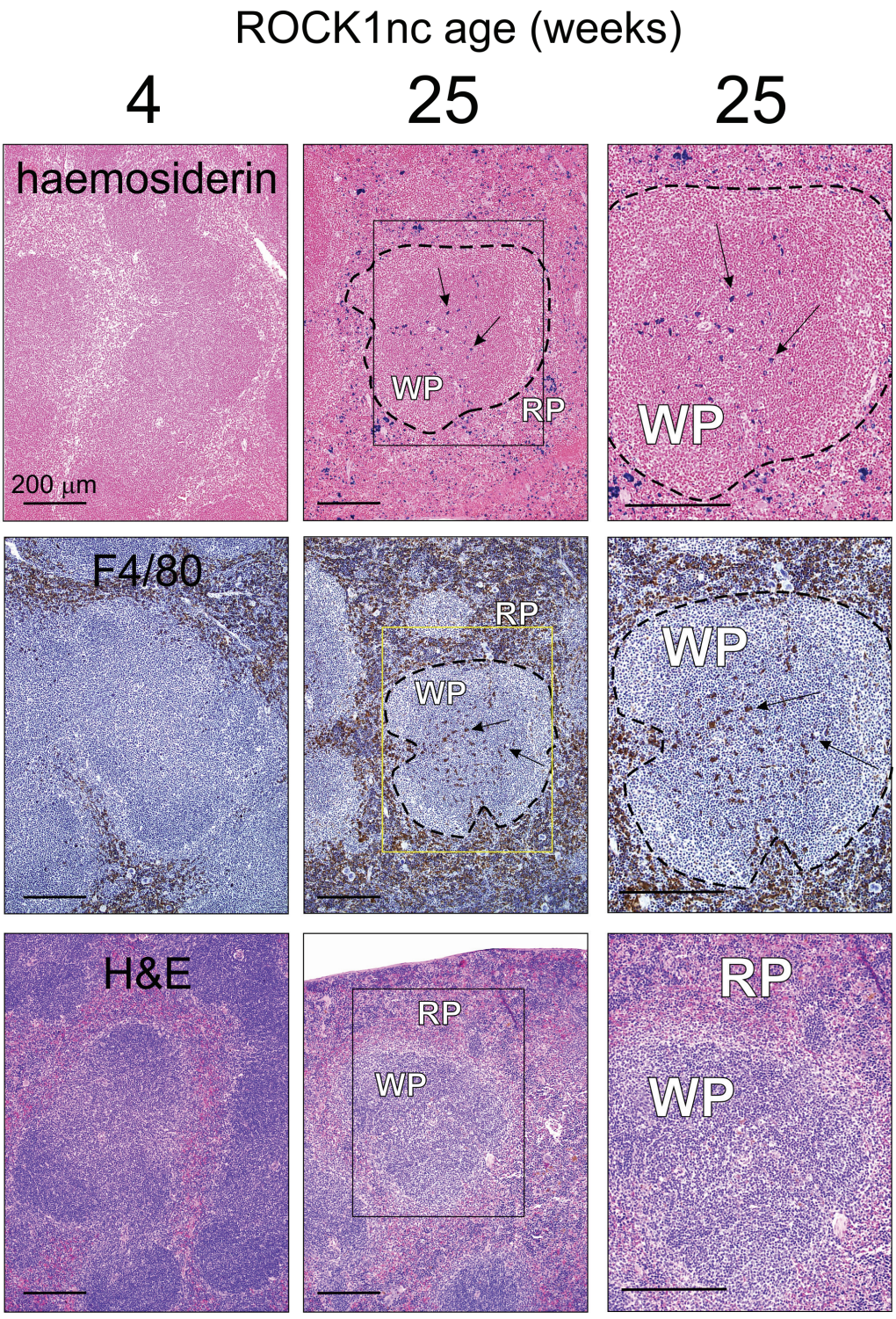

Figure 2.15. ROCK1nc mice accumulate splenic follicular haemosiderin and invasive macrophages with age

Representative images of formalin fixed spleens from 6 and 25 week old female ROCK1wt and ROCK1nc mice. Tissue is stained for haemosiderin (top panels, blue stain), macrophages (middle panels, F4/80-brown stain), and haematoxylin and eosin (bottom panels). Lymphoid follicles outlined by dashed black line. WP indicates white pulp, RP indicates red pulp. Black arrows indicate intra-follicular haemosiderin stain (top panels) and invasive macrophages (middle panel), respectively. Boxed area in middle panel shown in greater magnification in far right images. Bright field images acquired using a 10x objective lens on Olympus BX51 upright microscope.

2.3 Discussion

While there is much speculation about the role of apoptotic ROCK1 cleavage towards the clearance of dying cells there is very little clarity. These data I present conclusively demonstrate that the cleavage of ROCK1 is a necessary prerequisite for apoptotic blebbing and further suggests that these morphological changes are important for efficient efferocytosis and the maintenance of self tolerance. While a complete characterisation of the ROCK1nc phenotype has yet to be elucidated, the animals appear to be developing auto-immunity. In particular the female dominance of splenic haemosiderin deposition and the appearance of glomerular immune complexes strongly indicate the development of autoimmune disease. While the cause of erythrocyte destruction in ROCK1nc mice remains undefined, the phenotype may be caused by auto-immune haemolytic anaemia (AIHA) which is characterized by auto-antibody opsonisation of circulating erythrocytes thus targeting them for phagocytosis [218]. Interestingly, AIHA is observed in 10% of SLE patients and may be the only presenting symptom of SLE [219]. However, alternative explanations for the reduction in haematocrit and splenic iron deposition in ROCK1nc mice cannot be excluded.

In a recent paper Gabet and colleagues demonstrate that ROCK activity is necessary for the differentiation of erythrocytes [220]. They show that *in vitro* erythroblast differentiation is impaired with the ROCK antagonist Y27632 which prevents cellular condensation into uniform small cells. It was further reported that during erythroblast maturation ROCK activation is Rho independent and that the kinase is partially cleaved by activated caspase 3. The activation of caspases has been previously identified as a vital component of erythrocyte terminal differentiation and this reports suggests that ROCK cleavage may be an important physiological phenomenon associated with erythropoiesis [221]. As the spleen is an active site of erythropoiesis in adult mice it is possible that failure to cleave ROCK1 triggers a differentiation defect leading to apoptosis and phagocytosis which over time causes the haematological phenotype seen in ROCK1nc mice [222]. While interesting, these observations are limited; they demonstrate an association between ROCK1 cleavage and erythroblast maturation but fail to prove causation. In fact, a significant pool of full length ROCK1 remains in the maturing erythroblasts and the relative contribution of cleavage remains unclear. If ROCK1 cleavage was truly vital to erythropoiesis this paper would predict that ROCK1nc

mice have profound changes in the mature population of circulating erythrocytes, characterized by increased size. In fact the exact opposite is seen in homozygous ROCK1nc mice: circulating RBC are quantitatively smaller that those in wild type littermates. Moreover, the female dominant phenotype and the appearance of glomerulonephritis seen in ROCK1nc mice cannot be explained by defective erythropoiesis. Thus the collection of pathologies observed in ROCK1nc mice is better explained by the development of autoimmune disease rather than faulty erythropoiesis.

One of the outstanding issues remaining to be investigated is the effect non-blebbing apoptotic cells have on phagocytic clearance. As outlined previously apoptotic blebbing may affect multiple aspects of efferocytosis including; the externalization/localization of eat-me molecules, and cellular fragmentation that have traditionally proven very difficult to investigate. As a result the literature has an unexplained conflict; apoptotic blebbing is simultaneously important for rapid efferocytosis and the generation of auto-antibodies, two outcomes which appear opposed to one another. The generation of non-cleavable ROCK1 knock-in mice can now provide the conclusive experimental evidence to address the *in vitro* and *in vivo* importance of apoptotic blebbing. Preliminary data suggest that ROCK1 cleavage driven apoptotic blebbing is important to avoid auto-immune disease and I expect this model will provide many more valuable insights, such as the potential role of apoptosis and inflammation during tumour growth and progression.

3. ROCK mediates apoptotic cell protein release to modulate innate immune responses

3.1 Introduction

The clearance of apoptotic corpses is clearly a vital process that is largely dictated by the dying cell. As previously discussed, apoptotic cells are active participants in efferocytosis and undergo dramatic membrane changes to help facilitate recognition and phagocytosis. In addition to these modifications, apoptotic cells release chemoattractant molecules that encourage macrophages to locate the suicidal cell prior to clearance. Thus, the release of 'find-me' factors can be seen as the first critical step for efferocytosis. While research has provided a great deal of insight into the mechanisms of phagocyte engagement and engulfment of apoptotic cells, there are only a handful of apoptotic chemo-attractant signals that have been identified [223]. These come-find-me factors are composed of a wide range of molecules including: proteins (e.g. tyrosyl tRNA synthetase (TyrRS) and dimer of ribosomal protein S19 (dRP S19)), lipids (e.g. lysophosphatidylcholine (LPC) and sphingosine-1-phosphate (S1P)), or nucleotides (e.g. ATP)[62,223,224]. In addition, apoptotic micro-blebs, which are small membranous sub-cellular particles released from B-cells (the micro-bleb nomenclature is from the referenced paper, for consistency, these structures will now be referred to as micro-apoptotic bodies), have also been described as potent monocyte chemoattractants [225]. Regardless of their composition, all these factors are soluble and diffuse from apoptotic cells to encourage monocytes and macrophages to find the suicidal cell and phagocytose it. Curiously, some of these factors (e.g. TyrRS and dRP S19) are intracellular proteins and the release of such factors from apoptotic cells, with presumably intact membranes, has not been adequately characterised. These apparently conflicting observations make the search for new proteinacious apoptotic chemoattractant factors problematic as a mechanism for their release also needs to be provided.

While ROCK induced apoptotic blebbing appears to be important for macrophage recognition and engulfment the importance of blebbing and apoptotic body formation in the release of 'find-me' factors remains to be investigated. The ability of micro-apoptotic bodies, whose generation is likely ROCK dependent, to attract

monocytes suggests that ROCK may be an active participant in the release of chemoattractant factors from apoptotic cells.

3.2 Results

3.2.1 Apoptotic bodies and blebs lose membrane integrity

As discussed, apoptotic cells are presumed to have intact plasma membranes that are important in limiting the release of pro-inflammatory intracellular molecules. However, there have been several reports suggesting that apoptotic blebs can lose membrane integrity independently of the cell body [126,226]. Importantly, these cells have functional plasma membranes and thus would be regarded as early apoptotic and not secondarily necrotic despite the loss of membrane integrity in a sub-set of extruded blebs. These observations suggest a potential role for ROCK, via loss of bleb integrity, in the release of factors from apoptotic cells that may in turn impact efferocytosis.

To confirm whether apoptotic blebs lose membrane integrity, time-lapse images of apoptotic NIH 3T3 cells were acquired in the presence of propidium iodide (PI), a fluorescent membrane impermeable stain for RNA and DNA. Treatment of NIH 3T3 with TNFα and cycloheximide rapidly and uniformly induced programmed cell death with pronounced blebbing and apoptotic body formation within 3 hours (Figure 3.1). Initially, both the parental cell and newly formed blebs and apoptotic bodies have stable intact membranes as indicated by their exclusion of PI. However, within an hour of the onset of blebbing (4 hours after induction), the newly formed apoptotic bodies and blebs have the potential to rapidly lose membrane integrity and take up PI, this process can occur while still tethered to the parental cell or at distance following release of free floating membrane clad bodies (Figure 3.1 arrows and Figure 3.2). The loss of membrane stability of these newly formed structures precedes the loss of integrity, and thus secondary necrosis, of the remaining cellular corpse by several hours (Figure 3.1). This observation is consistent with several previous reports which indicate that apoptotic blebs lose membrane function well in advance of the cell body [126,226,227].

In order to further quantify the loss of membrane integrity of apoptotic bodies we assessed PI staining of NIH 3T3 apoptotic bodies at 4 hours after treatment with

TNFα and cycloheximide by fluorescence activated cell sorting (FACS). At this time point, and consistent with the time-lapse microscopy data, a significant number of cells were visually executing programmed cell death (actively blebbing and generating apoptotic bodies), but were not yet secondarily necrotic (Figure 3.6a and b). FACS gating on the small (low forward scatter) (Figure 3.3a) sub-cellular debris revealed that 20% of the apoptotic bodies were positive for PI, indicating that a significant number of these sub-cellular particles had lost membrane integrity (Figure 3.3b). Treatment of the apoptotic bodies with RNaseA alone or a combination of RNaseA+DNase1 reduced PI staining to 9% and 5.5%, respectively (Figure 3.3c). The reduction in PI staining of apoptotic bodies following treatment with RNase and DNase suggests that membrane permeability is sufficient to permit nuclease diffusion. RNaseA and DNase1 were found to be 10 and 34 kDa, respectively, suggesting that apoptotic body membranes are permissive to molecules with at least these masses. (Figure 3.3d). The loss of membrane integrity in apoptotic bodies was further validated using NIH 3T3 cells expressing membrane tagged GFP (mGFP). Following induction of apoptosis in mGFP-NIH 3T3 cells, 30% of the resulting apoptotic bodies had detectable levels of GFP (Figure 3.4a). Treatment of this sample with proteinase K, a broad spectrum serine protease with a mass of 28 kDa, significantly reduced the GFP positive apoptotic bodies by 69%, indicating that the majority of detectable particles have compromised membranes (Figure 3.4b). Taken together these observations suggest that many sub-cellular particles released from apoptotic cells have significantly compromised membranes that fail to exclude molecules as large as 34 kDa.

3.2.2 ROCK activity triggers apoptotic body formation but does not affect membrane integrity

While ROCK1 is important for triggering the formation of apoptotic blebs, its role modulating membrane stability during apoptosis is less clear. Within four hours of NIH 3T3 cell exposure to TNFα, there was a significant increase in the number of apoptotic bodies (Figure 3.5). When apoptosis was initiated in the presence of the ROCK inhibitor Y27632 or the myosin ATPase antagonist blebbistatin, the formation of apoptotic bodies was significantly impaired suggesting that the formation of these sub-cellular particles is dependent upon ROCK activation of acto-myosin contractility (Figure 3.5). Further analysis of apoptotic body

permeability to PI suggests that inhibition of ROCK does not affect the percentage of particles that take up the vital dye (Figure 3.6). However, it is interesting to note that PI staining in apoptotic bodies generated in the presence of blebbistatin is 48% of the staining observed in TNFα alone (Figure 3.6). This reduction in apoptotic body PI staining might be attributed to either increased membrane stability or impaired loading of RNA/DNA in apoptotic bodies. Nonetheless, it appears that during apoptosis, ROCK activity induces blebbing and apoptotic bodies, which then lose membrane integrity via ROCK independent mechanisms.

3.2.3 ROCK antagonism does not affect time course of apoptotic cell membrane disruption

Having established that up to 20% of apoptotic bodies have permeable membranes within 4 hours of TNFα treatment, we sought to determine if the much larger apoptotic cells shared a similar level of membrane disruption and were therefore secondarily necrotic. Traditionally the analysis of apoptotic stage is determined by co-staining with annexin V and PI. Cells that are double negative are non-apoptotic, annexin positive are early apoptotic, and double positive are secondarily necrotic. This approach, while widely accepted, may overestimate the necrotic population size. FACS analysis of cells with PI positive apoptotic bodies would be scored as necrotic, while timelapse microscopic analysis would indicate otherwise (Figure 3.7a). Thus we assume necrosis only in the population of highly PI positive cells, as indicated by the gating in Figure 3.7a. We found that PI uptake in large apoptotic cells was limited to 3.7% at 4 hours and was not significantly altered by either ROCK or myosin inhibition (Figure 3.7b). This suggests that, while a high degree of apoptotic bodies lose membrane integrity, their associated parental cell bodies remain largely intact. This is consistent with time-lapse images demonstrating apoptotic body PI uptake in advance of secondary necrosis. In addition, we examined the release of HMGB1, an established pro-inflammatory cytokine released only during primary and secondary necrosis [228]. Accumulation of HMGB1 in the extracellular compartment was only detectable 24 hours after TNFα induced programmed cell death, while at 12 hours all the protein appears to be retained within the cellular corpse (Figure 3.7c). This is consistent with published reports showing delayed HMGB1 release following apoptosis and a role for the protein as a proinflammatory molecule [228]. Treatment with either Y27632 or blebbistatin did not affect HMGB1 release. Taken together the failure of Y27632

and blebbistatin to alter the rate of secondary necrosis further confirms that their activity is limited to the suppression of apoptotic body generation.

3.2.4 Apoptotic cells release intracellular proteins in a ROCK dependent manner

The loss of apoptotic body membrane integrity raises several interesting possibilities: first, the intracellular contents of these particles may be passively released and accumulate in the extracellular space; second, the suppression of apoptotic body generation by ROCK may have a significant, albeit indirect, impact on protein release. To test these possibilities, we generated apoptotic cell conditioned medium (AC-CM) at 2, 4, 12, and 24 hours following treatment with TNFα and cycloheximide with and without the addition of Y27632 or blebbistatin and assessed the samples for lactate dehydrogenase (LDH) activity. Although LDH release is commonly regarded as an indicator of cytotoxicity and cell lysis, we hypothesized that its release may also be associated with programmed cell death via passive liberation from decaying apoptotic bodies. As suspected, apoptosis led to a significant release of LDH within 2 hours that continued to accumulate through 24 hours (Figure 3.8). Interestingly, antagonism of ROCK or myosin ATPase significantly decreased apoptotic LDH release at 2 and 4 hours. However, the effectiveness of these compounds diminished over time; at 12 hours only blebbistatin is effective, and by 24 hours neither treatment altered AC-CM LDH activity (Figure 3.8). The ability of Y27632 and blebbistatin to suppress acute, but not prolonged, LDH release is best attributed to the reduction in apoptotic body numbers available for protein release and is consistent with the passive release of protein due to apoptotic body degradation during programmed cell death.

3.2.5 Proteomic analysis of AC-CM by quantitative mass spectrometry

Having established a mechanism through which intracellular protein can be released from apoptotic cells, we next sought to identify proteins that are released and whether ROCK activity, and thus blebbing, is an important factor in that release. To accomplish this, we performed a quantitative proteomic analysis using a stable isotope labeling with amino acids in cell culture (SILAC) approach. This technique relies upon labeling proteins with arginine (Arg) and lysine (Lys) residues with stable, yet heavier, carbon and nitrogen isotopes. When cells are

cultured in media supplemented with these specific amino acids, they eventually become incorporated into newly translated proteins. Importantly, this heavy amino acid incorporation does not affect the physical or biochemical properties of the proteins. After multiple cell divisions the entirety of the cell proteome will be bearing heavy Arg and Lys residues. Individual proteins, due to their increased mass, can then be easily differentiated from unlabelled or alternately labeled proteins using liquid chromatography and mass spectrometry (LC-MS). The ability to discriminate individual protein species based on SILAC label then allows multiple samples, each with a different experimental condition and label, to be simultaneously analysed and the relative abundance of individual protein species to be quantitated.

Individual populations of NIH 3T3 fibrobasts were grown in defined SILAC medium containing, light (no isotope label), medium (Lys-4, Arg-6), or heavy (Lys-8, Arg-10) amino acids (Figure 3.9). Within 5 passages more than 95% of the cellular proteins incorporated the isotope labeled amino acids (data not shown). Each population of labeled NIH 3T3 cells was assigned a specific experimental treatment: light-control (no apoptosis); medium-TNFα (apoptosis); heavy-TNFα+Y27632 (apoptosis without blebbing). After 4 hours the AC-CM was prepared as indicated in Figure 3.9 and protein fragments subjected to LC-MS. I was able to reliably identify 60 proteins in the AC-CM as listed in Table 3.1, including LDH, a protein previously found to be released from apoptotic cells. Using LDH as a cutoff for SILAC ratio ranked proteins, 77% were enriched in AC-CM (in blue) compared to medium from non-apoptotic cells (SILAC ratio: medium/light) (Table 3.1, Figure 3.10a). Furthermore, the release of proteins during apoptosis appears to be highly dependent upon ROCK. In fact, up to 70% of the proteins released during apoptosis were suppressed with the ROCK antagonist, Y27632, to varying degrees (in orange) (Table 3.2, Figure 3.10b). Taken together, these data suggest that, not only do a wide range of intracellular proteins escape from apoptotic cells, but that release was dependent upon ROCK activity.

3.2.6 Validation of SILAC data

In order to validate the SILAC results, I western blotted NIH 3T3 lysate and 4 hour AC-CM for gelsolin and actin, two of the most highly enriched proteins identified in

the SILAC screen. While NIH 3T3 AC-CM contained large amounts of actin, no full length gelsolin was seen despite a robust cellular expression (Figure 3.11a). Nonetheless, a low molecular weight protein was detected with anti-gelsolin antibodies, suggesting that gelsolin may be released from apoptotic cells in a low mass form (Figure 3.11a). This is consistent with the SILAC data as the highly enriched gelsolin signal was detected in much lower molecular weight bands than expected (Table 3.1). We confirmed that the low molecular weight band seen in AC-CM was gelsolin by siRNA knockdown (Figure 3.11a). Interestingly, gelsolin is a substrate for caspase 3 which cleaves the protein into two fragments of 48 and 40 kDa, consistent with the gelsolin fragments detected in AC-CM [229]. To verify if gelsolin was released following caspase cleavage, I induced apoptosis in the presence of the caspase inhibitor z-VAD-fmk and found no protein release (Figure 3.11a). Importantly, the knockdown of gelsolin did not affect actin release and thus was unlikely to have affected either blebbing, apoptotic body formation, or the timecourse of programmed cell death (Figure 3.11a).

Although the AC-CM was visually verified to be clear of cells and apoptotic bodies there remained a possibility of sample contamination with intact apoptotic bodies that were subsequently lysed and the intracellular protein detected, yielding a false positive artifact of protein release. To address these concerns, purified AC-CM was given an additional high speed spin and was found to still contain both cleaved gelsolin and actin, suggesting that this protein is legitimately released from apoptotic cells (Figure 3.11b).

In order to determine whether gelsolin release was dependent upon membrane blebbing, we used the selective ROCK inhibitor Y27632 or the myosin ATPase inhibitor blebbistatin to reduce actomyosin contractility and hence blebbing. Both Y27632 and blebbistatin significantly reduced cleaved gelsolin release at all time points from 4 to 24 hours, although at 12 and 24 hours the magnitude of suppression was reduced (Figure 3.12). In addition, the pattern of actin release from apoptotic cells was identical to that of gelsolin (Figure 3.12a).

3.2.7 ROCK inhibition does not affect caspase cleavage

To confirm that ROCK antagonism does not affect gelsolin cleavage, and thus its release, we examined cellular lysates of NIH 3T3 at multiple time points following

treatment with TNFα +/- Y27632. As seen in Figure 3.13 both gelsolin and ROCK1 were readily cleaved by caspase 3 in apoptotic cells within 2 hours and cleavage was nearly complete by 4 hours, this cleavage remained unaffected in the presence of Y27632.

3.2.8 Apoptotic protein release alters macrophage migration

The release of protein from apoptotic bodies and blebs raises an interesting possibility that this material may participate in directing macrophages towards a dying cell to mediate corpse clearance. To provide proof of principle that apoptotic protein release is participating in extracellular signaling events, we chose gelsolin as a particularly promising candidate protein. Not only was gelsolin the most enriched protein discovered in NIH 3T3 AC-CM but has a clear extracellular role. While generally regarded as an intracellular F-actin binding and severing protein, gelsolin is also an abundantly secreted plasma protein with the capacity to bind, and modulate lysophospholipid signaling molecules [230]. Plasma gelsolin and gelsolin fragments have high affinity binding domains for several lysophospholipids including: lysophosphatidic acid (LPA), sphingosine-1-phosphate (S1P), and platelet activating factor (PAF) [231,232]. In fact, gelsolin binding directly to PAF can dose dependently attenuate neutrophil oxidative bursts [232]. Interestingly, plasma gelsolin may be particularly important in the regulation of inflammation, as plasma gelsolin levels invariably decline prior to the development of complications in a wide array of insults including; sepsis, trauma, and rheumatoid arthritis. In addition, there is a strong correlation between declining plasma gelsolin levels and poor prognosis for survival [233-237]. Furthermore, exogenous gelsolin reduces injury and lowers mortality in animal models of sepsis, inflammation, and injury [238,239]. Although plasma gelsolin is clearly implicated as a natural suppressor of many pro-inflammatory events there has been no known mechanism for the acute regulation of extracellular gelsolin levels. These observations may provide such a mechanism. Taken together, the release of gelsolin from apoptotic cells may be an important molecule mediating extracellular macrophage migration signals. To test this possibility, we assessed murine Raw264.7 macrophage transwell migration towards 4 hour NIH 3T3 AC-CM with or without gelsolin knockdown (Figure 3.14a). Raw264.7 macrophages had a robust migratory response towards AC-CM from NIH 3T3 transfected with non-targeting siRNA (Figure 3.14b and c). The macrophage migration towards AC-CM was significantly impaired by

approximately 70% following knockdown of gelsolin suggesting that gelsolin release from the apoptotic cells is an important factor aiding macrophage homing towards dying cells (Figure 3.14b and c).

Table 3.1. Apoptotic protein release

Protein	Accession	MASCOT Score	SILAC Ratio (M:L)
Gelsolin (light)	P13020	147	3.29
Vimentin	P20152	364	2.81
Lamin-A/C (isoform C)	P48678	411	2.56
Actin, cytoplasmic 1 or/and 2	P60710	2474	1.89
Calmodulin	P62161	181	1.57
Macrophage-capping protein	Q6AYC4	273	1.55
Heterogeneous nuclear ribonucleoproteins A2/B1	A7VJC2	184	1.47
Protein disulfide-isomerase A3	P27773	399	1.44
Vinculin	Q64727	448	1.41
Ubiquitin-like modifier-activating enzyme 1	Q02053	257	1.41
Glyceraldehyde-3-phosphate dehydrogenase	P04797	191	1.39
Phosphoglycerate kinase 1	P09411	558	1.39
Elongation factor 1-alpha 1	P10126	337	1.36
Peroxiredoxin-1	P35700	744	1.36
Filamin-C	Q8VHX6	389	1.34
14-3-3 protein theta	P68254	193	1.29
Latexin	P70202	183	1.28
14-3-3 protein zeta/delta	P63101	602	1.27
Rho GDP-dissociation inhibitor 1	Q5XI73	173	1.25
Transketolase	P40142	246	1.25
Phosphatidylethanolamine-binding protein 1	P70296	342	1.25
14-3-3 protein epsilon	P62259	758	1.25
Triosephosphate isomerise	P48500	173	1.24
Rab GDP dissociation inhibitor beta	P50399	587	1.24
Peroxiredoxin-2	Q61171	325	1.24
Phosphoglycerate mutase 1	Q9DBJ1	361	1.23
6-phosphogluconate dehydrogenase, decarboxylating	Q9DCD0	311	1.23
Aldose reductase	P45376	209	1.21
Malate dehydrogenase, cytoplasmic	O88989	147	1.20
Filamin-A	Q8BTM8	735	1.19
Importin subunit beta-1	P52296	128	1.18
14-3-3 protein gamma	P61982	478	1.18
Peptidyl-prolyl cis-trans isomerase A	P17742	1577	1.17
Nucleoside diphosphate kinase B	Q01768	230	1.17
Glutathione S-transferase A4	P24472	392	1.17
Macrophage migration inhibitory factor	P30904	127	1.17
Heat shock cognate 71 kDa protein	P63017	1464	1.14
Alpha-actinin-4	Q9QXQ0	1335	1.14
Cofilin-1	P18760	1025	1.14
Pyruvate kinase isozymes R/L	P53657	148	1.14
Aspartate aminotransferase, cytoplasmic	P05201	171	1.14
Alcohol dehydrogenase [NADP+]	Q9JII6	650	1.14
Destrin	Q7M0E3	137	1.13
Prostaglandin reductase 1	Q91YR9	265	1.13
Pyruvate kinase isozymes M1/M2	P52480	925	1.12
L-lactate dehydrogenase A chain	P06151	656	1.12
Alpha-actinin-1	Q7TPR4	808	1.11
Glutathione S-transferase Mu 1	P10649	199	1.08
Transaldolase	Q93092	196	1.08
Ubiquitin	P62976	194	1.05
Tropomyosin alpha-3 chain	Q63610	108	1.05
Malate dehydrogenase, mitochondrial	P04636	138	1.05
GTP-binding nuclear protein Ran	P62827	416	1.04
Eukaryotic initiation factor 4A-II	Q5RKI1	190	1.01
Heat shock 70 kDa protein 4	Q61316	145	0.96
Tubulin alpha-1C chain	Q6AYZ1	221	0.95
Clathrin heavy chain 1	Q68FD5	110	0.95
Glutathione S-transferase omega-1	O09131	75	0.95
Gelsolin (heavy - Cytoplasmic)	P13020	73	0.57
Collagen alpha-1(I) chain	P11087	439	0.57

Table 3.2. ROCK dependent apoptotic protein release

Protein	SILAC Ratio (M:L)	SILAC Ratio (H:L)	% TNFα (H:L)/(M:L)
Malate dehydrogenase, cytoplasmic	1.20	0.59	49
Calmodulin	1.57	0.81	51
Rho GDP-dissociation inhibitor 1	1.25	0.65	52
Latexin	1.28	0.73	57
Glutathione S-transferase A4	1.17	0.70	59
Phosphoglycerate mutase 1	1.23	0.76	62
Heterogeneous nuclear ribonucleoproteins A2/B1	1.47	0.91	62
Phosphoglycerate kinase 1	1.39	0.87	62
Gelsolin (light)	3.29	2.07	63
Aldose reductase	1.21	0.78	65
Phosphatidylethanolamine-binding protein 1	1.25	0.81	65
Peptidyl-prolyl cis-trans isomerase A	1.17	0.76	65
Macrophage migration inhibitory factor	1.17	0.76	65
Alpha-actinin-4	1.14	0.76	67
Protein disulfide-isomerase A3	1.44	0.96	67
Vinculin	1.41	0.95	67
Peroxiredoxin-1	1.36	0.91	67
Rab GDP dissociation inhibitor beta	1.24	0.86	69
14-3-3 protein zeta/delta	1.27	0.88	69
Heat shock cognate 71 kDa protein	1.14	0.80	70
Ubiquitin-like modifier-activating enzyme 1	1.41	0.99	70
Prostaglandin reductase 1	1.13	0.80	71
Cofilin-1	1.14	0.83	73
Filamin-C	1.34	0.98	73
14-3-3 protein epsilon	1.25	0.91	73
Vimentin	2.81	2.09	74
Pyruvate kinase isozymes R/L	1.14	0.85	75
14-3-3 protein gamma	1.18	0.88	75
Actin, cytoplasmic 1 or/and 2	1.89	1.43	76
Triosephosphate isomerase	1.24	0.95	76
Nucleoside diphosphate kinase B	1.17	0.91	78
L-lactate dehydrogenase A chain	1.12	0.87	78
Lamin-A/C (isoform C)	2.56	2.04	80
Peroxiredoxin-2	1.24	1.01	81
6-phosphogluconate dehydrogenase, decarboxylating	1.23	1.02	83
Alcohol dehydrogenase [NADP+]	1.14	0.95	83
Transketolase	1.25	1.06	84
Pyruvate kinase isozymes M1/M2	1.12	0.95	84
Filamin-A	1.19	1.08	91
Importin subunit beta-1	1.18	1.09	92
14-3-3 protein theta	1.29	1.24	96
Macrophage-capping protein	1.55	1.53	99
Destrin	1.13	1.15	102
Aspartate aminotransferase, cytoplasmic	1.14	1.45	128
Glyceraldehyde-3-phosphate dehydrogenase	1.39	2.16	155
Elongation factor 1-alpha 1	1.36	3.53	260

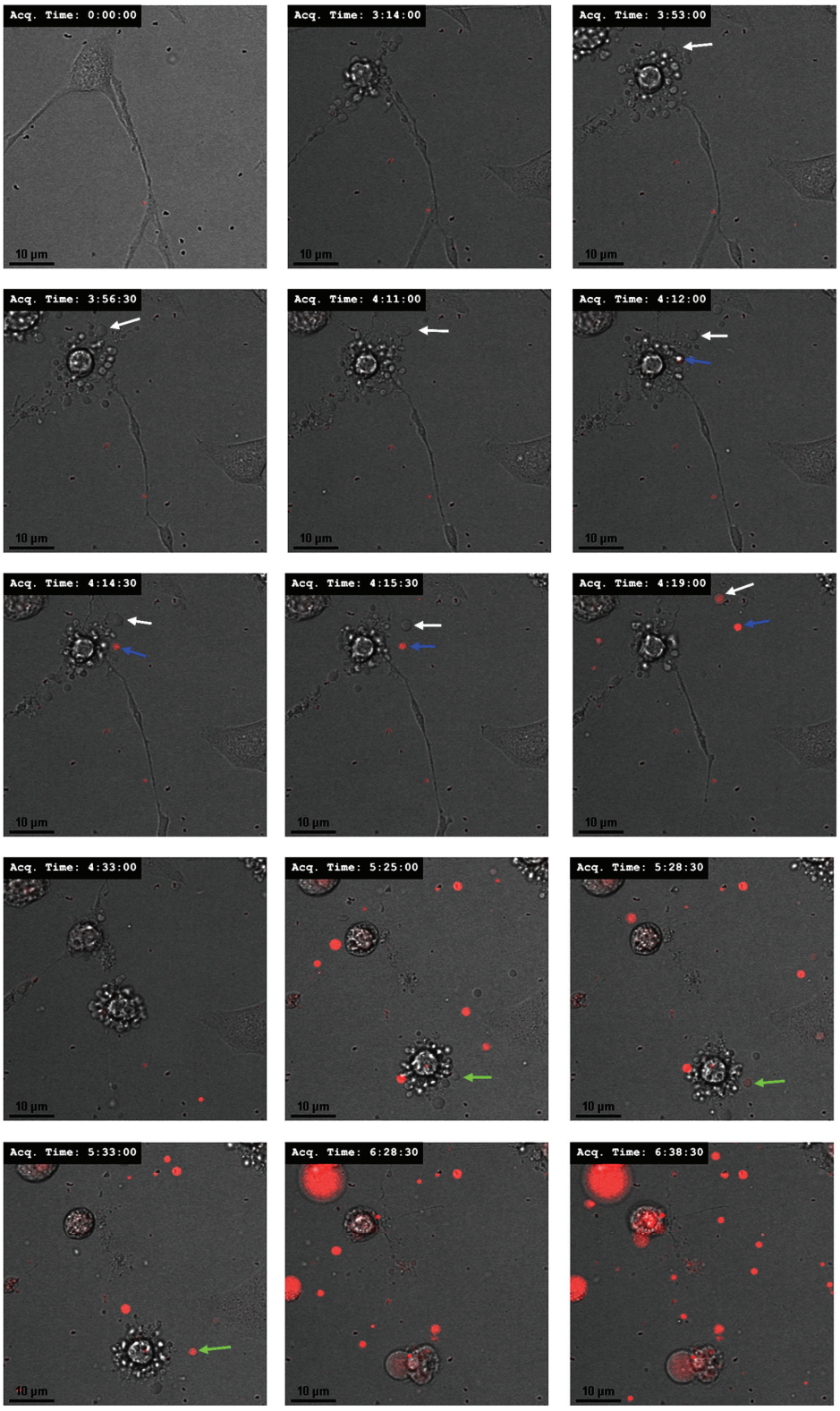

Figure 3.1. Apoptotic bodies lose membrane integrity before secondary necrosis
Confocal timelapse images of apoptotic NIH 3T3 cells demonstrating the generation of propidium iodide (red) positive apoptotic bodies. Arrows track discreet apoptotic bodies. Time index is indicated in hr:min:sec following application of TNFα.

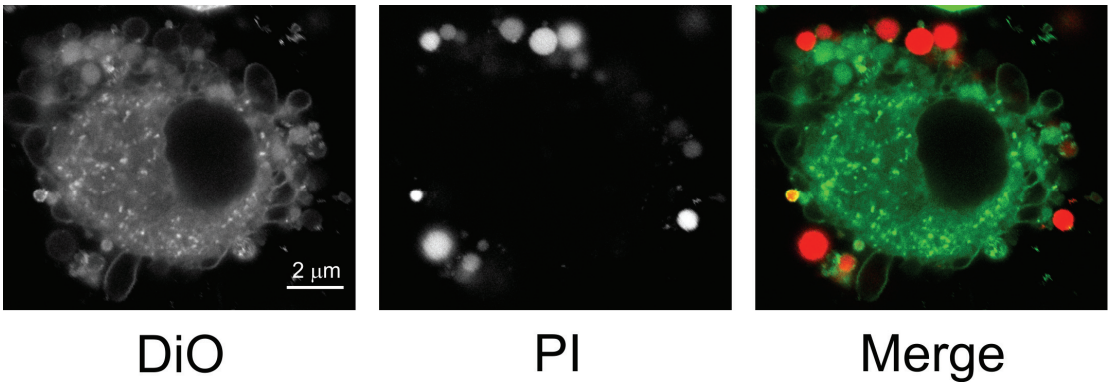

Figure 3.2. Apoptotic blebs lose membrane integrity before secondary necrosis.
Confocal images of live apoptotic NIH 3T3 cells in the presence of the fluorescent lipid stain DiO (green) and propidium iodide (PI)(red) and merge. Images acquired with a 60x oil immersion lens

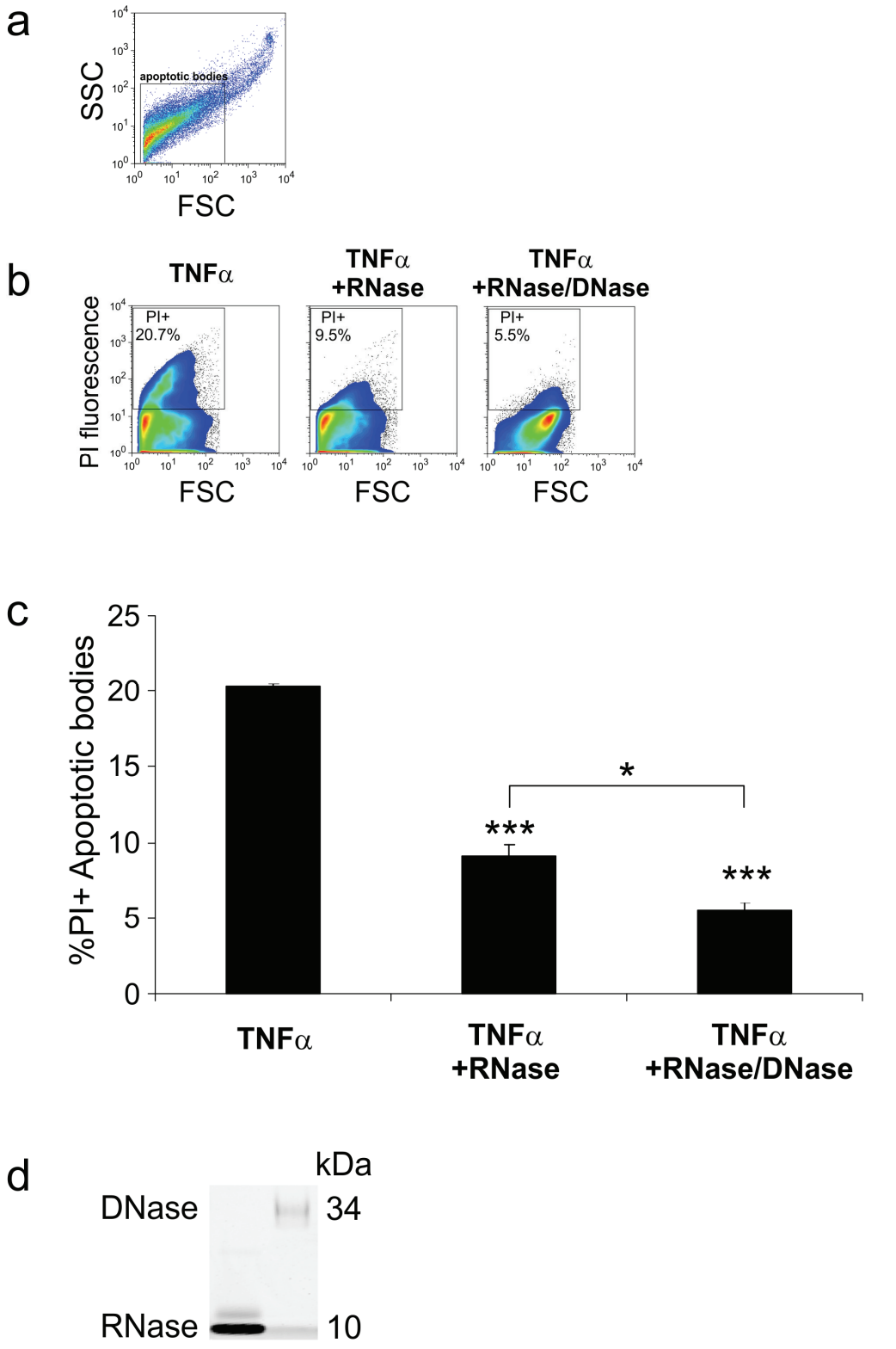

Figure 3.3. Apoptotic bodies are permeable to nucleases.
(a) Representative FACS dot plot of forward (FSC) and side (SSC) scatter of apoptotic NIH 3T3 cells at 4 hours. Gate indicates area of cellular debris containing apoptotic bodies. (b) Representative FACS plots of apoptotic bodes exposed to propidium iodide (PI) plotted versus FSC. Reduction of PI staining in apoptotic bodies treated with TNFα ± RNase or RNase+DNase as indicated. Gate indicates population and percentage of cells positive for PI stain. (c) Mean ± SEM percentage of PI positive apoptotic bodies treated with TNFα ± RNase or RNase+DNase as indicated. Statistical comparison performed by ANOVA followed by Tukey-Kramer multiple comparison test (n=3)(*, $p<0.05$; ***, $p<0.001$). (d) Coomasie stained SDS-PAGE demonstrating approximate molecular mass of commercial recombinant RNase and DNase as indicated.

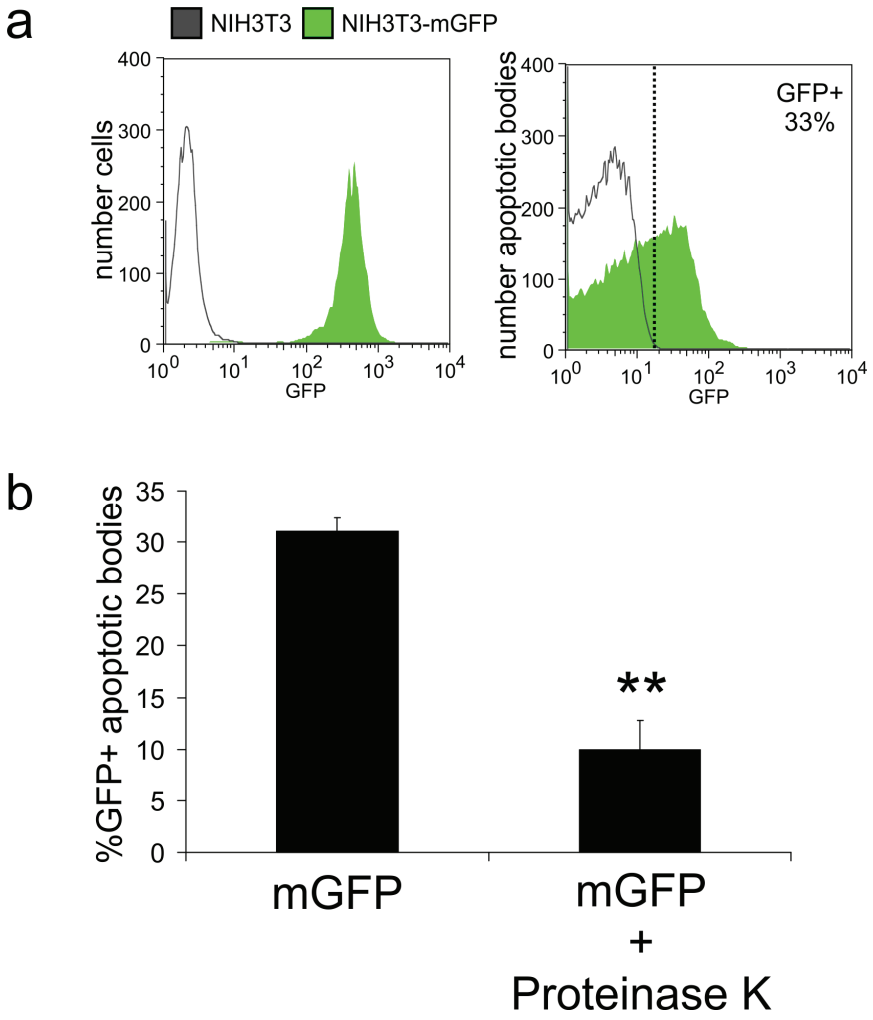

Figure 3.4. Apoptotic bodies are permeable to proteinase K.
(a) Representative FACS histogram plots of GFP fluorescence in NIH 3T3 cells transduced with CaaX box tagged GFP (left panel) and 4 hr apoptotic bodes from those cells (right panel). Cutoff indicates detectable GFP labelled apoptotic bodes. (b) Mean ± SEM of GFP positive apoptotic bodies ± 50 ug/ml proteinase K for 2 hours. Statistical comparison performed by t-test (n=3)(**, P<0.01).

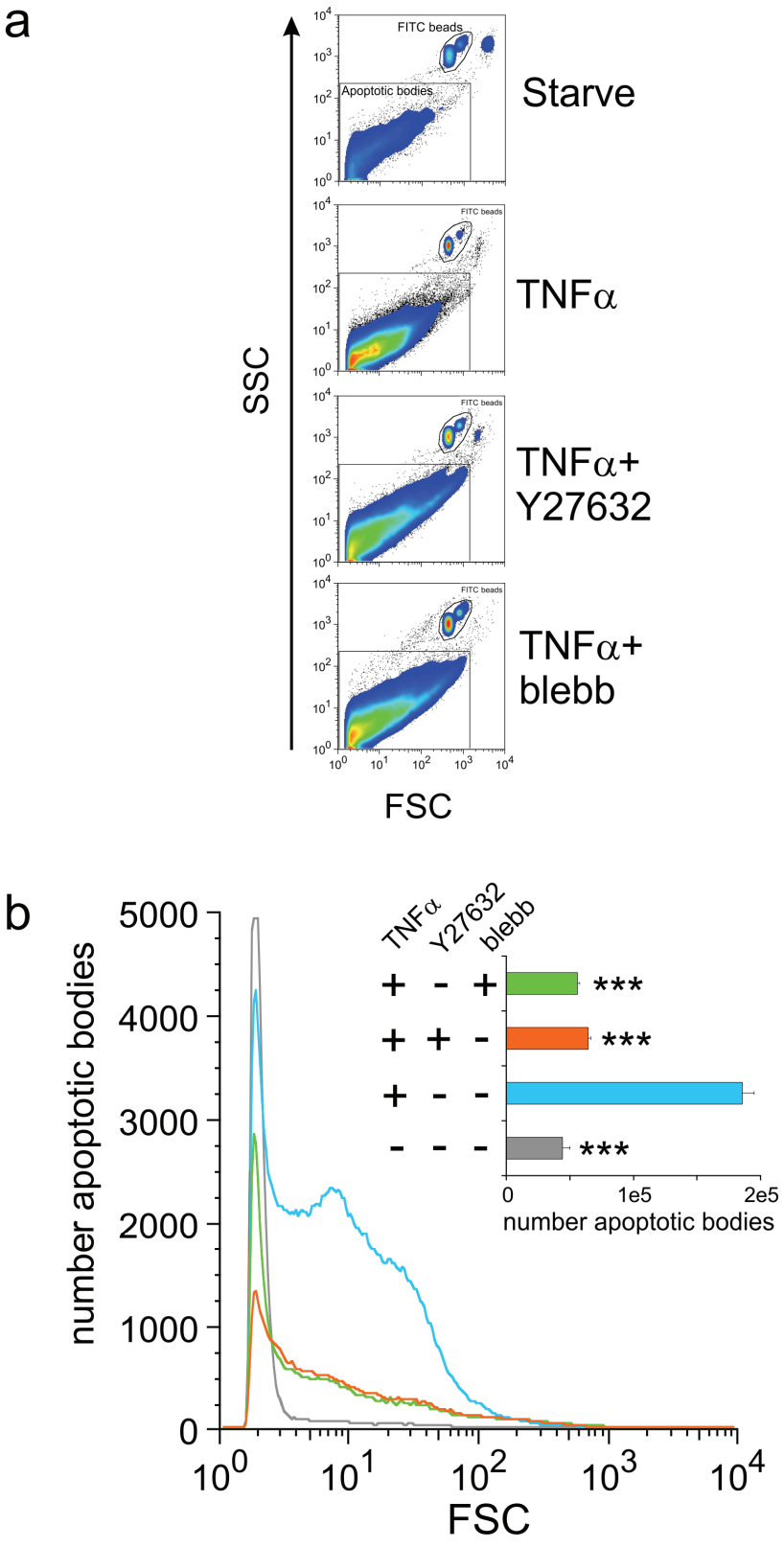

Figure 3.5. ROCK induced acto-myosin contractility induces apoptotic body formation.
(a) Representative forward (FSC) and side (SSC) scatter FACS dot plots of 4 hour apoptotic NIH 3T3 cells following indicated treatments. Gates indicate apoptotic body population and exogenous FITC labelled beads used to aid quantitation. 10 000 beads counted in each treatment. (b) Representative FACS histogram demonstrating the number of apoptotic bodies generated following treatment with TNFα ± Y27632 or blebbistatin as indicated. (inset) Mean ± SEM of apoptotic body numbers generated with indicated treatments. Statistical comparison performed by ANOVA followed by Dunnetts multiple comparison test (n=3)(***, $p<0.001$).

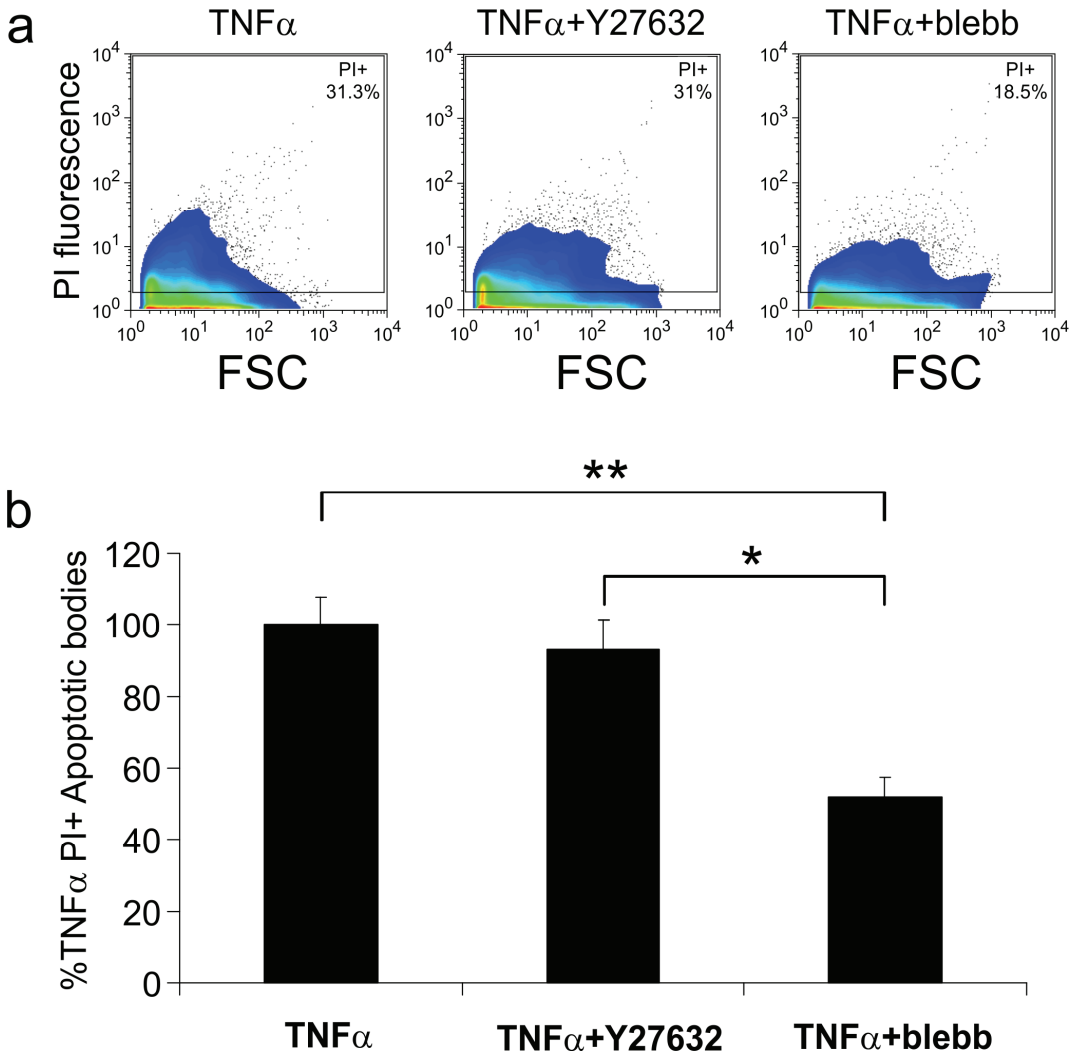

Figure 3.6. ROCK does not affect apoptotic body membrane stability.
(a) Representative FACS dot plots of 4 hour apoptotic body PI fluorescence following treatment with TNFα ± Y27632 or blebbistatin as indicated. Gate indicates apoptotic body population positive for PI. (b) Mean ± SEM of PI positive apoptotic bodies, relative to TNFα alone, following indicated treatments. Statistical comparison performed by ANOVA followed by Tukey-Kramer multiple comparison test. (n=3)(*, $p<0.05$; **, $p<0.01$)

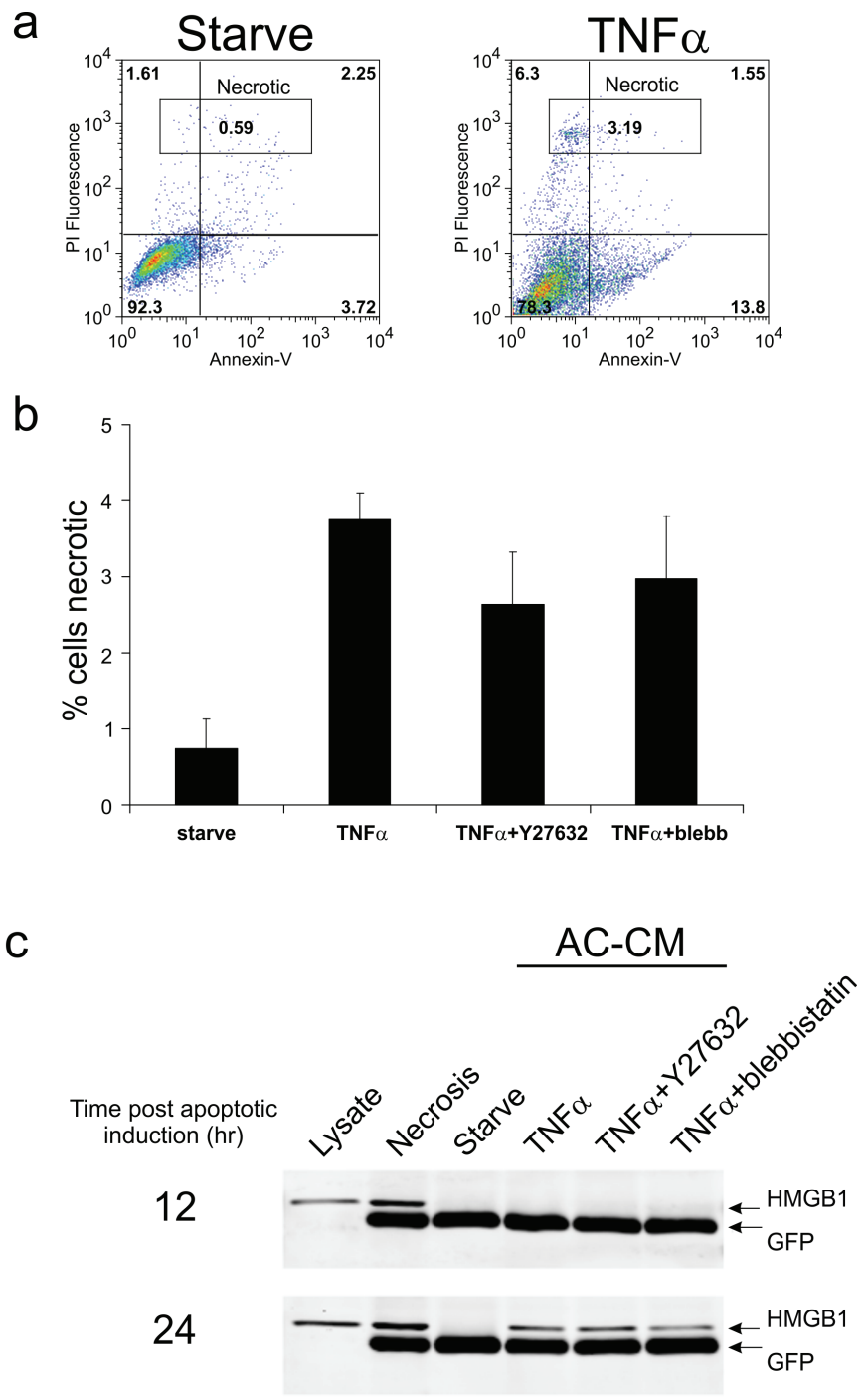

Figure 3.7. ROCK and acto-myosin contractility do not alter onset of secondary necrosis. (a) Representative FACS dot blots of 4 hour apoptotic cells stained with PI and fluorescent annexin V (AnX) following treatment with TNFα. Quadrants, with indicated population percentages, indicate classic division used to determine apoptotic stage: PI-/AnX-, non-apoptotic; PI-/AnX+, early apoptotic; PI+/AnX+, secondacrily necrotic. Quadiant indicates population of cells, with percentages, that are highly PI positive and taken as truly necrotic. (b) Mean ± SEM of percent necrotic NIH 3T3 cells following treatment with TNFα ± Y27632 or blebbistatin as indicated (n=3). No significance was detected by ANOVA between TNFα treated groups. (c) Representative western blot of SDS-PAGE 12 and 24 hour NIH 3T3 whole cell lysate, freeze-thaw necrosis lysate, starvation supernatant, and concentrated apoptotic cell conditioned medium (AC-CM) ± Y27632 or blebbistatin as indicated probed with anti-HMGB1 antibody. Cellular samples were prepared using centrifugal concentrators with 10 kDa cutoff and were normalized to exogenous GFP addition prior to concentrating sample. Bands corresponding to HMGB1 and GFP are indicated

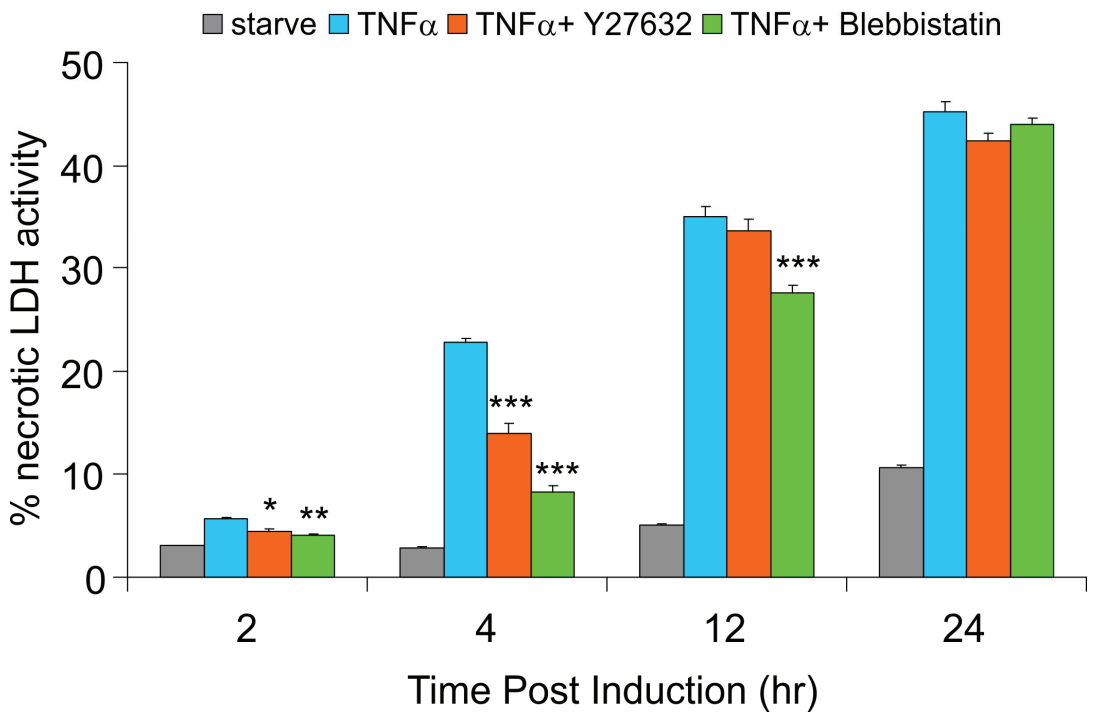

Figure 3.8. Acto-myosin dependent release of lactate dehydrogenase from apoptotic cells
Mean ± SEM of lactate dehydrogenase (LDH) activity in NIH 3T3 apoptotic cell conditioned medium at indicated times treated with TNFα ± Y27632 or blebbistatin. AC-CM was concentrated and normalized to exogenous GFP. Sample activity is normalized as a percent of LDH activity detected in freeze-thaw necrosis sample at each time point. Statistical comparison performed by ANOVA followed by Dunnetts multiple comparison test versus TNFα alone at each time point (n=3) (*, $p<0.05$; **, $p<0.01$; ***, $p<0.001$).

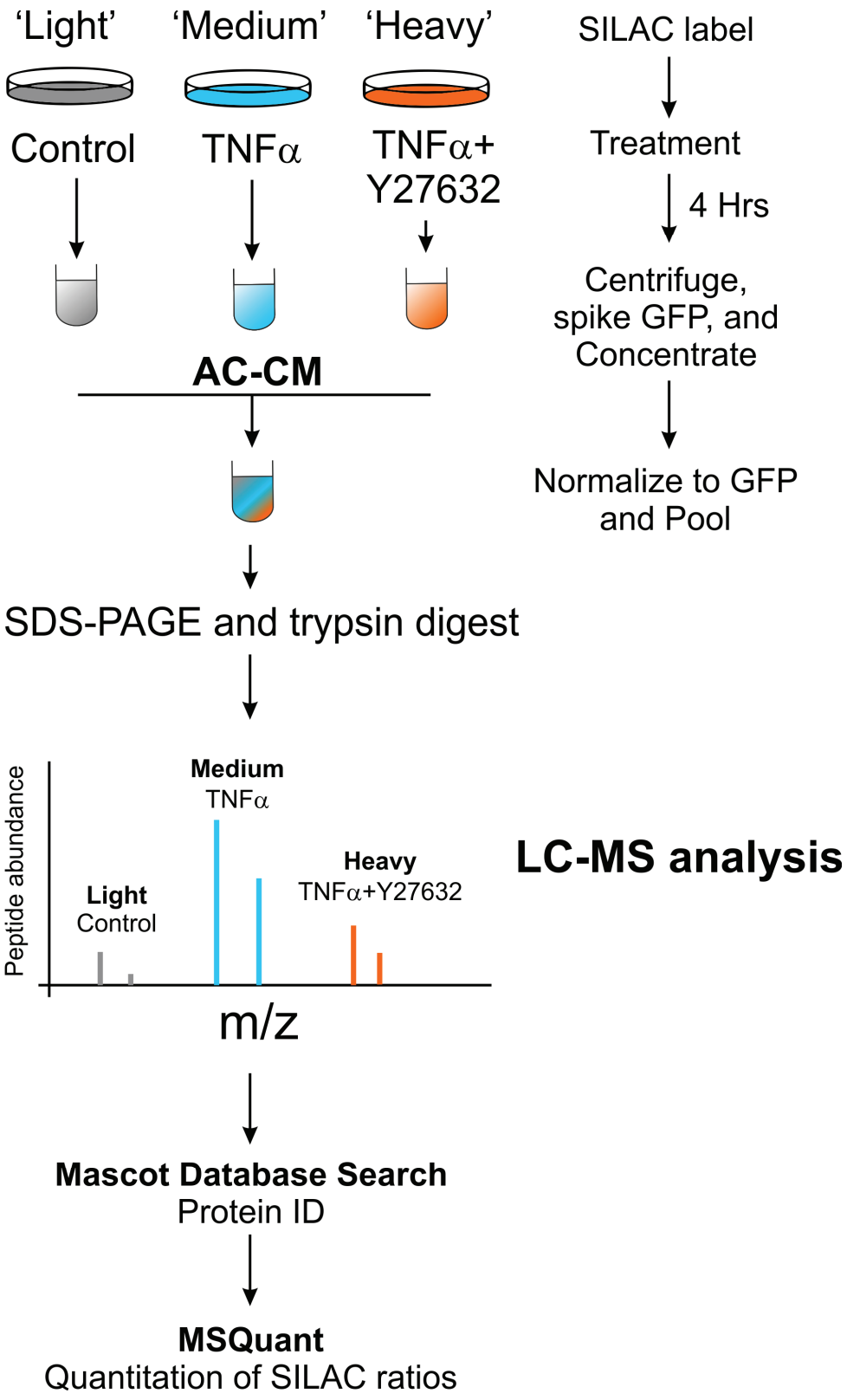

Figure 3.9. Experimental flow chart for quantitative SILAC mass spectrometry. AC-CM, apoptotic cell conditioned medium. LC-MS, liquid chromatography and mass spectrometry.

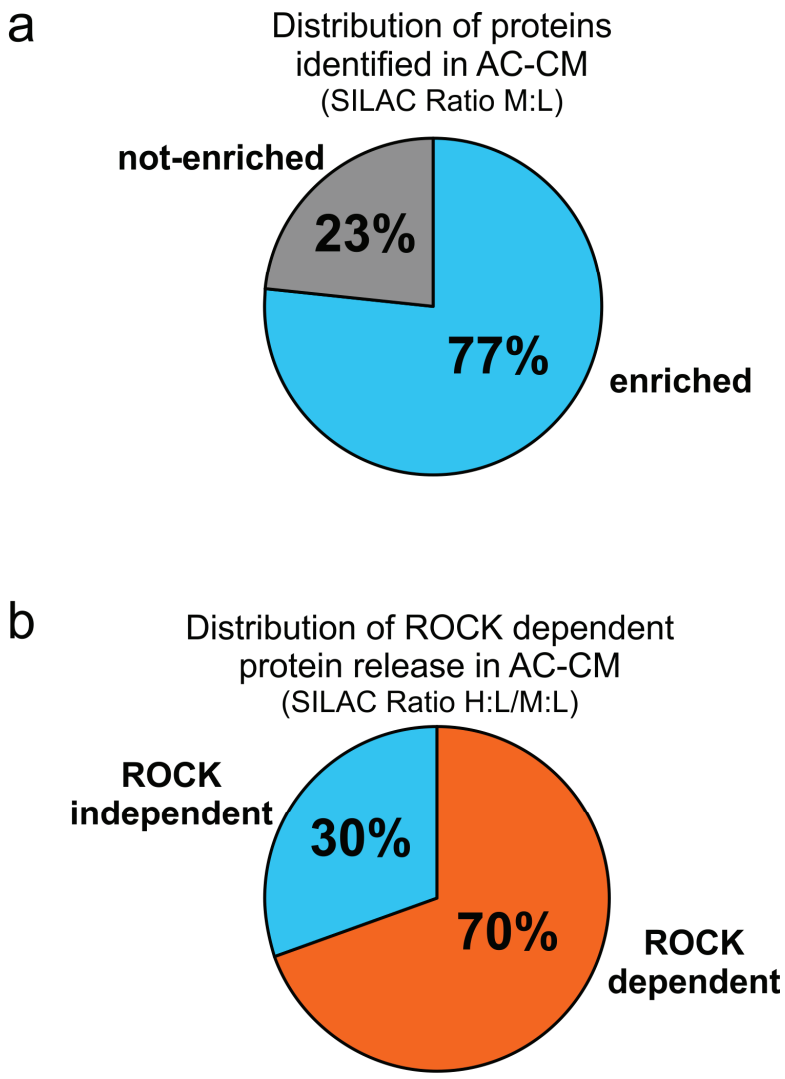

Figure 3.10. ROCK catalyses release of many proteins during apoptosis
(a) Pie chart illustrating percentage of proteins identified by SILAC in 4 hr NIH 3T3 AC-CM that were enriched during TNFα induced apoptosis. (b) Pie chart illustrating the percentage of apoptotic released proteins that are ROCK dependent as determined by SILAC.

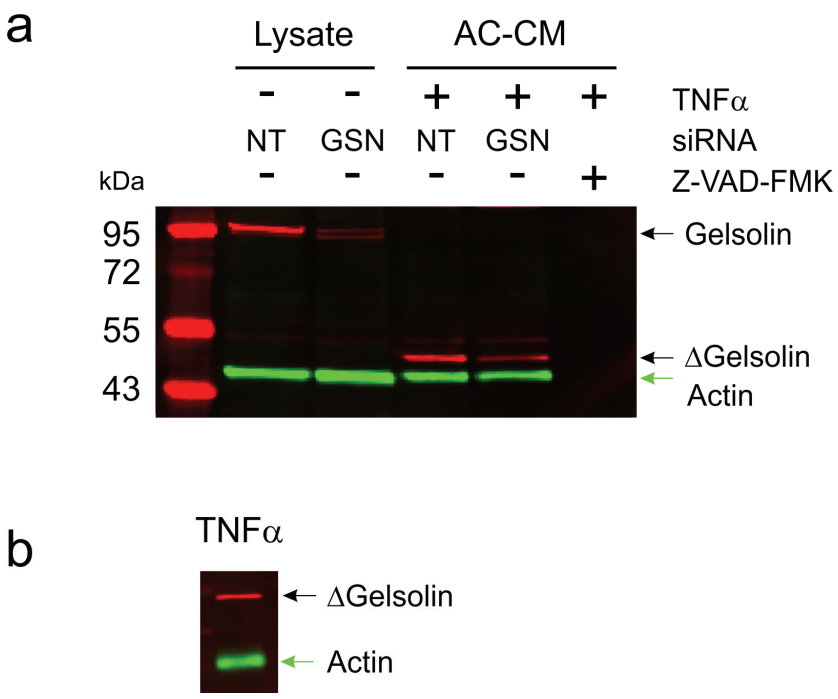

Figure 3.11. Apoptotic cells release gelsolin following caspase cleavage.
(a) Representative western blot of NIH 3T3 lysate and concentrated AC-CM probed with anti-gelsolin and anti-actin antibodies and visualized with specific fluorescent antibodies using LiCor. Cells were transfected as indicated with either non-targeting (NT) or gelsolin (GSN) siRNAs. z-VAD-fmk (20 μM) supplemented in media with TNFα. (b) Western blot of concentrated AC-CM subjected to additional high speed (16,000x g) centrifugation. Blot probed with gelsolin and actin antibodies and visualized as indicated above.

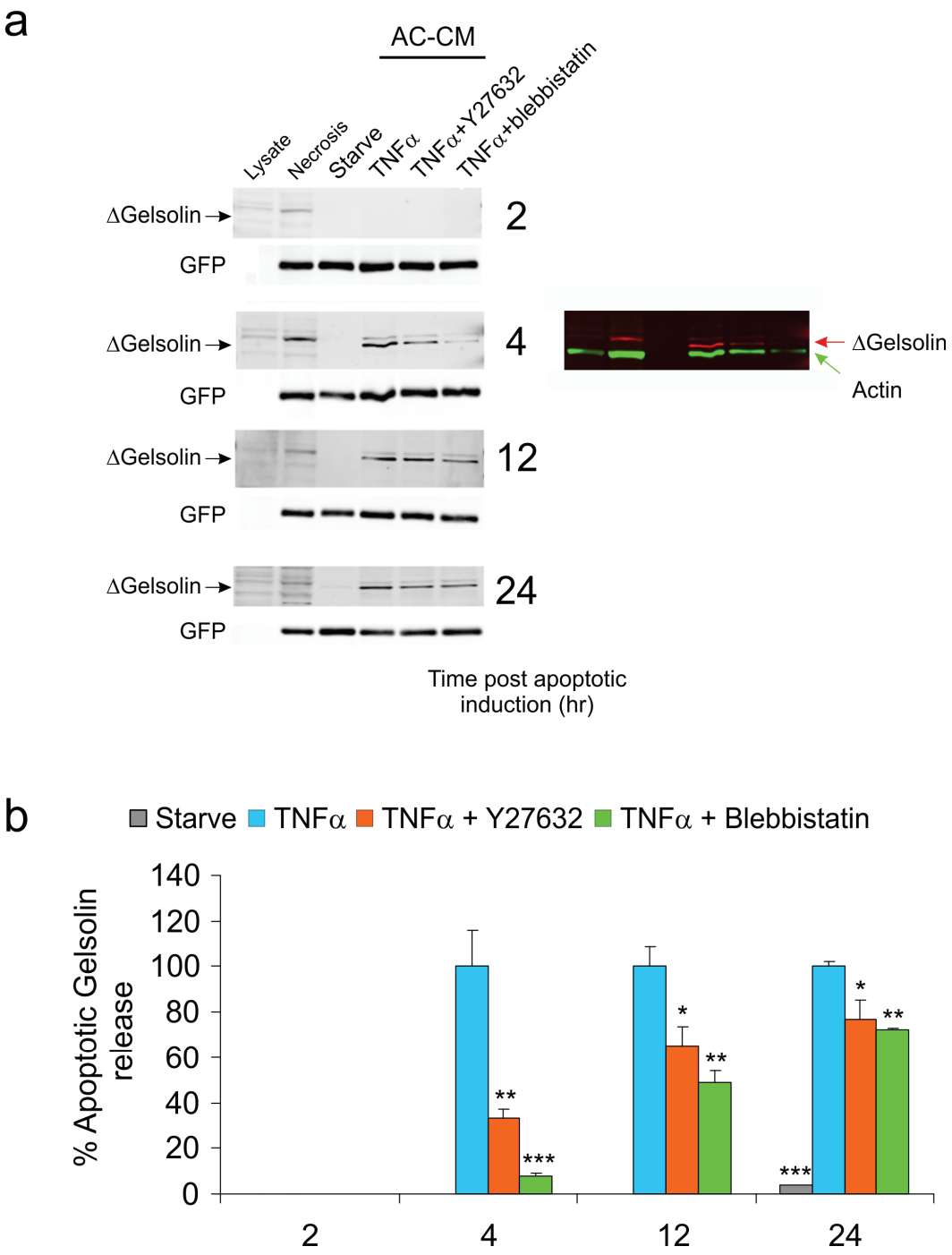

Figure 3.12. Apoptotic gelsolin release is dependent on acto-myosin contractility.
(a) Representative western blots of concentrated NIH 3T3 AC-CM collected at 2, 4, 12, and 24 hours as indicated. Blots probed for gelsolin (left panels) and actin (right panel), the band corresponding to caspase cleaved gelsolin (ΔGeslolin) is indicated. Exogenous GFP, added before sample concentrating, is used as loading control. Imaging performed using LiCor. (b) Quantitation of cleaved gelsolin band intensity mean ± SEM at indicated time and treatments. Statistical comparison performed by ANOVA followed by Dunnetts multiple comparison test versus TNFα alone at each time point (n=3) (*, $p<0.05$; **, $p<0.01$; ***, $p<0.001$).

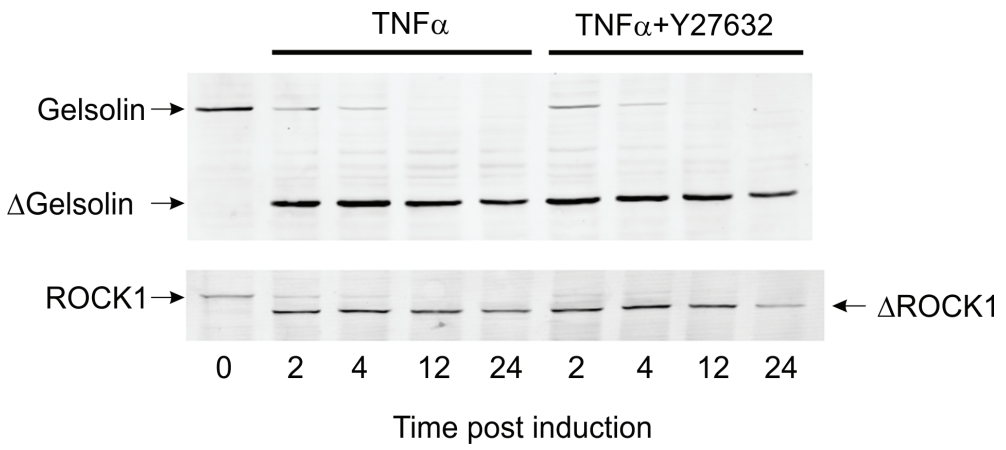

Figure 3.13. Rock inhibition does not affect apoptotic gelsolin cleavage.
Representative western blot of apoptotic NIH 3T3 lysate at indicated times following treatment with TNFα ± Y27632. Blots probed for gelsolin (upper) and ROCK1 (lower). Full length and caspase cleaved gelsolin (ΔGelsolin) and ROCK1 (ΔROCK1) products are indicated.

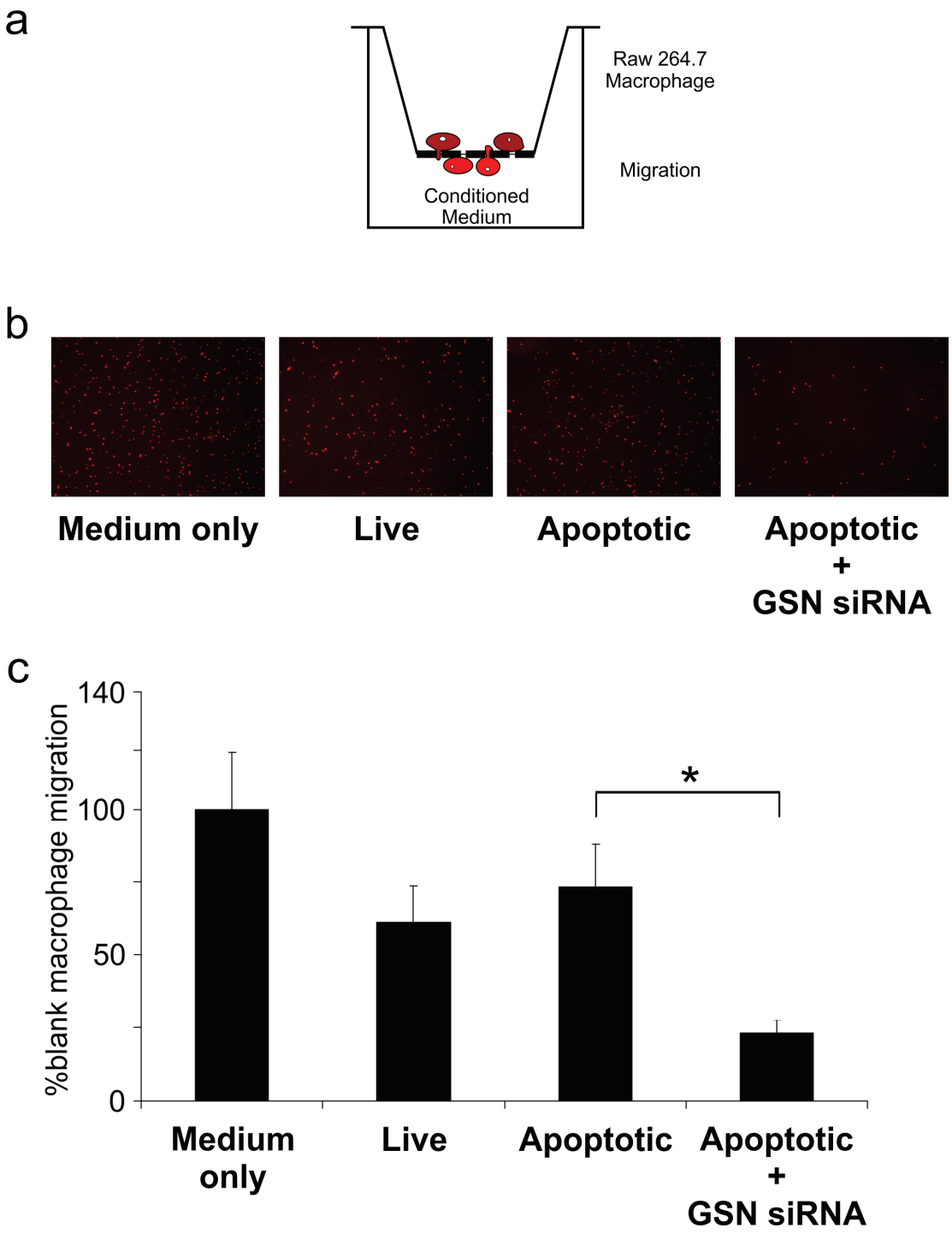

Figure 3.14. Apoptotic gelsolin release ensures macrophage migration.
(a) Schematic diagram of transwell migration cell. Mouse Raw264.7 macrophage in starve medium are deposited in upper chamber and exposed to conditioned medium in lower chamber for 2 hours. Migrated cells are fixed, stained and microscopically scored. (b) Representative 4x images of migrated RAW 264.7 macrophages exposed to the indicated NIH 3T3 conditioned media. NIH 3T3 cells were transfected with either non targeted (NT) or gelsolin (GSN) siRNA 72 hours prior to induction of apoptosis with low dose TNFα and UVB. Migrated macrophages are stained with PI after fixation and permeabilization. (c) Quantitation of RAW 264.7 transwell migration to indicated conditioned medium. Bars indicate the mean sum of the number of migrated macrophages from three fields (as in b) normalized to medium only migration. Statistical comparison performed by ANOVA followed by Tukey-Kramer multiple comparison test (n=3) (*, $p<0.05$).

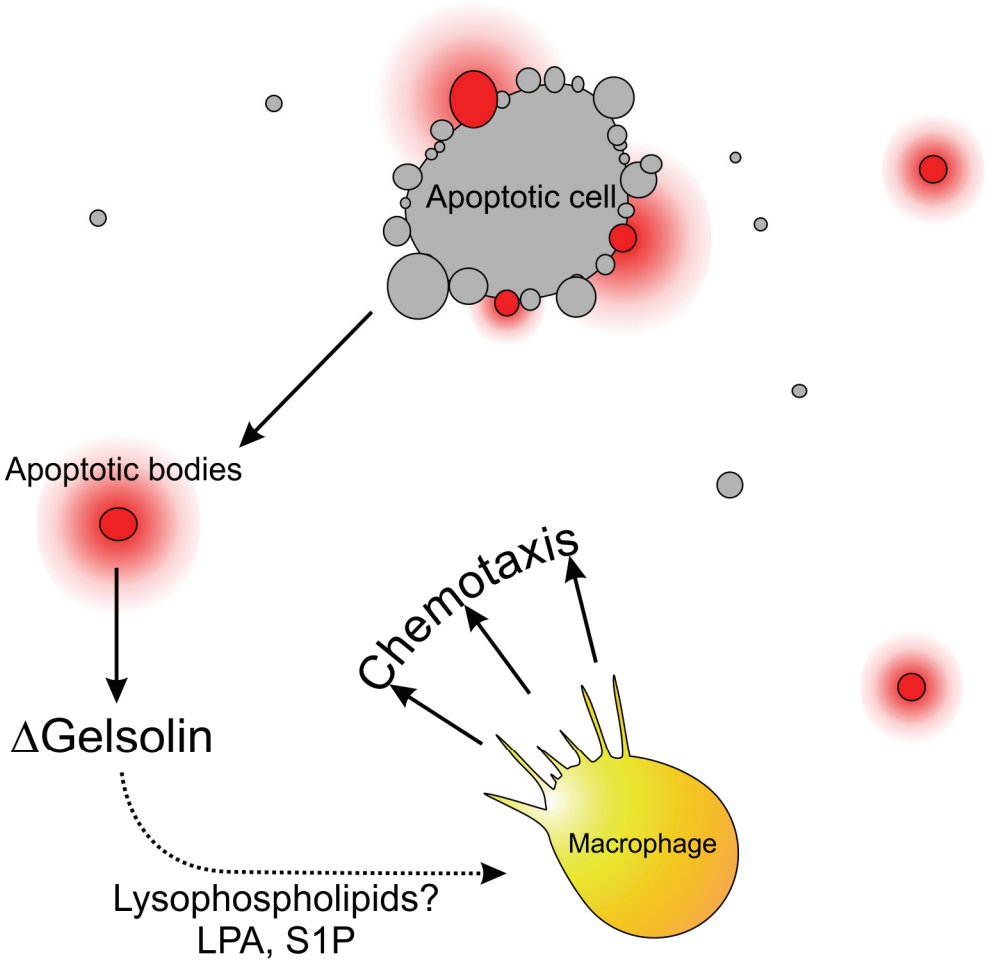

Figure 3.15. Schematic model of apoptotic gelsolin release
Apoptotic blebs and bodies indicated in grey and red. Red structures indicate loss of membrane integrity and protein leakage. ΔGeslolin-caspase cleaved gelsolin. LPA-lysophosphatidic acid. S1P-sphingosine-1-phosphate.

3.3 Discussion

One of the defining features of apoptotic cells is their intact and functional membranes which appear to prevent pro-inflammatory activation by limiting the release of intracellular protein. As such, apoptotic protein release has not been considered to be a component of efferocytosis. In fact, protein release is generally regarded to occur only during secondary necrosis. Our data demonstrate that acute protein release from apoptotic cells is a *bona fide a*poptotic process and is indirectly influenced by ROCK-induced actomyosin contractility. The mechanism of apoptotic bleb and body degradation in early apoptosis provides a simple and robust route for intracellular protein to participate in complex extracellular signaling events during apoptosis. Furthermore, these observations highlight a novel biological role for ROCK induced apoptotic body formation and blebbing. The generation of independent sub-cellular apoptotic bodies which diffuse away from the apoptotic cell prior to membrane breakdown and release of their intracellular contents would dramatically increase the range at which macrophages detect apoptotic cells. The behavior of these sub cellular particles as “suicide notes” to attract surveilling macrophages may be a common and important mechanism to mediate safe and rapid clearance, thus avoiding unwarranted inflammatory activation (Figure 3.15). This possibility suggests that the release of protein from apoptotic cells does not appear to necessarily lead to immune activation and may in fact be an active participant in acute corpse clearance. A further implication is that protein released during apoptosis is likely to have limited inflammatory potential and that only during primary and secondary necrosis are specific pro-inflammatory mediators released. Indeed, in post apoptotic cells the release of the pro-inflammatory cytokine HMGB-1 is only observed hours after the onset of secondary necrosis [228].

Due to the existing dogmatic preconceptions of apoptotic membrane integrity, the focus in the search for come-find-me signals has largely ignored the potential contribution of many intracellular proteins. As previously mentioned, the release of TyrRS and dRP S19, two intracellular proteinaceous come-find-me factors, from apoptotic cells conflicts with the current model of early apoptotic cell membrane impermeability. The insight we now provide may resolve this long standing dilemma and expand the scope of come-find-me factors to include more intracellular proteins. Although we failed to find either TyrRS or dRP S19 as part of

our systematic quantitative SILAC survey of AC-CM, we identified the release of 46 proteins from early apoptotic NIH 3T3, none of which have previously been identified as come-find-me factors. Critically, many of these proteins are dependent upon ROCK induced blebbing and apoptotic body formation for their release, recapitulating the importance of these structures in the proposed mechanism of apoptotic protein release. Such an acute and dramatic release of protein is likely to have an important biological impact in the surrounding microenvironment and several of these molecules may be apoptotic come-find-me factors. As proof of principle, we investigated the potential role of gelsolin, the most abundantly enriched protein in NIH 3T3 AC-CM, and found that it encourages macrophage migration towards apoptotic cells. Gelsolin itself may behave as a come-find-me-factor, or may act by modifying additional extracellular signals to affect responses [240,241](Figure 3.15). The ability of plasma gelsolin to bind and modify the activity of lysophospholipids has been well established and release of caspase cleaved gelsolin from apoptotic cells may be a significant modifier of such lipid signals. As previously mentioned, apoptotic cells release a variety of lipid chemoattractant signals including S1P that, in turn, affect macrophage migration and survival [241-244]. Alternatively apoptotic release of S1P has also been shown to mediate extrusion of apoptotic cells by initiating contraction of an epithelial sheet, thus preserving barrier function [245]. Whatever the mechanism, the release of gelsolin from apoptotic cells would be expected to modify the existing lysophospholipid signaling networks and thus mediate profound changes in the extracellular environment. While we have demonstrated that released gelsolin has the potential to act as an apoptotic come-find-me factor, it may not be a universal signal. Nonetheless, it is interesting to note that actin, which is abundant and ubiquitously expressed, was also highly enriched in AC-CM. Extracellular actin has been proposed to act as reservoir to retain circulating plasma gelsolin near sites of tissue damage where it can modulate immune responses, such a mechanism could be identical following apoptotic actin release [230]. While a gelsolin knockout mouse was first described in 1995 there are no reports specifically demonstrating defective apoptotic cell clearance [246]. There are however several reports which suggest that apoptosis in the knockout mouse is altered [247-249]. Induction of apoptosis in mice with the Fas stimulatory antibody Jo-2 has been shown to dramatically increase hepatocyte apoptosis in gelsolin$^{-/-}$ mice compared to gelsolin$^{+/+}$ littermates [247]. This observation is curious because gelsolin expression in the liver is limited to sinusoidal lining cells while the bulk of the

tissue, such as hepatocytes, express little or no protein [247]. Thus gelsolin appears to be an important factor limiting apoptosis, even in tissues where it is not expressed which suggests that the protein has a potentially important extracellular function. While it remains unclear precisely how gelsolin mediates this effect, the possibility remains that extracellular gelsolin, either plasma and/or caspase cleaved, may be mediating important anti-inflammatory signals associated with apoptosis and its absence leads to increased programmed cell death and tissue damage. It is important to note that the gelsolin knockout eliminates both the plasma and cytoplasmic isoforms. Due to the systemic deficiency of gelsolin in this model the relative importance of plasma versus apoptotically released gelsolin in the attraction of macrophages and the resolution of cell death cannot be determined.

Clearly gelsolin was only one of many molecules identified in NIH 3T3 cells AC-CM, any of which may modulate macrophage and immune responses towards apoptotic cells. The actual protein content of extracellular supernatant following apoptotic body and bleb breakdown is likely to be highly dependent upon cell type. This work is a first step in systematically identifying the range of proteins released from apoptotic cells and extensive further investigation is required to determine; how consistent protein release is across cell types; which proteins in AC-CM have extracellular roles; and what their mechanism of actions might be.

4. Activating Somatic ROCK1 Mutations in Cancer

(Text extracted from Lochhead, P*., Wickman, G*., Mezna, M., Olson, M.F. Activating Somatic mutations in human cancer. Oncogene (2010) 29, 2591-2598. *Co-first authors.)

4.1 Introduction

The identification of mutated genes that drive human oncogenesis is an ongoing major objective worldwide. The development of high-throughput detection methodologies has facilitated the identification of novel somatic mutations associated with numerous cancers (http://www.sanger.ac.uk/genetics/CGP/ and http://cancergenome.nih.gov/). Statistical analysis of mutation frequency can be used to classify them as active "driver" mutations that provide a selective advantage during cancer initiation and progression, or silent "passengers" which are expanded from progenitor cells, yet provide no overt selective advantage. While this approach has tremendous value in identifying important genes in cancer, it remains incomplete until the biological consequences of detected mutations are determined to differentiate drivers from passengers.

The Cancer Genome Project has thus far identified 3 nonsynonymous mutations in the ROCK1 gene, an essential effector kinase downstream of Rho GTPases that is an important mediator of cell migration. ROCK1 is an unusual AGC kinase family member as its kinase domain assumes an active conformation without activation loop phosphorylation [9]. Instead, ROCK1 activity is restrained by its inhibitory C-terminus; relief from auto-inhibition results from Rho-GTP binding or by caspase cleavage at a C-terminal site [46,57]. There is a wealth of data implicating Rho GTPases in human cancer [148,250] suggesting that ROCK1 and ROCK2, as key mediators of Rho signaling, may play important roles in oncogenesis [154,202,251]. In support of this, pre-clinical studies have demonstrated beneficial effects of ROCK inhibition on tumour incidence rates, volume, invasiveness and metastasis [53,206,209,210,252-254]. In addition, elevated ROCK1 and/or ROCK2 expression have been detected in several human cancers, which positively correlates with poor outcome [151,152,255,256]. While alterations in the regulation of ROCK1 signaling as a contributory factor to human cancer may be well-accepted, this is the first report of ROCK1 activation as a direct consequence of somatic mutations.

I found that these somatic ROCK1 mutations lead to elevated kinase activity and drive actin cytoskeleton rearrangements that promote increased motility and decreased adhesion; both characteristics of cancer progression. Mapping of the kinase-interacting regions of the carboxy-terminus combined with structural modeling provides insight into how these mutations likely affect the regulation of ROCK1. Consistent with the frequency of ROCK1 mutations in human cancer, these results support the conclusion that there is selective pressure for the ROCK1 gene to acquire “driver” mutations that result in kinase activation.

4.2 Results

4.2.1 Cancer Associated Mutations in ROCK1

As previously mentioned, cancer genome sequencing has revealed three novel ROCK1 mutations in human malignant disease (http://www.sanger.ac.uk/cgi-bin/genetics/CGP/cosmicsearch?_q=rock1). The 3 somatic mutations in ROCK1 are: AA insertion between base pair (bp) 1214-1215, resulting in frameshift and premature termination at Y405*; C to G transition at bp 3377, resulting in premature termination at S1126*; and C to T transversion at bp 3577, resulting in the amino acid substitution P1193S (Figure 4.1). The Y405* and S1126* mutants were both identified in primary human breast cancers, while the third mutation, P1193S, was identified from the established human non-small cell lung carcinoma line NCI-H1770) [257].

4.2.2 Cancer associated somatic mutations of ROCK1 are activating

To determine how ROCK1 mutations affected activity, MYC-tagged wild-type (WT), kinase-dead K105G, and Y405*, S1126* and P1193S proteins were expressed in NIH 3T3 mouse fibroblast cells. WT, K105G and P1193S migrated at 158 kDa, while Y405* and S1126* migrated as expected at 47 kDa and 113 kDa, respectively, as determined by western blotting (Figure 4.2). *In vitro* kinase assays of the MYC-immunoprecipitated proteins revealed that the activity of all three ROCK1 mutants was increased significantly (2.5-3.5 fold) relative to WT (Figure 4.2). The kinase-dead K105G mutant had no detectable activity, indicating that the active forms possessed intrinsic kinase activity that did not result from contaminating MYC-tag co-immunoprecipitating kinases (Figure 4.2). This work was performed in collaboration with Dr. Pam Lochhead.

4.2.3 ROCK1 Mutations are Constitutively Active in Cells

To further explore the cellular consequences of ROCK1 mutations the enzymes were transiently expressed in NIH 3T3 fibroblasts. The activity of ROCK1 was assessed by immunofluorescence microscopy of actin stress fibres and phosphorylation of the regulatory myosin light chain (pMLC) at serine 18 and 19, two hallmarks of ROCK activation. Co-staining for MYC-tag ROCK1 and F-actin revealed large increases in both the number and thickness of actin stress fibres, in cells transfected with Y405*, S1126*, and P1193S but not with K105G (Figure 4.3). Expression of WT ROCK1 appeared to increase the appearance of stress fibres although to a much lesser extent than the more biochemically active mutants. Examination of pMLC in MYC-tag positive cells reveals a staining pattern identical to that seen with actin stress fibres. Interestingly, the enhancement of pMLC and actin stress fibres appear far more pronounced following transfection with Y405* and S1126* versus P1193S.

Following transfection of NIH 3T3 fibroblasts with the ROCK1 mutants significant changes in the cells were observed. Within six hours of transfection the cellular area of NIH 3T3 cells that expressed ROCK1 Y405*, S1126*, or P1193S was reduced to 52, 39, and 59%, respectively, of cells expressing GFP (Figure 4.4a). While the active ROCK1 mutants clearly initiated a contractile phenotype the kinase dead K105G construct appeared to increase cell spreading compared to GFP, suggesting a dominant negative activity over native wild type ROCK1 (Figure 4.4a). When the effects of the active ROCK1 mutants on cell morphology were examined, Y405*, S1126*, and P1193S expression markedly modified cell shape, shifting the distribution of morphologies from predominantly spread to contracted and rounded (Figure 4.4b). Furthermore, the magnitude of the distribution shift is consistent with cellular activity observed in previous experiments.

4.2.4 ROCK1 mutants enhanced motility and migration

Given the prominent role of ROCK1 in tumour cell invasion and metastasis [258], I sought to assess the effects of the somatic ROCK1 mutations on motility and adhesion. Expression of the MYC-tagged ROCK1 proteins in NIH 3T3 fibroblasts, assessed by flow-cytometry, was comparable for WT, S1126* and P1193S, while expression of K105G and Y405* was lower (Figure 4.5a and b). Analysis of individual cell motility by time-lapse microscopy over 20 hours revealed that

S1126* and P1193S expressing NIH 3T3 cells were more motile than GFP-expressing control cells, with significantly longer cumulative track lengths (Figure 4.6a and b). Although track lengths of WT ROCK1 expressing cells were apparently longer than GFP-control cells, they were not statistically significant (Figure 4.6b), while Y405* expression was insufficient to reliably assess its effects. Expression of S1126* also increased Euclidean distance travelled and cell velocity (Figure 4.7a and b). No effect on cell persistence was observed following transfection with any ROCK1 construct (Figure 4.7c). I next examined the effects of ROCK1 mutants on adhesion using a transwell dissociation assay [259]. This assay relies upon the migration of ROCK1 expressing NIH 3T3 cells in an FBS gradiant through an 8 μm pore transwell membrane followed by dissociation, and adherence to the bottom of the well (Figure 4.8a). Cellular dissociation is then quantitated by counting the number of cells adhered to the plate. All three ROCK1 mutants significantly increased the number of cells that had crossed and dissociated from the transwell membrane (Figure 4.8b) indicating reduced cell adhesiveness, a property associated with increased metastatic potential. Expression of S1126* also was sufficient to further increase dissociation of the highly-metastatic MDA MB 231 breast cancer cell line in this assay (Figure 4.8c).

4.2.5 C-terminus of ROCK1 contains multiple kinase interacting Domains

Next I addressed how the three ROCK1 mutations; Y405*, S1126*, and P1193S led to kinase activation. Since these three ROCK1 mutations affect the C-terminus it is likely that they trigger activation by disrupting inhibitory interactions between N- and C-terminal domains. While the role of the C-terminus in ROCK1 autoinhibition is thoroughly established, the kinase interacting regions mediating inhibition had not previously been mapped. Thus, I probed a 21-mer peptide array (Figure 4.9a) comprised of amino acids 1-75 containing the N-terminal dimerization region and amino acids 853-1354 of the C-terminus with [^{35}S]-labeled ROCK1 kinase domain (amino acids 1-404). As expected, the probe bound to the ROCK1 N-terminal residues 27-75 that mediate kinase dimerization (Figure 4.9b and c)[9]. In addition, the kinase domain strongly bound 4 C-terminal regions (Figure 4.9b; regions 2d, 2f, 2h and 2i), indicating that potentially there are multiple sites engaged in kinase regulation. Region 2d overlapped with the latter half of the RBD. The first segment of the split Pleckstrin Homology (PH) domain contained

regions 2f, while the second segment overlapped with 2i. Binding region 2h was contained within the cysteine-rich C1 domain. Kinase binding to the region containing P1193 (2g) was weak though detectable (Figure 4.9b). To further characterize these kinase binding regions, I expressed FLAG-tagged protein fragments in *E. coli* and tested their abilities to bind recombinant GST-ROCK1 kinase domain (200 ng) spotted onto nitrocellulose membranes (Figure 4.10a). Regions 2g, 2h and 2i significantly bound ROCK1 kinase domain, while 2d binding was detectable but did not achieve significance (Figure 4.10b). Region 2f could not be tested due to protein insolubility. The P1193S mutation significantly reduced kinase binding by over 30% (Figure 4.9b)

4.2.6 Specific ROCK1 C-terminal Interacting Domains Mediate Kinase inhibition

To test the role of these domains in kinase regulation, representative 21-mer peptides from each binding region were synthesized and tested in an IMAP fluorescence-polarization ROCK1 kinase assay. Kinase activity was significantly inhibited by peptides 2f and 2g (31 and 68% of control respectively) while peptides corresponding to regions 2d, 2h, and 2i failed to inhibit ROCK1 activity (Figure 4.11a). Analysis of ROCK1 inhibition by mutant 2g (P1193S) revealed a significant reduction in kinase inhibition compared to wild type 2g (Figure 4.11b).

4.2.7 ROCK1 C-terminal Interacting Domain Modeling

While the data presented above make it easy to conceive how the Y405* and S1126* mutants, which respectively lack all or most of the kinase-interacting and autoinhibitory regions 2f, 2g and 2h, would be constitutively activated, the mechanism of kinase activation due to P1193S mutation is unclear. Thus, given the high degree of conservation between the ROCK1 and ROCK2 PH-C1-PH domains in general, and the 2f, 2g and 2h regions in particular (Figure 4.12), the ROCK1 kinase-interacting and inhibitory regions were modeled onto the NMR solution structures of the PH-C1-PH domains of ROCK2 in order to gain greater insight into potential structural modifications induced by P1193S [260](Figure 4.13). As can be seen in Figure 4.13a P1193 breaks a short α-helix prior to a β-sheet that leads on towards the C1 domain (highlighted in green). I predict that the P1193S mutation does not provide the appropriate α-helix break, and as a consequence will disorder the split PH domain and likely disrupt the C1 domain as

well. In addition, the structural rigidity provided by a proline residue would be reduced when substituted with a serine residue, which might result in less ordered folding. Such structural alterations are likely responsible for the reduced kinase domain binding and attenuation of kinase inhibition observed in domains bearing the P1193S mutation. In addition, modeling of the 2f, 2g and 2h regions reveals that they form multiple surfaces located directly opposite to a series of charged lysine and arginine residues that cooperate to mediate lipid interaction and to orientate the PH-C1-PH domains in membrane bilayers (Figure 4.13b). As a result, the critical kinase interaction and inhibitory domains would be exposed to the cytosol and thus accessible for interaction and inhibition of the ROCK catalytic domain (Figure 4.13b). These results indicate that multiple surfaces in the ROCK1 C-terminus likely contribute to kinase-domain binding and regulation. These interactions range from relatively weak and non-regulatory (2d) to strong and inhibitory (2g). In addition to the significant contribution of region 2g that contains P1193, region 2h and 2i appear to be an important kinase binding regions, possibly contributing to stabilizing N and C-terminal interactions.

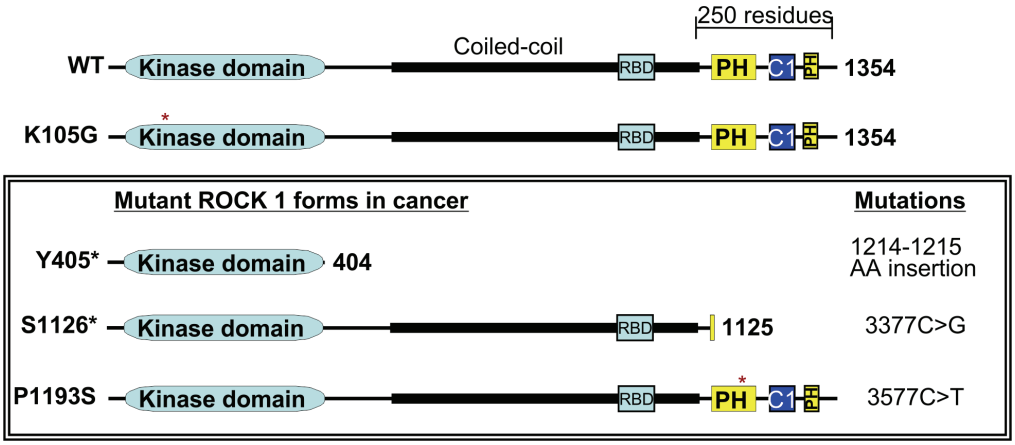

Figure 4.1. ROCK1 domain structure for wild-type (WT) and cancer associated mutations. RBD=Rho binding domain. Split Pleckstrin Homology (PH) domains (yellow) have an inserted C1 domain (dark blue). Asterisk indicates position of amino acid substitution (red). Drawn to scale.

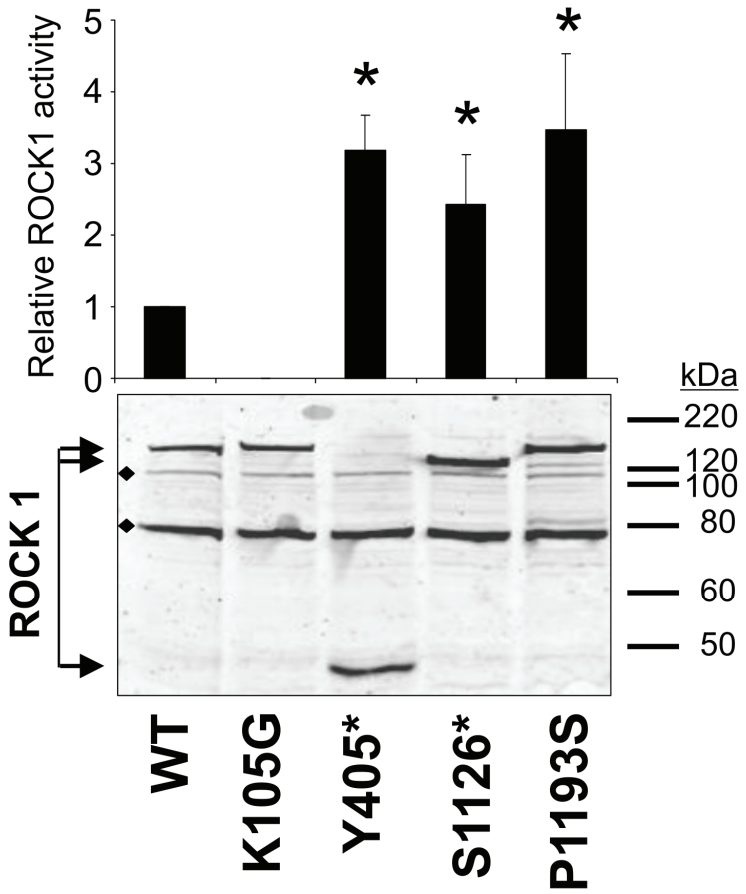

Figure 4.2. ROCK1 somatic cancer mutants are active.
Upper panel, ROCK1 kinase activity of indicated MYC-tagged constructs immunoprecipitated, as described previously (coleman et al., 2001), from transfected NIH 3T3 cells. Results are mean ± SEM vs. WT (n=3)(*, $p<0.05$ vs WT, by t-test). Lower panel, cellular lysates were separated by SDS-PAGE and immunoblotted with anti-MYC antibody. Arrows indicate ROCK1 proteins. ◆ , non-specific bands. Results are mean ± SEM activity (n=3)(* $p<0.05$, relative to WT, by *t-test*). Figure courtesy of Pam Lochhead.

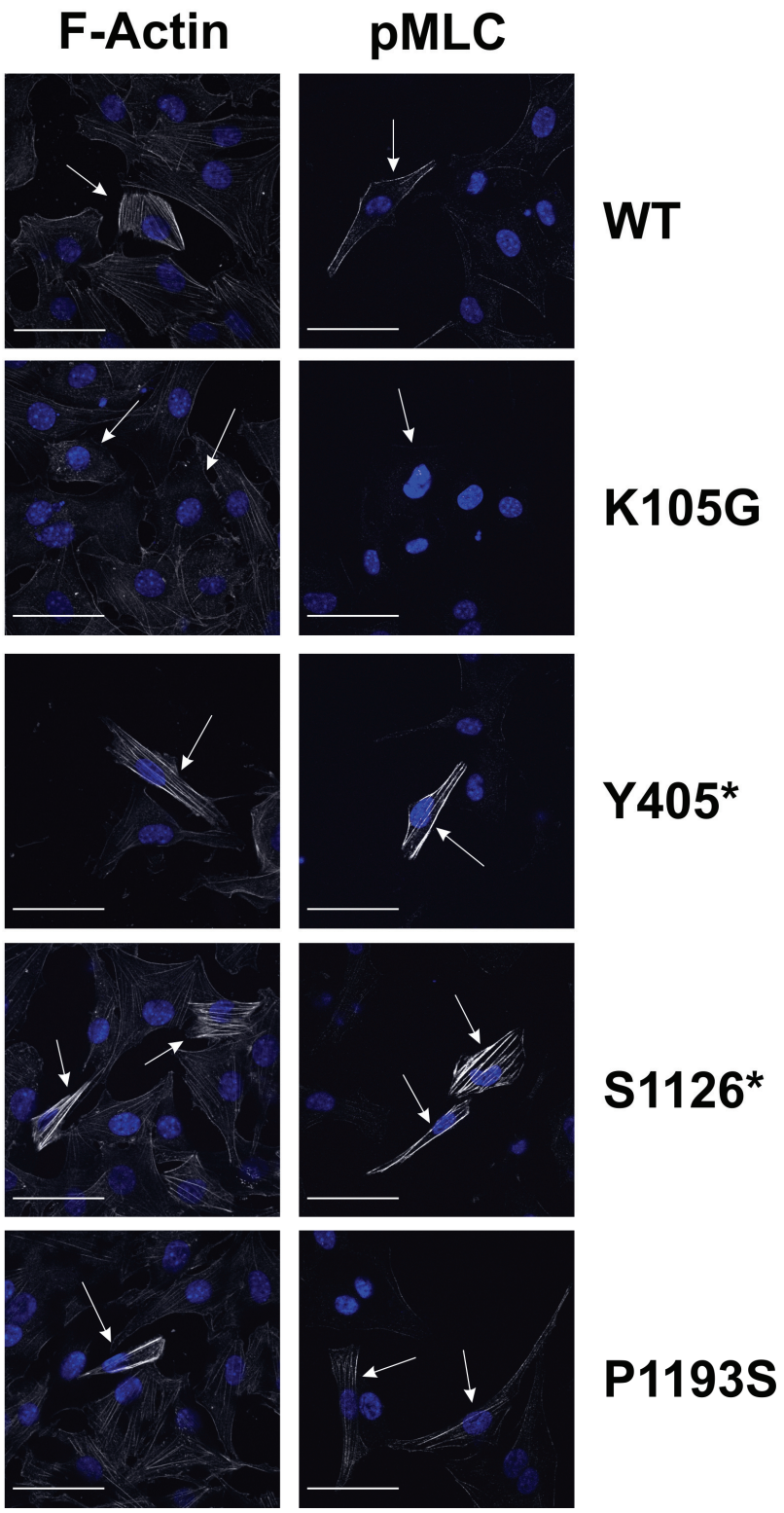

Figure 4.3. ROCK1 mutants are active in cells.
Representative immunofluorescence confocal images of serum starved NIH-3T3 fibroblasts stained for actin (left panels) and phosphorylated myosin light chain (pMLC; right panels). Cellular nuclei, stained with DAPI, are shown in blue. Arrows indicate cells positive for MYC-tag ROCK1. Scale bars represent 50 μm. After transfection, cells were serum starved overnight then fixed and stained as described previously (Coleman *et al.*, 2001). Confocal images were obtained using an Olympus FV1000 using a 60x oil-immersion objective.

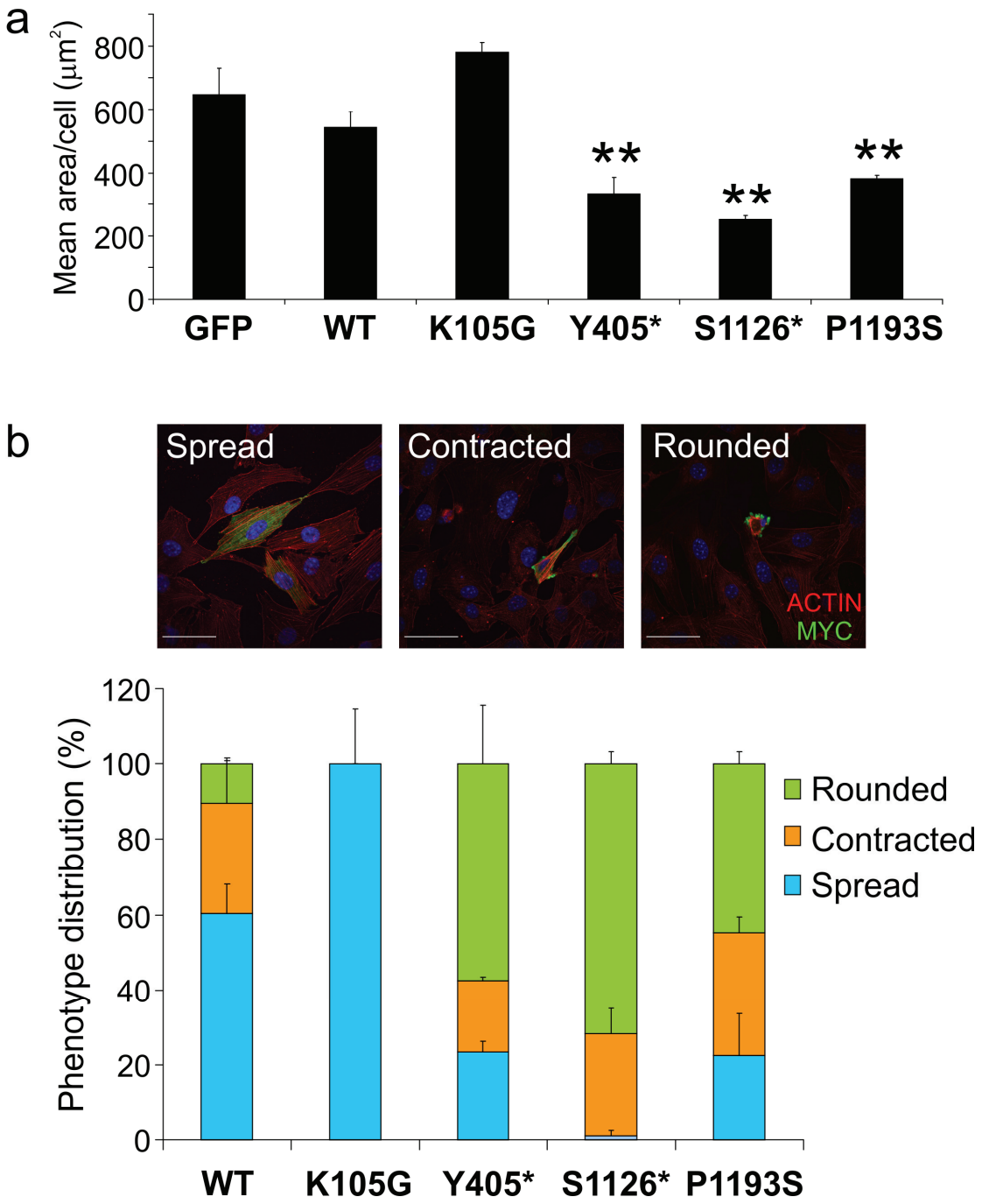

Figure 4.4. ROCK1 somatic cancer mutants promote cellular actin rearrangements.
(a) Mean cell area of ROCK1 transfected NIH 3T3 cells. For cell size determinations, 6 random fields of MYC-tag positive cells were captured per treatment. Images were analysed for percentage MYC-tag positive area divided by the cell number. Data are mean ± SEM (n=3), statistical comparisons determined by ANOVA followed by Dunnett's multiple comparison test. (* $p<0.01$ vs GFP). (b) Representative images of cell morphologies (spread, contracted, and rounded) stained for F-actin (red) and ROCK1-expression (MYC; green). For cell morphology, images were captured and scored for spread, contracted or rounded. Average distribution of morphologies from 3 experiments for each ROCK1 variant in bottom panel.

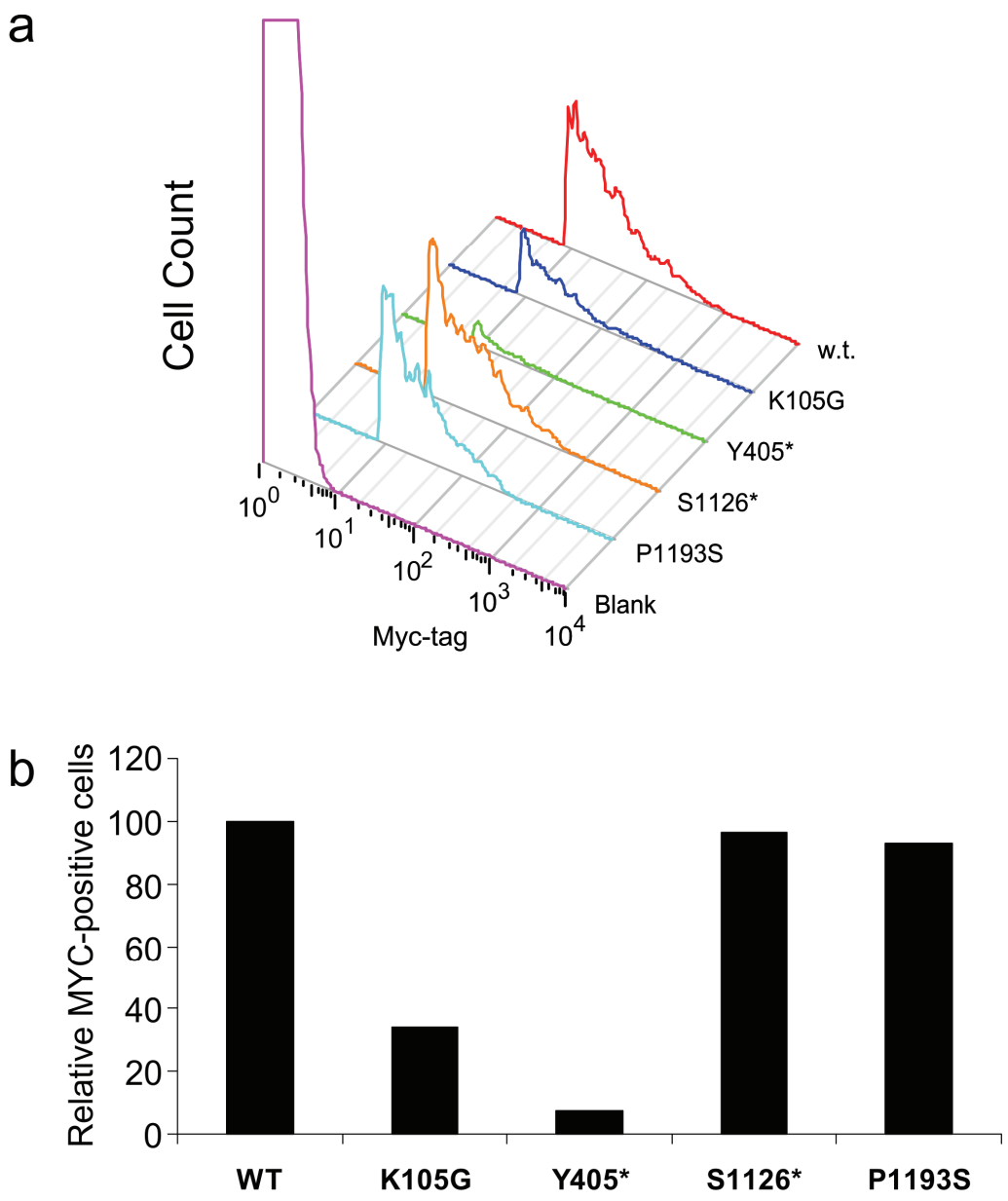

Figure 4.5. Expression of MYC-tagged ROCK1 constructs in NIH 3T3 mouse fibroblasts.
(a) Representative FACS expression profiles of cells positive for expression of MYC-epitope tagged ROCK1 plasmids. After transfection, cells were incubated overnight in 10% FBS medium. The following day the cells were collected and fixed in 2% paraformaldehyde for 10 minutes. Cells were then washed and permeabilized with 0.1% Triton X-100 for 5 minutes. MYC-tagged ROCK1 constructs were detected with an anti-MYC (9B11) antibody conjugated with AlexaFluor 647. 10,000 events were collected on a BD FACScaliber and MYC-tag positive cells were gated against blank transfected cells. Traces represent histograms of MYC-tag positive cell number vs MYC-tag intensity. (b) Representative expression profile of MYC-tag positive cells as determined by FACS. Data represent percentage of MYC-tagged positive cells relative to WT ROCK1 expression.

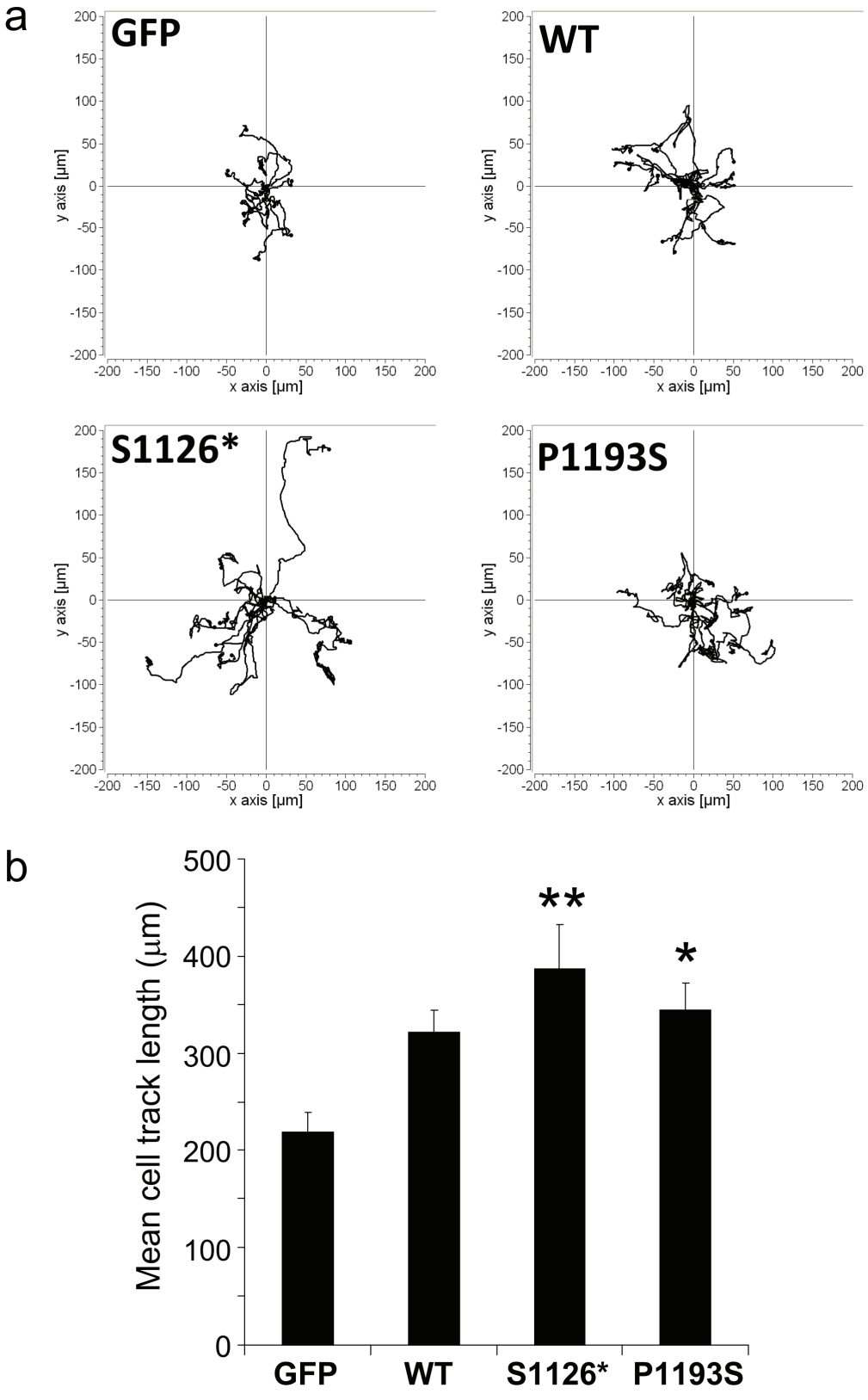

Figure 4.6. ROCK1 somatic cancer mutants promote cell migration.
(a) Representative cell tracks of 10 cells expressing indicated ROCK1 constructs. Cells were co-transfected with ratio of 1:2 of GFP and ROCK1 constructs and plated into a glass bottom 6 well plate in complete medium. 3h after nucleofection the medium was replaced with reduced serum (3.3% FBS) medium. Three bright field and GFP timelapse images were captured for each treatment every 2 minutes for 20 h. In those fields the motility of 10 cells in all 3 fields was analysed using Metamorph and Image J. (b) Mean cumulative tracklengths $\pm$ SEM of NIH 3T3 analysed an in (a). Statistical comparison performed by ANOVA followed by Dunnett's multiple comparison test (n=4)(* $p<0.05$ vs GFP; ** $p<0.01$ vs GFP).

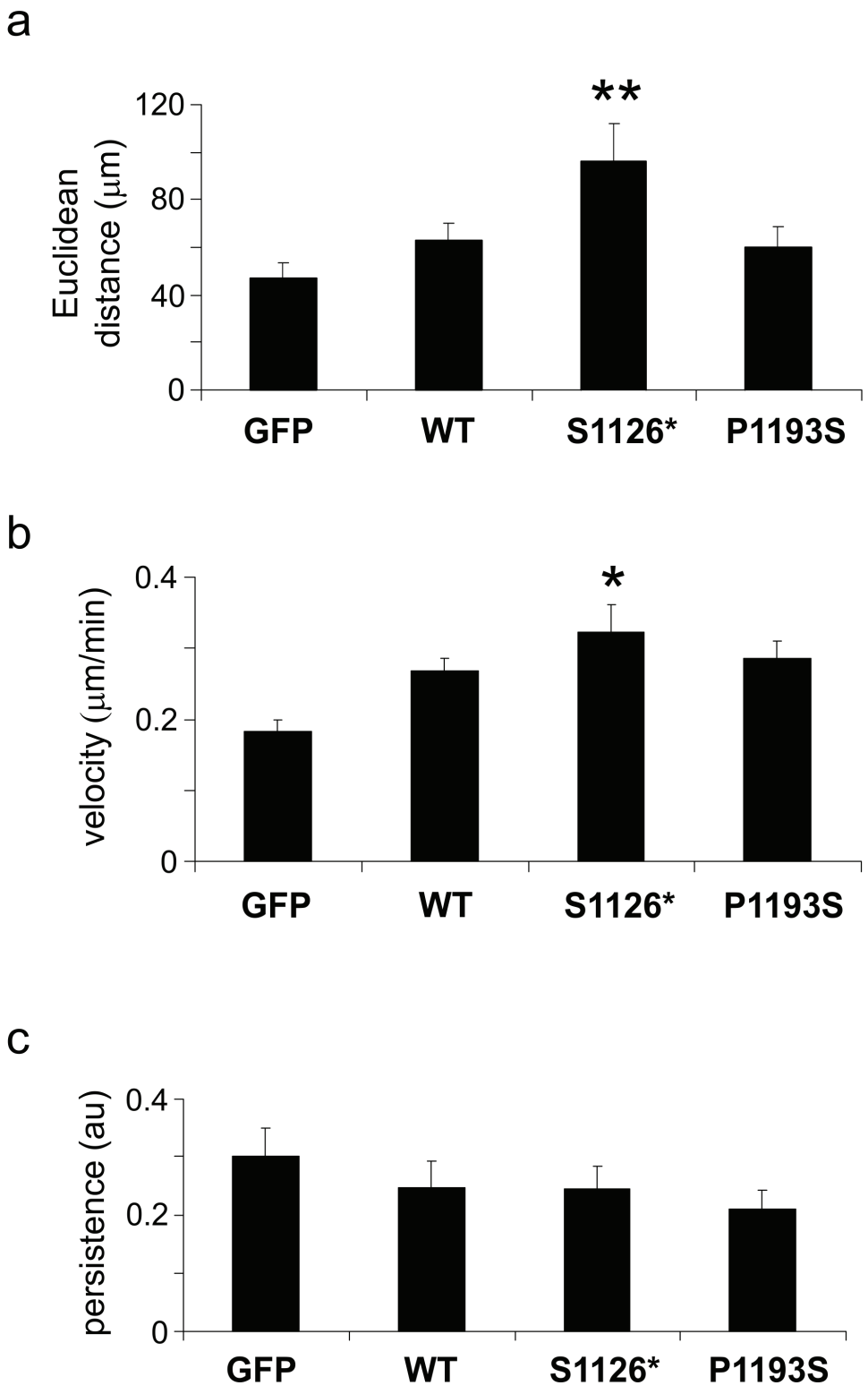

Figure 4.7. ROCK1 somatic cancer mutants promote random cell motility.
(a) Data represent mean Euclidean distance travelled ± SEM. (b) Data represent mean cell velocity ± SEM over 20 hours. (c) Data represent mean persistence (Track length/Euclidean distance) ± SEM. Euclidean distance and persistence were calculated from individual cell tracks obtained with the Chemotaxis and Migration Tool plugin for ImageJ from time-lapse image stacks. Statistical analysis performed by ANOVA followed by Dunnett's multiple comparison test (*, $p<0.05$; ** $p<0.01$ vs GFP).

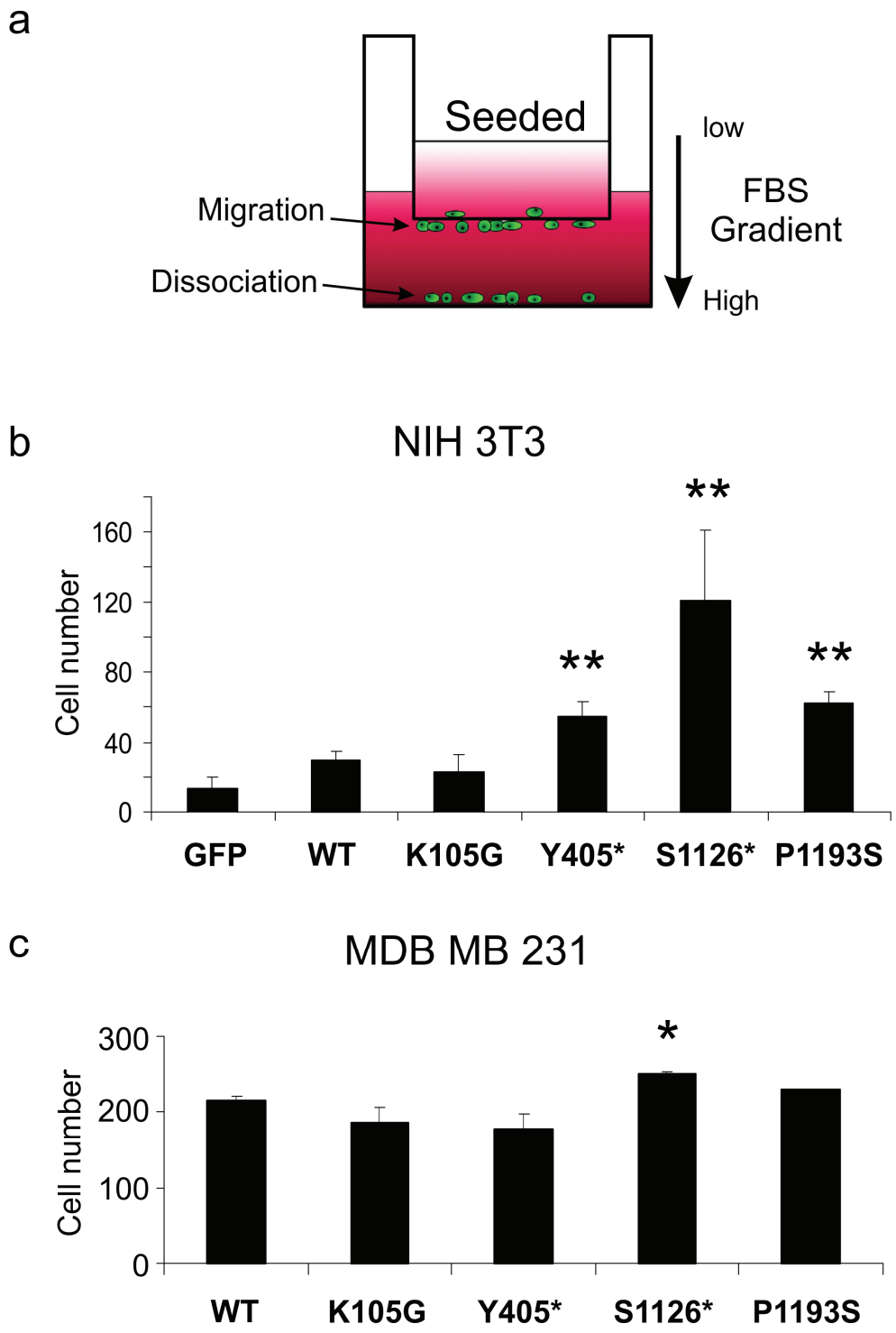

Figure 4.8. ROCK1 somatic cancer mutants encourage cellular dissociation.
(a) Schematic diagram of transwell dissociation assay. Cells were co-transfected with a ratio of 1:2 of GFP and ROCK1 constructs and incubated in 10% FBS medium within an 8 μm pore Transwell insert for 3h. Following incubation, the insert medium was aspirated and replaced with serum free medium, insert was placed in fresh well containing 10% FBS media and incubated 18 h. The number of GFP positive cells that invaded and dissociated from the membrane were then counted from five independent 20x fields. (b) Mean number of dissociated cells following chemotaxis of ROCK1 transfected NIH 3T3 cells through Transwell membranes. Results are mean ± SEM, statistical analysis performed by ANOVA followed by Dunnett's multiple comparison test (n=4)(** $p<0.01$ vs GFP). (c) Mean number of dissociated cells following chemotaxis of ROCK1 transfected MDA MB 231 breast cancer cells. Results are mean ± SEM. Statistical analysis performed by ANOVA followed by Dunnett's multiple comparison test (n=3)(*, $p<0.05$ vs WT).

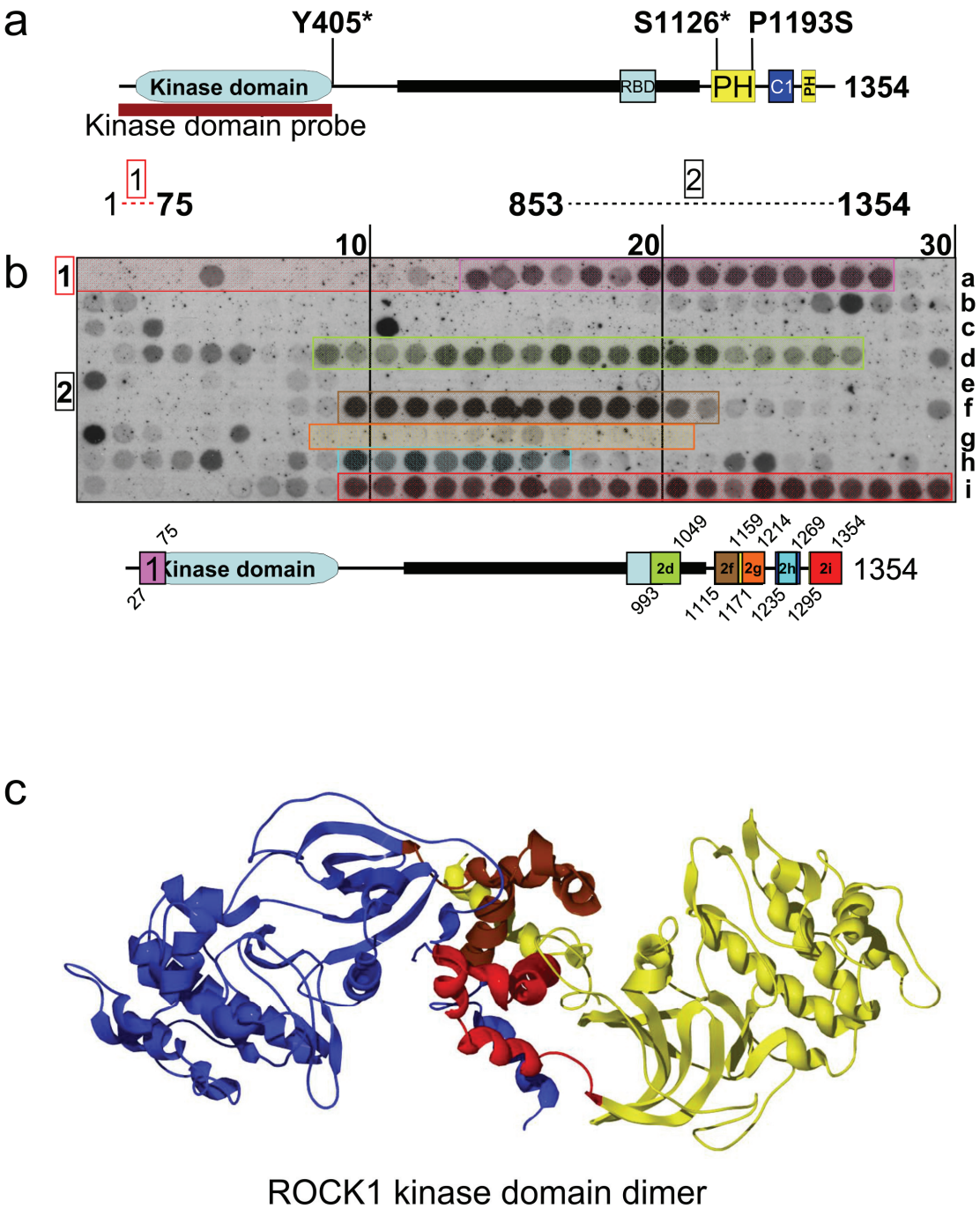

Figure 4.9. ROCK1 kinase domain has multiple and distinct c-terminal interacting sites.
(a) Schematic representation of ROCK1 domain structure, regions analysed on peptide array, and the probe used (upper panel). The probe consisted of MYC-tagged ROCK1 kinase domain (amino acids 1-404). 21-mer peptides offset by 2 amino acids covered region 1 (red) amino acids 1 – 75 and region 2 (black) amino acids 853-1354. (**b**) Autoradiogram of the peptide array probed with ^{35}S labelled protein MYC-tagged ROCK1 kinase domain (upper panel). The 5 binding regions are outlined with pink, green, brown, orange, blue and red. The locations of these regions in ROCK1 are indicated in the schematic diagram (lower panel). (c) Ribbon diagram showing the N-terminal kinase interacting region 1 (red or brown) modeled onto the ROCK1 kinase domain (blue or yellow) dimer structure (PDB ID:2etr) using protein co-ordinates imported from PDB into DeepView (v4.0.1) for modeling. Images were generated following export to POV-Ray (v3.6).

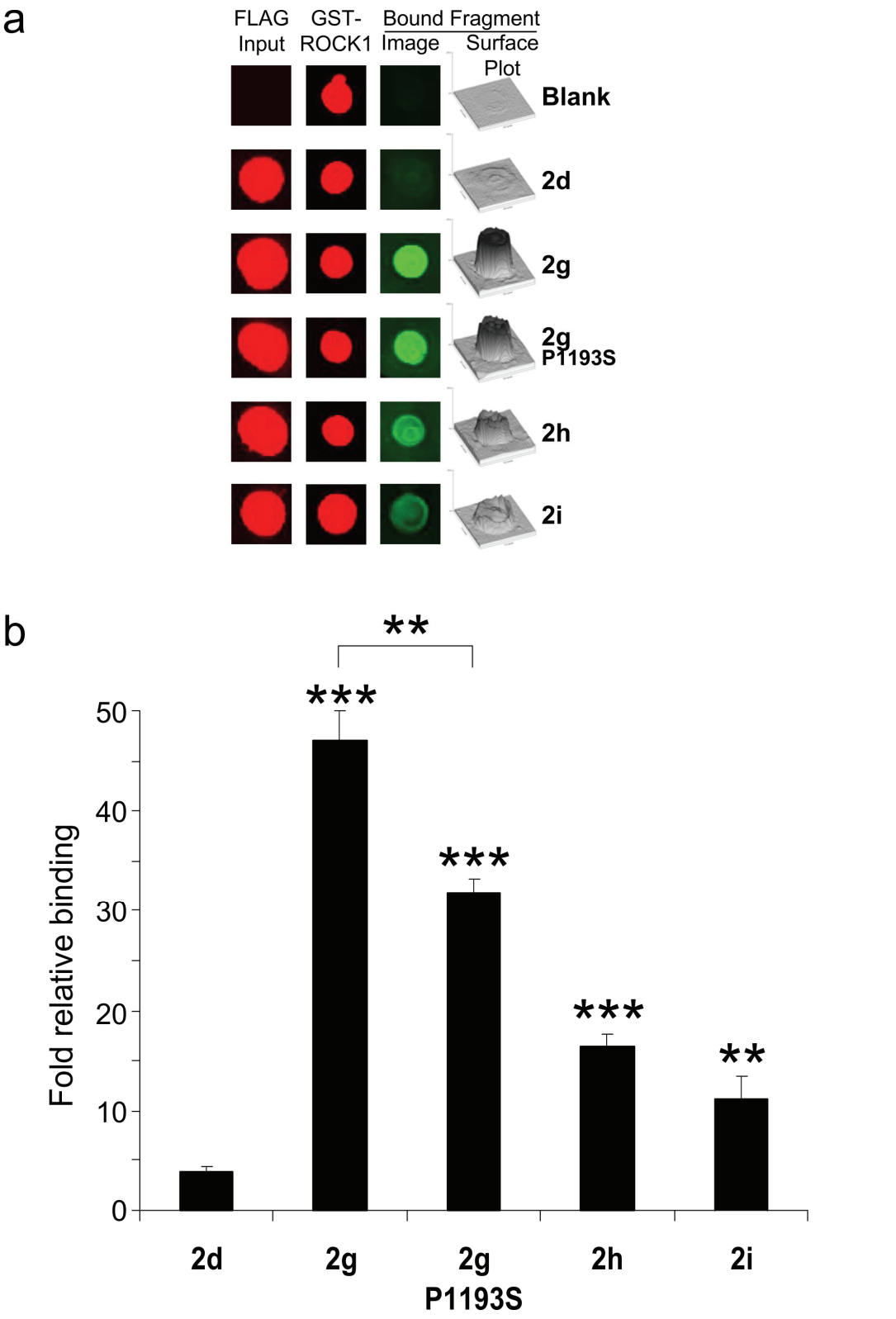

Figure 4.10. Validation of ROCK1 C-terminal interacting regions.
(a) Representative dot blots of protein fragments binding to immobilized ROCK1 kinase domain. Membranes were probed with rabbit anti-GST and mouse anti-FLAG antibodies to detect ROCK1 and FLAG-labelled binding proteins respectively. Infra-red fluorophore conjugated secondary antibodies were detected at 700 and 800 nm using a Li-Cor Odyssey. Surface plot indicates signal intensity for each condition in third dimension. (b) Mean dot blot signal intensities over blank. Statistical analysis calculated by ANOVA followed by Bonferroni's multiple comparison test (n=3-9) (*$p<0.05$ vs blank; **, $p<0.01$ vs blank, ***, $p<0.001$ vs blank).

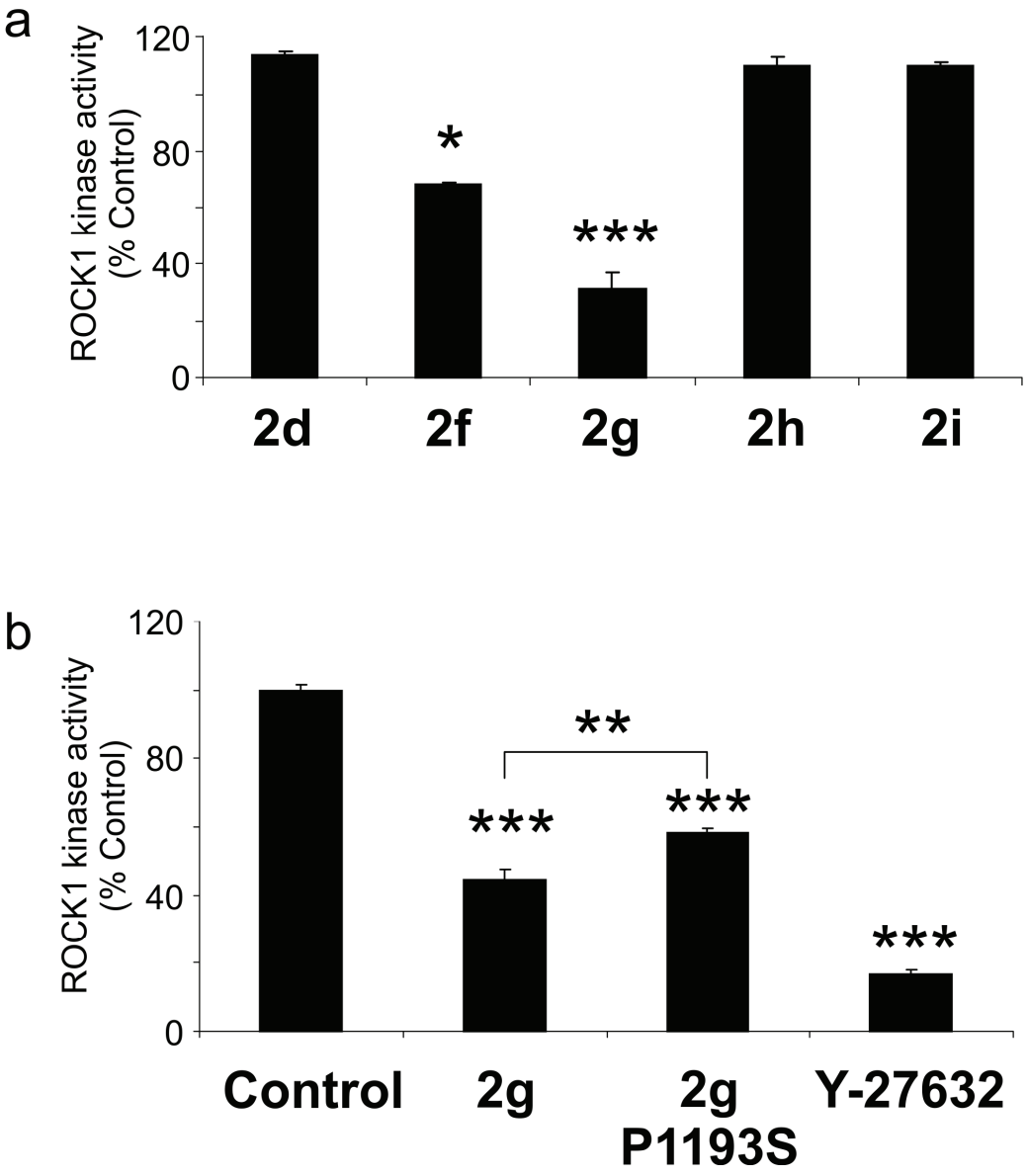

Figure 4.11. ROCK1 kinase-binding regions inhibit kinase activity.
(a) Mean ± SEM of ROCK1 activity in fluorescent polarization assay following incubation with 100 μM of the indicated synthetic ROCK1 peptides (corresponding to the following spots on the peptide array 2d (d17), 2f (f16), 2g (g15), 2h (h12), and 2i (i12)). (b) Mean ± SEM of ROCK1 activity in fluorescent polarization assay following incubation with 100 μM of the synthetic peptides 2g, 2g P1193S, and with 10 μM Y-27632. Statistical analysis calculated by ANOVA followed by Dunnett's multiple comparison test (n=2-5)(*, $p<0.05$; **, $p<0.01$ ***; $p<0.001$ vs control).

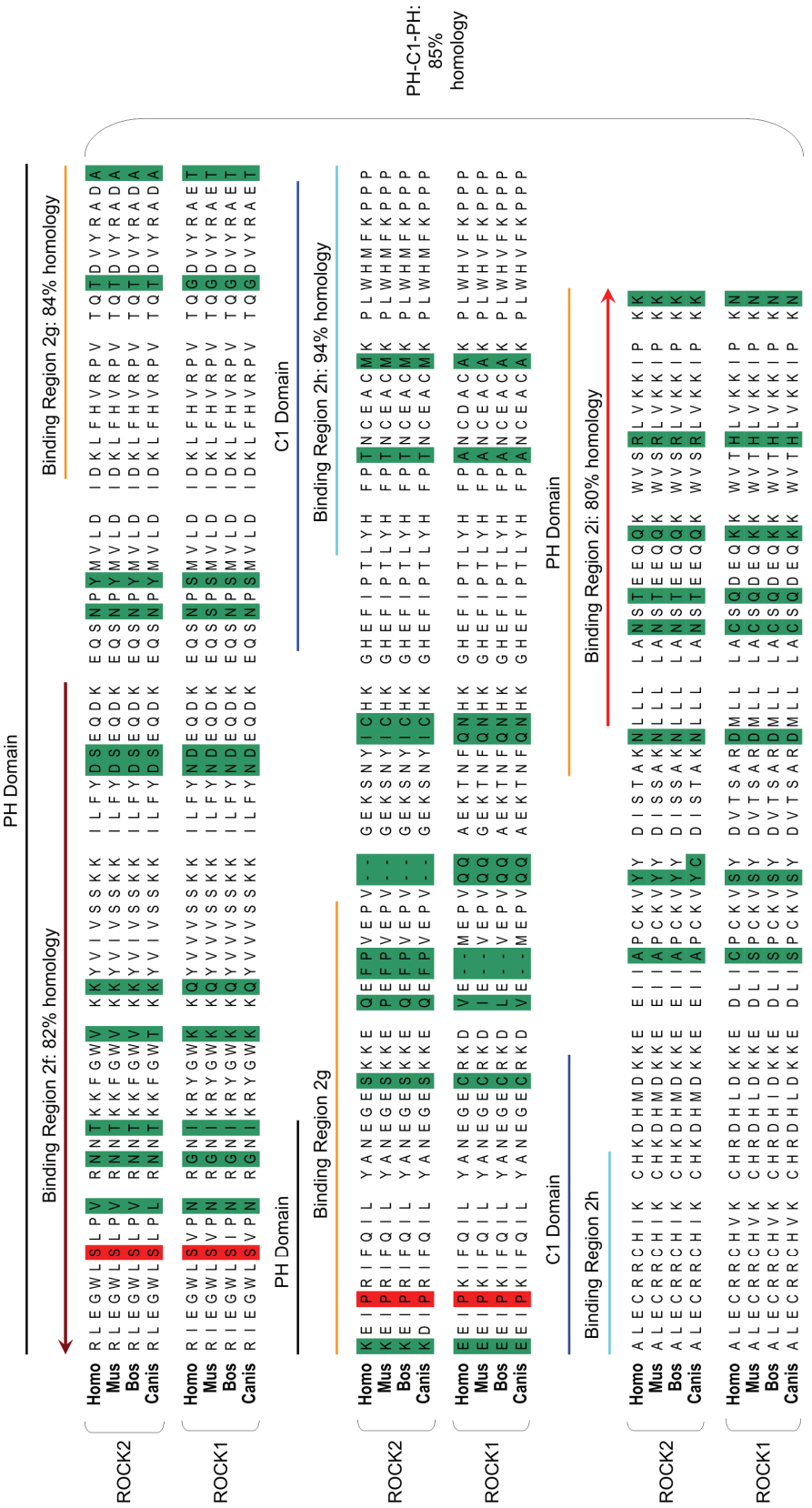

Figure 4.12. ROCK1 and ROCK2 are highly conserved in the C-terminal regulatory domain. Amino acid sequence alignment of the PH-C1-PH domains of mammalian ROCK1 and ROCK2. Non-conserved amino acids are highlighted in green. ROCK protein domains, according to ROCK1 NCBI reference sequence NP_005397, are indicated above alignment. Kinase interaction regions are indicated above alignment with percent homology. Mutated residues, S1126 and P1193, are highlighted in red.

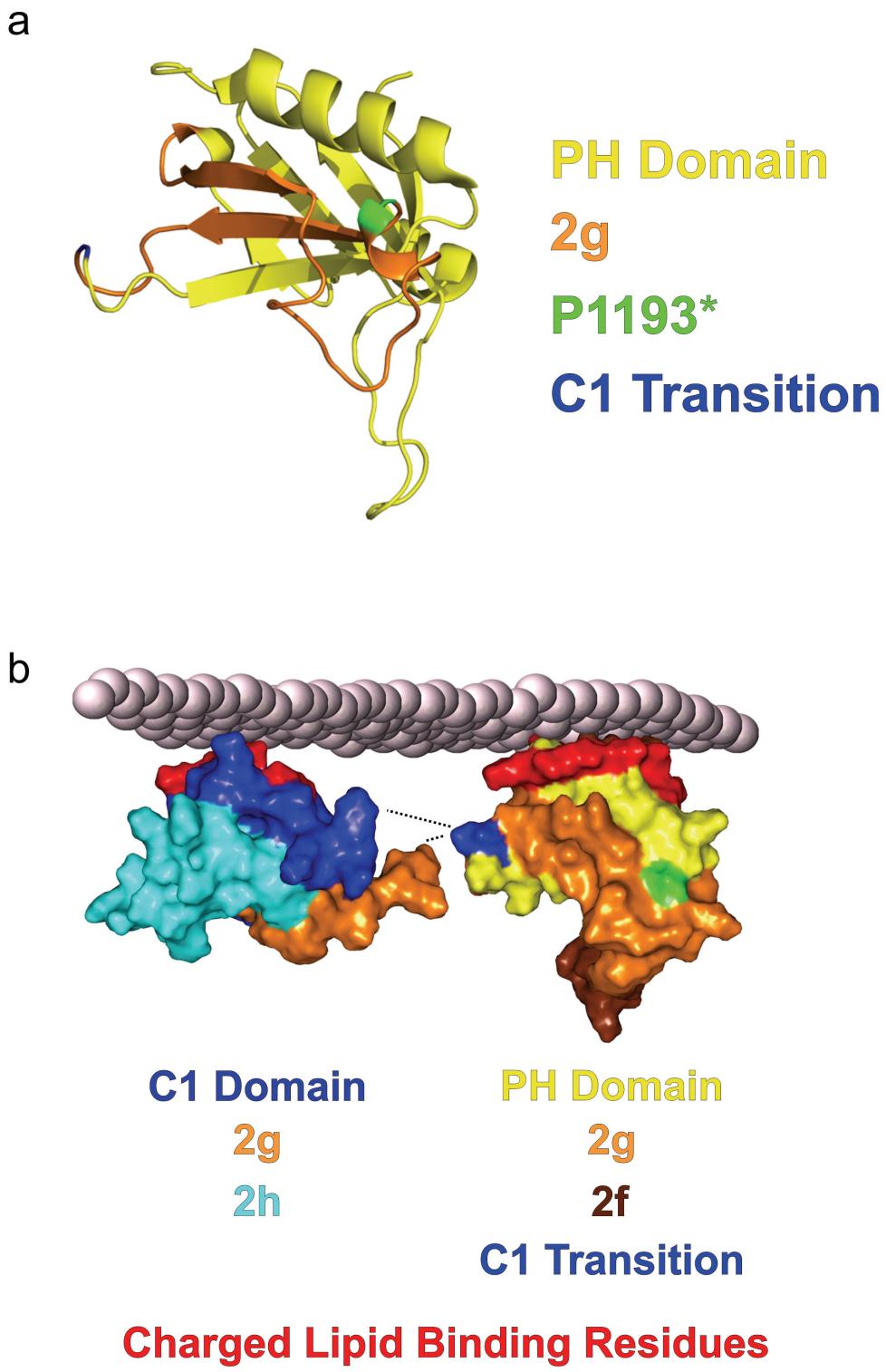

Figure 4.13. Structural modelling of the ROCK1 interacting regions.
(a) Ribbon diagram demonstrating that P1193 (green) is located between an α-helix and a β-sheet in the PH domain (yellow). A part of the kinase interacting region 2g is highlighted in orange. In full length ROCK the interrupting C1 domain would be expected to continue from the orange ribbon (2g) and re-join the PH domain at the indicated residue in blue. Residues and domains modeled and rendered onto the ROCK2 PH structure (PDB ID: 2rov) from PDB co-ordinates using Pymol. (b) Surface modelling of PH and C1 domains with predicted membrane orientation. ROCK1 binding and inhibitory domains 2g (orange), 2f (brown), and 2h (light blue) modelled onto separately solved PH (yellow) and C1 (dark blue) structures of ROCK2 (PDB ID: 2rov and 2row, respectively). Location of P1193 is indicated in green. Residues highlighted in red mediate lipid binding[260]. Charged headgroups of the inner leaflet of a phospholipid bilayer are drawn in gray. Dashed lines indicate the expected structural attachments between the PH and C1 domains. Structures were modelled and rendered in Pymol.

4.3 Discussion

In summary, the three ROCK1 mutations, Y405*, S1126*, P1193S have enhanced kinase activity, promote contraction, increase motility and decrease adhesion; indicating that these mutations are all constitutively active, consistent with them being active cancer drivers. These kinase mutations associated with cancer have revealed 2 ROCK1 mutants similar to previously characterized activating deletions; caspase-cleavage [57] and an experimentally derived truncation [53]. In addition, a novel activating single amino acid substitution was identified revealing new information about ROCK1 regulation. Mapping of the C-terminal kinase interacting regions and structural modeling has revealed that ROCK1 likely keeps kinase activity in check via interactions with multiple surfaces.

In a recent paper the phosphorylation of myosin light chain was also found to be altered in cancer cells bearing somatic mutations in death-associated protein kinase 3 (DAPK3)[261]. Expression of the kinase dead mutants of DAPK in several cancer cell lines was found to significantly decrease MLC phosphorylation, which was then associated with increased proliferation, survival, and adhesion leading the authors to conclude that somatic DAPK mutations are drivers of cancer. Although the effect on myosin light chain phosphorylation following mutant DAPK expression is the opposite of what I see with mutant ROCK1 the results are not in direct contradiction. Firstly, both kinases have multiple substrates and the importance of pMLC in the cancer promoting effects of either mutant kinase was not assessed in either report. Secondly, while I used NIH 3T3 cells almost exclusively, the DAPK3 report makes frequent use of many different cancer cell lines, any one of which, is likely to have altered signaling pathways. Finally, neither study attempts to assess the *in vivo* relevance of ROCK1 or DAPK mutation in tumour growth, survival, or metastasis. Combined these differences make a meaningful interpretation of a role for pMLC (either increased or decreased) in driving cancer impossible. Nonetheless, somatic mutation of either ROCK1 or DAPK3 does seem to promote the generation and/or progression of malignant disease.

Three somatic mutations have also been described in the ROCK2 gene in human cancers; a T to C transversion at position 3508 in the LB2518 malignant melanoma cell line that results in a S1194P substitution (equivalent to S1162 in

ROCK1) in the first PH domain, insertion of A at 3518-3519 in the CP50-MEL-B malignant melanoma cell line resulting in a frameshift and termination at Y1174* (equivalent to Y1142 in ROCK1) in the first PH domain, and deletion of T at 412 resulting in a frameshift and termination at W138* in a primary stomach carcinoma (http://www.sanger.ac.uk/cgi-bin/genetics/CGP/cosmicsearch?_q=rock2). Given the results of this study, the clustering of the Y1174* and S1194P mutations in the first PH domain suggests that they would be activating mutations, although the W138* mutation retains little of the kinase region. As previously mentioned, the activation of ROCK2 in skin epithelial cells leads to contractility dependent hyperproliferation and promotion of a cancerous 'niche' [154]. It is of particular interest that one of the ROCK2 mutations was not only found in a malignant melanoma but is predicted to lead to constitutive activation. Expression of this mutant would be expected to cause collagen deposition and mechanical feedback driving tumour proliferation and survival

There are numerous examples of kinase activation by cellular proteolysis [262], as exemplified by caspase cleavage of ROCK1 [57] and granzyme B cleavage of ROCK2 [78]. The organization of ROCK1 and ROCK2 domains containing N-terminal kinase domains and C-terminal autoinhibitory domains lends them to activation by proteolysis or by mutations that result in premature termination. Therefore, it could be predicted that other kinases organized in a similar manner would also be subjected to activating mutations that affected C-terminal regulatory regions. Indeed, the Cdc42-regulated MRCKα (aka CDC42BPA), which plays a similar role in actin cytoskeleton regulation as ROCK1 and ROCK2, has an example of a frameshift and termination at K697* in the HCC1395 breast ductal carcinoma cell line that removes autoinhibitory C1 and PH-like domains [263]. Interestingly, 4 non-synonymous mutations were identified for MRCKβ (aka CDC42BPB), all of which occur C-terminal to the kinase domain and therefore are potentially activating, with the most likely mutation to be activating consisting of a frameshift and termination at R1092* found in an intestinal adenocarcinoma tumour.

The increased activity of the ROCK1 mutations suggests independence from the upstream regulator Rho, similar to Ras-independent activating B-Raf mutations. Although the rate of ROCK1 mutations was low, these results justify screening a larger set of cancers to determine a more representative rate and indentify

additional mutations. Furthermore, these observations additionally validate the value of high-throughput sequencing for identification of new cancer genes, and for providing valuable unbiased insight into protein regulation and function.

5. Materials and Methods

5.1 Chapter 2 methods

5.1.1 ROCK1nc knock-in animal generation

5.1.1.1 Home office project and personal licensing

All animal work reviewed and approved of in project and personal licenses issued by the UK Home Office.

5.1.1.2 Targeting vector generation

The 5.1 kb 3' homology arm for targeting ROCK1 was isolated from a BAC clone containing the murine ROCK1 gene by gap repair recombineering in DY380 cells as described by [264]. BAC clones were from the Sanger AB2.2 mouse genomic DNA library (representative of the mouse 129 strain) and identified as: 107N12, 208K1 and 459E7.

A retrieval vector was generated by PCR-amplifying short (approximately 500bp) arms that represent the extreme ends of a larger target sequence (in this instance, the 5.1 kb 3' homology arm) and sub-cloning these into pCR-blunt 2.1 (Invitrogen) in such a way that the adjacent sequences were separated by an *Asc*I site to allow linearization of the vector between the amplified arms.

DY380 cells carrying the target BAC were grown at 30C to an OD600 of 0.5-0.6 then shifted to 42°C for 15 minutes to heat-shock induce lambda phage recombination proteins which drive the retrieval. Heat-shocked cells were harvested and washed twice in sterile distilled H_2O. Pelleted cells (25µl) were resuspended in residual H2O then mixed with 50-100 ng (5ul volume max) of the gel-purified, *Asc*I-linearised retrieval vector. Following, electroporation, the bacterial cells were allowed to recover by shaking at 30°C in 900ul SOC then plated on LB-agar plates supplemented with ampicillin (the antibiotic-resistance in the backbone of the retrieval vector).

The 3.1 kb 5' homology arm of ROCK1 proved refractory to recombineering and was generated from BAC DNA by high fidelity PCR amplification. An amino acid point mutation aimed at making the resultant ROCK1 caspase-resistant was then

introduced into exon 27 of the ROCK1 gene using a mutated oligonucleotide primer with Stratagene QuickChange II XL site-directed mutagenesis kit.

The mutated plasmid was sequenced to confirm the introduction of the desired mutation (which generated a novel *Pst*I restriction site) and the conservation of other exons within the fragment. In sequencing, a number of polymorphisms were identified in the 129 strain-derived genomic DNA (confirmed by sequencing from independent PCR products from tail DNA) relative to the C57Bl/6 DNA sequence archived by Ensemble. Two changes were identified within exon 27 and were conservative with reference to the encoded amino acid sequence. The 5' and mutated 3' arms were cloned directionally into pDupDel Neo (gift of Prof. Oliver Smithies and available commercially from Open Biosystems) using restriction sites introduced during PCR cloning and recombineering respectively. This placed the mutated exon 27 proximal to the selection cassette to decrease the chance of loss of the mutation during homologous recombination (Figure 2.1). Since pDupDel Neo contains a high activity form of the neomycin resistance gene, the original selection cassette was removed by Cre deletion in EL350 cells [264] and a low activity version (expressed from a PGK/EM7 hybrid promoter) from pL452 [265] was inserted by the reverse process and selection on kanamycin. The resultant targeting vector was linearised with *Not*I restriction enzyme in preparation for transfection of mouse embryonic stem cells. This work was performed by the Beatson Institute Transgenic Technology core service.

5.1.1.3 Mouse embryonic stem cell (mES) vector transfection

G4 murine embryonic stem cells (gift of Dr. Andras Nagy and Marina Gertsenstein [266]) were grown under ES medium (DMEM (high glucose), 15% FBS, 2mM Glutamax, 0.1 mM non-essential amino acids, 0.1 mM β-Mercaptoethanol 1000 U/ml ESGRO (Millipore), 33 μg/ml Gentamycin) on mouse embryonic fibroblast (MEF) feeder layers. Cells were harvested from two T175 flasks 24hrs after their final split and plated for 20 minutes to remove the majority of MEFs. Cells were pelleted, washed once with PBS and counted.

Following resuspension in room temperature Embryomax transfection buffer (Millipore) at $1x10^7$ cells/ml, five volumes of $8x10^6$ cells were mixed with 40μg of linearised targeting vector and the mixtures transferred to 4mm electroporation

cuvettes (Biorad) before electroporation at 250V, 500μF and infinite resistance. After recovery at room temperature for 20 minutes, cells were washed out of the cuvettes with regular ES medium and the contents of each cuvette split across four 10cm plates of MEFs. After 24 hrs, medium was changed to ES medium supplemented with 240 μg/ml G418. The plates were maintained under this medium (with daily changes) for 6 days.

Colonies selected for G418 resistance were picked onto five 96-well plates of MEFs and grown under selection for 3 days. Plates were then archived for subsequent recovery and cells grown on parallel gelatinized plates. 96-well plates containing expanded ESC colonies were washed twice with 200μl PBS per well and 50μl of trypsin added. Following 5 minutes at 37^{o}C, cells were pipetted up and down then 50μl of ES medium added to terminate trypsinisation. A 50μl volume of trypsinised cells was transferred to a parallel round-bottomed 96-well plate containing 50μl of 2x freezing medium (40%FBS-40% ES medium-20% DMSO) to act as a master-plate. The plate was overlaid with 100μl of embryo-tested mineral oil, sealed and frozen in a polystyrene box at -80 ^{o}C before transfer to liquid nitrogen storage. The remaining trypsinised cells were transferred to gelatinized plates prepared thus: 50μl of 0.1% (w/v) porcine gelatin in PBS was applied to each well of a 96-well plate and allowed to stand at RT for 20 minutes. After this time, the plate was drained and 50μl of ES medium added. Cells from the trypsinised 96-well plate were transferred to the parallel gelatinized plate with additional ES medium (up to a final volume of 250μl) and allowed to grow for 4 days whereupon the medium was yellowed. The plates were then drained and washed twice with PBS. 50μl of lysis buffer (10mM Tris.HCl, pH 7.5, 10mM EDTA, 10mM NaCl, 1mg/ml proteinase K, 0.5%(w/v) SDS) was added to each well, the plates sealed with adhesive sheets and incubated in a humidified chamber at 55 ^{o}C overnight. The genomic DNA was precipitated by the addition of 100μl of ice-cold ethanol-salt mix (75 mM NaCl in 100% ethanol) to each well. Plates were allowed to stand for a minimum of 1 hour at room temperature before being drained by careful inversion onto paper towels. The plate was then washed three times with 200μl/well of 70% ethanol and allowed to air-dry for 20-30 minutes. This work was performed by the Beatson Institute Transgenic Technology core service.

5.1.1.4 mES screening for homologous recombination

Screening of neomycin resistant mES cells for homologous recombination was accomplished with separate PCR reactions against the 3' and 5' homology arms of the insert vector. Spotted genomic DNA was diluted in 50 ul TE buffer (Tris 10mM pH 8.0, and EDTA 1mM) for 24 hours at 37°C and then screened, remaining DNA was re-frozen. The primary screen tested recombination in the 3' targeting vector homology arm and used primers within the neomycin selection cassette and outside the homology arm (Figure 2.2), this reaction is expected to yield a 3.5 kb product in correctly recombined samples. PCR reaction used 200 ng template DNA, 1 unit Phire hotstart DNA polymerase (Finnzymes), 0.2 mM dNTP, and 1 μM primers. Positive samples were re-analysed. Samples verified positive for 3' recombination were then tested for 5' homology arm recombination and used primers outside the homology arm and within the neomycin selection cassette (Figure 2.3). This secondary screening reaction is expected to yield a 5.5 kb product in correctly recombined samples. PCR reaction used the Expand high fidelity PCR system (Roche) with 400 ng template DNA, 1 unit polymerase, 0.5 mM dNTP, and 500 nM primers. All PCR reactions were examined for product by agarose gel electrophosesis visualized with ethidium bromide. Product size was estimated from DNA ladders (Hyperladder I, Bioline). Successfully targeted clones were then expanded and stocks generated for subsequent injection into mouse blastocysts.

5.1.1.5 mES blastocyst injection and embryo implantation

Targeted stem cells were grown on MEF monolayers and harvested for injection following plating out of MEFs. Stem cells (8-15) were injected into C57Bl/6 blastocysts and then implanted into the uteri of pseudo-pregnant female ICR mice. Male chimeras of high ESC contribution were identified in the subsequent litters by coat colour. These were crossed with C57Bl/6 females and the offspring genotyped for ROCK1nc. Genotypically positive mice were then crossed to a Cre-deleter strain (on a C57Bl/6 background) to remove the neomycin selection cassette. Mice homozygous for ROCK1nc were then interbred to generate a homozygous strain for use in our proposed studies. This work was performed by the Beatson Institute Transgenic Technology core service.

5.1.1.6 Animal genotyping

For routine genotyping the animals were tail clipped at weaning and samples sent to Transnetyx genotyping service for analysis.

5.1.2 In vitro ROCK1 kinase assay

ROCK1 kinase assays were performed with purified full length MYC-tagged wild type and D1113A ROCK1 expressed in HEK 293T cells. These MYC-tag ROCK1 constructs were generated as previously reported [73]. Briefly, confluent HEK 293 cells were transfected with 10 μg of plasmid with lipofectamine2000 (Invitrogen) in 10 cm plates and incubated at 37°C for 24 hours. Control sample had no plasmid transfected. The transfected cells were then washed, collected, and lysed with RIPA buffer. Anti-MYC-tag antibody was added to approximately 450μg of cellular lysate overnight at 4°C. Protein bound to antibody was precipitated with protein G sepharose and washed in kinase wash buffer (50 mM Tris pH 7.5, 10 mM $MgCl_2$, 0.1 mM PMSF, 1 mM Na Vanadate, 50 mM NaCl, 1 mM DTT, 10% glycerol, 0.03% Brij-35) divided into 4 20 μl aliquots and frozen at -20°C. Uniformity of protein expression was determined by Coomasie staining of PAGE gels. 200 ng of purified BSA was loaded on gel to verify protein concentration. Kinase activity was then analysed with a fluorescence polarization assay. Briefly, 200 ng of MYC-tagged ROCK1 in kinase buffer was supplemented with 100 μM ATP and 500 nM Fluorescein-tagged ROCK1 peptide substrate derived from S6Kinase (5FAM-AKRRRLSSLRA). The reaction was incubated for 1 hour at room temperature in a plate shaker. Following incubation 1:400 dilution of IMAP binding reagent (Molecular Devices) in kinase buffer was added and further incubated for 1 hour at room temperature on plate shaker. Kinase activity was then determined by reading fluorescence peptide polarisation in a Tecan Safire^2 multimode microplate reader by exciting the sample at 470 nm and measuring the emission at 525 nm.

5.1.3 Mouse embryonic fibroblast (MEF) generation

MEFs were generated from E13.5 embryos resulting from homozygous ROCK1wt and ROCK1nc breeding pairs. The appearance of the mating plug indicates embryonic day 0.5 (E0.5) and 13 days later the pregnant females are euthanized by cervical dislocation and uterine horns containing embryos extracted. Further dissection of the embryos takes place in laminar flow hood to minimize bacterial

contamination. Briefly, the embryos are dissected from the uterus and washed in PBS. Embryonic heads and livers were removed and sent for genotyping. The remaining tissue from all embryos was pooled and roughly chopped before incubation in 0.05% trypsin (1ml trypsin/embryo) for 10 min at 37°C. Embryos were then further dissociated by trituration in serological pipettes of decreasing size, then counted and plated at $5x10^6$ cells in a 180 cm flask. Cells were cultured in DMEM supplemented with 10% FBS, penicillin/streptomycin (100 units/ml, 100 μg/ml, respectively) and maintained at 37°C in 5% CO_2 atmosphere. Cells were split twice before cryopreservation. Typically ROCK1wt and ROCK1nc MEF cultures proliferated to passage 8-10 before senescing. No difference in proliferation rate or senescing age was seen in either ROCK1 genotype.

5.1.4 Microscopy

5.1.4.1 Fluorescent

After plating on glass coverslips ROCK1wt and ROCK1nc MEFs were serum starved overnight then treated with 10% FBS for 5 min ± 10 μM Y27632. The cells were then fixed and permeabilized with paraformaldyhyde with 0.5% triton X-100 at room temperature for 5 min before washing and staining. Following fixation the samples were blocked with 1.5% BSA and 10% normal goat serum in PBS for 10 min. Fixed cells were probed with rabbit anti-phosphorylated myosin light chain (pMLC) (thr18/ser19) antibody (cell signaling) diluted 1:100 in blocking buffer for 1 hour at room temperature. Following washing the cells were stained with anti-rabbit IgG antibody conjugated to Alexa Fluor 488 (1:1000, Invitrogen) and f-actin filaments were visualized with Texas Red conjugated phalloidin (1:250, Invitrogen) in PBS. Samples were then washed and mounted with Vectashield hard set mounting medium with DAPI (Vector labs). Fluorescent microscopic images were acquired with a 60x oil immersion lens on an Olympus FV1000 laser scanning confocal microscope.

5.1.4.2 Timelapse

ROCK1wt and ROCK1nc MEFs were plated on glass bottom dishes (Iwaki) then serum starved overnight prior to induction of apoptosis with TNFα and cycloheximide (CHX) (50 ng/ml and 10 μg/ml, respectively). Bright field differential interference contast (DIC) time-lapse microscopy images were acquired with a 20x

objective using a Nikon Eclipse Ti microscope with a heated stage and 5% CO_2 gas line. Immediately after induction of apoptosis the cells were relocated to the microscope and time lapse images were taken every 30-60 seconds for several hours.

5.1.5 In-cell western blot

MEFs (50,000/well) were plated in a 96 well plate and then serum starved overnight before stimulation with 10% FBS for 5 min ± 10 μM Y27632. Staining for pMLC was performed as previously described. Total cell number was determined by nuclei staining with the fluorescent marker DRAQ5 (1:700, Biostatus). Fluorescence was determined by imaging the plate with an Odyssey LiCOR scanner and signal intensity with Odyssey software. pMLC signal was normalized to DRAQ5 signal.

5.1.6 Western blot

Apoptotic ROCK1wt and ROCK1nc MEFs were generated with TNFα and CHX as previously indicated. Four hours after treatment the cells were collected by scraping centrifuged and lysed in RIPA buffer (10 mM TRIS pH 7.5, 5 mM EDTA, 150 mM NaCl, 40 mM NaPPi, 50 mM NaF, 1% (v/v) NP-40, 0.5% (v/v) sodium deoxycholate, 0.025% (w/v) SDS, 1mM Na_3VO_4, 1 mM PMSF). Samples were then normalized to total protein concentration determined by Bradford colorimetric assay (BCA) and separated on a 10% SDS-PAGE gel. Gel was then transferred to nitrocellulose blotting paper and blocked with BSA. Multiple membranes were probed for ROCK1 (BD-transduction labs), PARP (BD Pharmingen), pMLC (Cell Signaling), and α-tubulin as a housekeeping protein (Santa Cruz). Antibody binding was visualized with fluorescent secondary antibodies using an Odyssey LiCOR scanner.

5.1.7 Flow cytometry

Apoptotic MEFs were generated as indicated. After 24 hours samples were collected, centrifuged, and diluted to 1e5 cells/ml in a total volume of 100 μl in binding buffer (100 mM HEPES pH 7.4, 140 mM NaCl, 2.5 mM $CaCl_2$) prior to staining with with 5 μg/ml PI and 5 μl commercial annexin V-alexafluor 488 conjugate for 10 min at room temperature. Samples are then diluted to 0.5 ml in

binding buffer then 10,000 apoptotic cells were gated using forward (FSC) and side scatter (SSC), PI and annexin fluorescence determined in channel FL1 and FL3. Quadrant gating was determined from stained non-apoptotic NIH 3T3 sample.

5.1.8 Histological tissue collection, fixation, processing, and staining

Animals were euthanized by either cervical dislocation or rising concentrations of CO_2 and tissues were rapidly dissected and fixed by immersion in 10% buffer formaldehyde. Fixed tissue was then processed by histology core service (paraffin embedding, sectioning, and stained). Prior to staining the samples are de-waxed in xylene and re-hydrated in 97% ethanol then washed in tap water. Samples were then stained with haematoxylin and eosin (H&E) and Perls prussian blue. Perls Prussian blue stain uses an equal part solution of ferrocyanide and hydrochloric acid for 10 min before washing and counterstaining with eosin. In addition, fixed tissue sections were also probed for the presence of cleaved caspase 3, mouse IgG, and F4/80 antigen (mouse macrophages) with specific antibodies. Cleaved caspse 3 is detected in fixed spleen following antigen retrieval with commercial proteinse K solution (DAKO) for 5 minutes and incubation with rabbit anti-cleaved caspase 3 antibody (1:200, Abcam) for 1 hour at room temperature. Cleaved caspase 3 is then visualized with commercial vectastain anti-rabbit IgG (Vector Labs) ABC immunoperoxidase kit which produces a brown precipitate on sample. Samples are then counter stained, dehydrated and mounted. The presence of mouse IgG in fixed kidney sections was detected directly with anti-mouse IgG antibodies conjugated to Alexa Fluor 488 (Invitrogen) and then mounted in vectashield hard set mounting medium with DAPI (Vector Labs). Mouse macrophages were detected in fixed spleen by staining with rat anti-F4/80 (1:100, Abcam) in PBS for 30 minutes at 37°C following proteinase K antigen retrieval. F4/80 antibody binding was detected with commercial vectastain anti-rat IgG (Vector Labs) ABC immunoperoxidase kit. Samples are then counter stained (haematoxylin), dehydrated and mounted.

5.1.9 Haematology

After CO_2 euthanasia 0.5 ml whole blood was withdrawn from descending abdominal aorta and dispensed in clinical potassium-EDTA tube. Samples were

then immediately sent to clinical veterinary pathology lab at the University of Glasgow Veterinary School for a complete clinical haematology analysis.

5.2 Chapter 3 methods

5.2.1 Cell culture

NIH 3T3 cells were maintained in DMEM supplemented with 10% donor bovine serum. Murine RAW 264.7 macrophages were maintained in DMEM supplemented with 10% fetal bovine serum.

5.2.2 Western blot

Cell lysates were generated with RIPA lysis buffer (10 mM TRIS pH 7.5, 5 mM EDTA, 150 mM NaCl, 40 mM NaPPi, 50 mM NaF, 1% (v/v) NP-40, 0.5% (v/v) sodium deoxycholate, 0.025% (w/v) SDS, 1mM Na_3VO_4, 1 mM PMSF). Cell lysates and concentrated conditioned medium was diluted 1:4 with sample buffer and warmed to 70 °C for 10 min. Samples were run on 10% SDS-polyacrylamide gels, transferred to polyvinylidene fluoride membranes blocked in 5% (w/v) skim milk in TBS prior to probing with anti-GFP (BD Biosciences), anti-gelsolin (Abcam), anti-HMGB1 (Cell Signaling), anti-actin (Santa Cruz), anti-ROCK1 (Transduction Labs). Primary antibodies were probed with alexafluor 680 (Invitrogen) and IR800 (Rockland) conjugated secondary antibodies and analysed using LiCOR-odyssey. Band intensity analysed using odyssey application software.

5.2.3 Creation of membrane tagged GFP expressing NIH 3T3 cells

Generation of ecotropic virus for CaaX-GFP transduction was carried out as previously described [267]. NIH 3T3 cells were infected with 1 ml of virus and 4 μl polybrene (4 mg/ml) overnight. The next day the medium was replaced and cells selected with puromycin. GFP fluorescence was verified by FACS.

5.2.4 Induction of apoptosis, and generation of conditioned medium

NIH 3T3 apoptosis was induced with a combination of 50 ng/ml tumour necrosis factor alpha (TNFα)(R&D Systems)) and 10 μg/ml cycloheximide (CHX)(Sigma), unless otherwise indicated, and diluted in unsupplemented DMEM medium following an overnight starvation. Cells were then incubated at 37°C for 2-24

hours. Medium was further supplemented with: Y27632 (10 μM)(EMD), blebbistatin (50 μM)(Tocris), z-VAD-fmk (20 μM)(R&D Systems) where appropriate.

Apoptotic cell conditioned medium (AC-CM) was generated by pelleting apoptotic cells in media at 2000x gravity for 10 min. AC-CM was routinely determined to be clear of cells and debris by microscopic examination. Necrotic cell supernatant was generated from starved cells by 3 freeze thaw cycles in dry ice. AC-CM was concentrated by centrifugation with 10 kDa cutoff Millipore centrifugal filter units at 4500x gravity for 30 min. Samples were concentrated approximately 30 fold. Prior to concentrating, 0.260 μg of recombinant GFP was added to each sample as an internal standard.

5.2.5 Microscopy

Timelapse microscopy images were acquired with a 20x objective using a Nikon A1R confocal microscope with a heated stage and 5% CO_2 gas line. Grey scale image is transmitted light. Cells were grown on optical glass coverslips and apoptosis was induced in starve medium supplemented with TNFα, CHX and 5 μg/ml propidium iodide (PI). Immediately after induction of apoptosis, cells were relocated to confocal microscope and time lapse images were taken every 30 seconds for 8 hours in both transmitted light and red fluorescence.

High resolution still images of unfixed apoptotic cells were acquired with a 60x oil immersion objective using same conditions as above. The medium was further supplemented with FAST DiO (3,3'-dilinoleyloxacarbocyanine perchlorate) diluted 1:500 from 2.5 mg/ml dissolved in 100% DMSO.

5.2.6 Flow cytometry

5.2.6.1 Apoptotic body PI permeability

For the assessment of apoptotic body PI permeability 4 hour apoptotic NIH 3T3 samples were generated with the further addition of 5 μg/ml PI (Sigma), 100 μg/ml RNaseA (Qiagen), and/or 200 units/ml DNase1 (Roche). Non-apoptotic NIH 3T3 cells were collected following trypsinization, quenched in growth medium and used as control. Apoptotic samples were analysed with a BD FACSCalibur flow

cytometer. 100,000 apoptotic bodes were gated using forward (FSC) and side scatter (SSC), and PI fluorescence determined in channel FL3. PI stained non-apoptotic control was used to gate samples.

5.2.6.2 Apoptotic body proteinase K permeability

Apoptotic body proteinase K permeability was assessed in NIH 3T3 cells expressing membrane tagged GFP. 2 hours after addition of TNFα and CHX, proteinase K (50 μg/ml) (Melford) was added to the cells and incubated for a further 2 hours. The apoptotic samples were analysed with a BD FACSCalibur flow cytometer. 100,000 apoptotic bodes were gated using forward (FSC) and side scatter (SSC), and GFP fluorescence determined in channel FL1. GFP positive apoptotic bodies gated against non-GFP expressing apoptotic bodies.

5.2.6.3 Apoptotic body generation

The generation of apoptotic bodies from NIH 3T3 cells at 4 hours was assessed following treatment with TNFα, CHX, and Y27632 (10 μM) or blebbistatin (50 μM). Apoptotic samples were collected, diluted 2:3 in PBS and an equivalent volume of FITC-calibrite beads added to each sample. Apoptotic bodes were gated on forward (FSC) and side scatter (SSC). FITC beads were gated based on fluorescence. The number of apoptotic bodies is counted alongside 10,000 gated FITC beads.

PI permeability of apoptotic bodies generated in the presence of Y27632 and blebbistatin was assessed following the addition of PI to the sample and incubating for 10 min at room temperature. PI fluorescence of 25,000 apoptotic bodies for each treatment was scored in channel FL3. PI stained non-apoptotic control was used to gate samples.

5.2.6.4 Apoptotic cell permeability

Apoptotic NIH 3T3 samples were generated as indicated. After 4 hours samples were incubated with 5 μg/ml PI and 5 μl annexin V-alexafluor 488 conjugate (Invitrogen) for 10 min at room temperature. 10,000 apoptotic cells were gated using forward (FSC) and side scatter (SSC), PI and annexin fluorescence

determined in channel FL1 and FL3. Quadrant gating was determined from stained non-apoptotic NIH 3T3 sample.

5.2.7 Lactate dehydrogenase activity measurements

LDH activity measured with Roche cytotoxcity detection kit according to manufacturers recommendations. After concentration, the samples were diluted 1:10 in DMEM prior to LDH activity measurement. After normalization to GFP, as determined by western blot, 100 μl of sample mixed with equal concentration of dye solution and incubated for 20 min in the dark in 96 well plate. Reaction stopped with 50 μl stop solution and solution absorbance measured with TECAN safire2 at 490 nm. Sample activity expressed as a percentage of activity detected in necrotic sample.

5.2.8 SILAC

NIH 3T3 cells were grown in DMEM supplemented with dialysed FBS containing specific labeled arginine (Arg) and lysine (Lys) amino acids for 5 passages. Cells were labeled with light/unlabeled (Lys-0, Arg-0), medium (Lys4, Arg6), and heavy (Lys8, Arg10) medium. Amino acids are labeled with the following isotopes: Lys4, $^{2}H_4$; Lys8, $^{13}C_6$, $^{15}N_2$; Arg6, $^{13}C_6$; Arg10, $^{13}C_6$, $^{15}N_4$ (Silantes). Label incorporation was determined to be >95% by mass spectrometry. Labeled populations of labeled NIH 3T3 assigned the following treatments: Light, control; Medium, TNFα+CHX; Heavy, TNFα+CHX+Y27632. After 4 hours the supernatant was processed and concentrated as mentioned. Samples were normalized to GFP internal standard by western blot and 10 ml of each sample was mixed and run on 10% SDS-PAGE. The gel was stained with Coomassie and destained in acetic acid. Gel was then processed and subjected to mass spectrometry and database search by Beatson Institute Mass Spectometry Service staff, Willie Bienvenut, Sergio Lilla, and David Sumpton.

5.2.9 Gelsolin knockdown

Gelsolin was knocked down by nucleofection of NIH 3T3 cells with Dharmacon on-target plus smart pool against mouse gelsolin (L-057211-00-0005). $1x10^6$ cells were transfected in solution R with 3 μg non-targeted or gelsolin siRNA. After nucleofection the cells were incubated in DMEM+10% FBS for 72 hours prior to

induction of apoptosis. 60-70% gelsolin knockdown was typically observed by western blot.

5.2.10 RAW 264.7 transwell migration

AC-CM was generated from NIH 3T3 at 4 hours after induction of apoptosis with or without gelsolin knockdown by siRNA nucleofection. AC-CM was used as a chemoattractant for $5x10^5$ Raw264.7 macrophages in starve medium were seeded in the top chamber of 8 μm transwell insert. Cells were incubated for 2 hours at 37°C and then fixed with ice cold methanol, cells that failed to migrate were removed by swab. Migrated cells were stained with PI (5μg/ml) and then quantitated by counting migrated macrophages in 3 random fluorescent microscopy fields (10x).

5.3 Chapter 4 methods

5.3.1 Cell culture, transfections and plasmids

NIH 3T3 cells were maintained and transient transfections were performed as described previously (Coleman et al., 2001). For Nucleofection, cells were prepared according to the Amaxa™ protocol.

pCAG MYC ROCK1 was described previously [57] and mutations were introduced using QuikChange (Stratagene) site-directed mutagenesis kit according to manufacturer's protocol.

5.3.2 Cell extraction and immunoblotting

Whole cell lysates were prepared and western blotted as described previously [57]. Rabbit anti-MYC 9B11 (Cell Signaling Technology) and Alexa-Fluor680 (Molecular Probes) antibodies were used and detected by infra-red imaging (Li-Cor Odyssey).

5.3.3 Immunoprecipitations and kinase assays

MYC-ROCK1 was immunoprecipitated from transfected NIH 3T3 cells with rabbit anti-MYC antibody and Protein G Sepharose (Sigma) for 2 h at 4 C, beads were washed 3x with lysis buffer. Immunoprecipitated ROCK1 was assayed at 30°C for 10 min in a total volume of 50 μl containing 50 mM Tris/HCl, pH 7.5, 0.1 mM

EGTA, 0.1% (v/v) 2-mercaptoethanol, 10 mM $MgCl_2$, 0.1 mM [γ-32P]ATP (2×106 c.p.m./nmol) and 50 μM LIMKtide (LKKPDRKKRYTVVGNPYWMA). The reaction was stopped by spotting onto p81 paper and submerging in 1% (v/v) orthophosphoric acid. The papers were washed 3 times, dried and Cerenkov counted.

5.3.3.1 Fluorescence polarization ROCK1 kinase assay

50 ng recombinant GST-ROCK1 fusion (Invitrogen) was incubated with 100nM Fluorescein-tagged ROCK1 peptide substrate derived from S6Kinase (5FAM-AKRRRLSSLRA), 100 μM ATP and 100 μM of interacting peptides or Y-27632 as indicated in a total 50μl kinase buffer (10mM Tris/HCl pH 7.2, 10mM $MgCl_2$, 0.05% $NaNO_3$ and 0.1% Phospho-free BSA). The reaction was incubated for 30-45 minutes at room temperature in a plate shaker. Following incubation 65 μl of 1:400 IMAP binding reagent in kinase buffer was added to each well. The mixture was further incubated for 30min at room temperature with gentle shaking then fluorescence polarisation was read in a Tecan Safire^2 multimode microplate reader by exciting the sample at 470nm and measuring the emission at 525nm.

5.3.4 Peptide arrays

In vitro transcribed and translated (IVTT) [^{35}S]-Methionine-labeled ROCK1 was generated from pcDNA3 using the TNT kit (Promega) according to the manufacturer's protocol. 21-mer peptides offset by 2 amino acids covering amino acids 1-75 and 853-1354 of human ROCK1 were arrayed onto membranes (Cancer Research UK, London, UK). Arrays were blocked in 5% (w/v) bovine serum albumin/Tris-buffered saline (BSA/TBS) for 1 h prior to incubation with 50 μl [^{35}S]-Methionine labeled IVTT ROCK1 in 5% (w/v) BSA/TBS for 1 h. Membranes were washed three times in TBS/0.1% (v/v) Tween, dried and exposed to film.

5.3.5 Immunofluorescence

Following nucleofection the cells were incubated for 3 hours in growth medium and then serum starved overnight. Cells were fixed and stained as described previously [57]. Confocal images were obtained using an Olympus FV1000 using a 60x oil-immersion objective.

For cell size, 6 random fields of MYC-tag positive fluorescence cells were captured per treatment with a 20x objective, subsequently the images were analysed for percentage MYC-tag positive area divided by cell number.

For cell morphology, 6 random fields of MYC-positive and actin were captured per treatment with a 10x objective and the number of cells with spread, contracted or rounded morphology were determined.

5.3.6 FACS expression

After transfection, cells were incubated overnight in growth medium (DMEM supplemented with 10% FBS). The following day the cells were collected and fixed in 2% paraformaldehyde for 10 minutes. Cells were then washed and permeabilized with 0.1% Triton X-100 for 5 minutes. MYC-tagged ROCK1 constructs were detected with an anti-MYC (9B11) antibody conjugated with AlexaFluor 647. 10,000 events were collected on a BD FACScaliber and MYC-tag positive cells were gated against blank transfected cells.

5.3.7 Protein fragment production

The binding peptide sequences were amplified by PCR from wild type pCAG ROCK1 constructs and subcloned into modified p-GEX-6-P1 expression vector containing a FLAG sequence. The P1193S mutation was introduced within the 2g construct using the quickchange XL site directed mutagenesis kit. The expression vectors were then used to transform BL21 e-coli strain. Peptide expression was induced with 0.1 mM IPTG from 5-18 h. Following bacterial lysis the samples were centrifuged to remove debris at 10000 g for 20 min, the supernatant was then mixed with PBS equilibrated glutathione-sepharose beads overnight at 4C. The beads were then washed 5x in PBS and finally re-suspended in protease buffer (50 mM TRIS-HCL, 150 mM NaCl, 1 mM EDTA, 1 mM DTT pH 7.0), the expressed peptides were then liberated from GST by cleavage with an overnight incubation at 4°C with PreScission protease (GE Life Sciences). Following cleavage the supernatant was collected by centrifugation and the protease removed with p-aminobenzamidine beads. The resulting protein was assessed by coomasie staining of PAGE gels as well as anti-flag western and dot blot.

5.3.8 Cell motility

NIH 3T3 cells were co-transfected with 1:2 ratio of GFP and pCAG ROCK1 constructs. Following Nucleofection, cells were incubated for 3 h in a 6 well glass bottom dish in complete medium followed by incubation in serum reduced medium (3.3% FBS). Three bright and GFP timelapse fields were captured with a 10x objective for each treatment every 2 min for 20 hours. Individual cell motility was analysed using Metamorph and Image J.

5.3.9 Protein binding assay

Approximately 200 ng of recombinant GST fusion ROCK1 (Invitrogen) was spotted directly onto nitrocellulose blotting paper and briefly allowed to dry. The membrane was then blocked in 5% milk in TBS for 20 min at room temperature. The membrane was then cut into individual spots and separately incubated with individual binding proteins diluted in 5% milk TBS and incubated at 4C overnight. Following washing, ROCK1 and bound protein were detected with Anti-GST and Anti-FLAG antibodies respectively. Membranes were imaged and quantitated using 2 colour infra-red imaging (Li-Cor Odyssey).

5.3.10 Transwell dissociation assay

NIH 3T3 cells were co-transfected with 1:2 ratio of GFP and pCAG ROCK1 constructs. Following nucleofection, $2x10^5$ cells were incubated with growth medium for 3 h in a 24 well transwell insert (8 μm pore). Following incubation, the growth media in each insert was aspirated and replaced with serum free medium and insert was placed in new well containing 10% FBS medium and incubated 18 hours. Inserts were then discarded and the number of GFP positive cells in the well bottom was assessed. Three GFP fields were captured with a 20x objective for each treatment and the number of positive cells was scored across all fields.

5.3.11 Protein modeling

The ROCK1 kinase interacting regions were modeled onto the ROCK1 kinase domain (2ETR), followed by alignment and identification of corresponding amino acids with the ROCK2 sequence onto the ROCK2 PH (2ROV) and C1 domains

(2ROW). The protein co-ordinates as indicated were imported from PDB into Pymol for modeling and rendering.

References

1. Wickman GR, Samuel MS, Lochhead PA, Olson MF. The Rho-Regulated ROCK Kinases in Cancer. In: van Golen K, editor. The Rho GTPases in Cancer. New York: Springer; 2010. p. 163–92.

2. Loirand G, Guérin P, Pacaud P. Rho kinases in cardiovascular physiology and pathophysiology. Circulation research. 2006 Feb 17;98(3):322–34.

3. Peng F, Wu D, Gao B, Ingram AJ, Zhang B, Chorneyko K, et al. RhoA/Rho-kinase contribute to the pathogenesis of diabetic renal disease. Diabetes. 2008 Jun;57(6):1683–92.

4. Nakagawa O, Fujisawa K, Ishizaki T, Saito Y, Nakao K, Narumiya S. ROCK-I and ROCK-II, two isoforms of Rho-associated coiled-coil forming protein serine/threonine kinase in mice. FEBS Lett. 1996 Aug;392(2):189–93.

5. Wilkinson S, Paterson HF, Marshall CJ. Cdc42-MRCK and Rho-ROCK signalling cooperate in myosin phosphorylation and cell invasion. Nat Cell Biol. 2005 Mar;7(3):255–61.

6. Shimizu T, Ihara K, Maesaki R, Amano M, Kaibuchi K, Hakoshima T. Parallel coiled-coil association of the RhoA-binding domain in Rho-kinase. J Biol Chem. 2003;278(46):46046–51.

7. Dvorsky R, Blumenstein L, Vetter IR, Ahmadian MR. Structural insights into the interaction of ROCKI with the switch regions of RhoA. J Biol Chem. 2004;279(8):7098–104.

8. Doran JD, Liu X, Taslimi P, Saadat A, Fox T. New insights into the structure-function relationships of Rho-associated kinase: a thermodynamic and hydrodynamic study of the dimer-to-monomer transition and its kinetic implications. Biochem J. 2004;384(Pt 2):255–62.

9. Jacobs M, Hayakawa K, Swenson L, Bellon S, Fleming M, Taslimi P, et al. The Structure of Dimeric ROCK I Reveals the Mechanism for Ligand Selectivity. J. Biol. Chem. 2006 Jan;281(1):260–8.

10. Yamaguchi H, Kasa M, Amano M, Kaibuchi K, Hakoshima T. Molecular mechanism for the regulation of rho-kinase by dimerization and its inhibition by fasudil. Structure. 2006;14(3):589–600.

11. Amano M, Chihara K, Kimura K, Fukata Y, Nakamura N, Matsuura Y, et al. Formation of actin stress fibers and focal adhesions enhanced by Rho- kinase. Science. 1997;275(5304):1308–11.

12. Amano M, Chihara K, Nakamura N, Kaneko T, Matsuura Y, Kaibuchi K. The COOH terminus of Rho-kinase negatively regulates rho-kinase activity. J Biol Chem. 1999;274(45):32418–24.

13. Riento K, Guasch RM, Garg R, Jin B, Ridley AJ. RhoE binds to ROCK I and inhibits downstream signaling. Mol Cell Biol. 2003;23(12):4219–29.

14. Ward Y, Yap SF, Ravichandran V, Matsumura F, Ito M, Spinelli B, et al. The GTP binding proteins Gem and Rad are negative regulators of the Rho- Rho kinase pathway. J Cell Biol. 2002;157(2):291–302.

15. Nobes CD, Lauritzen I, Mattei MG, Paris S, Hall A, Chardin P. A new member of the Rho family, Rnd1, promotes disassembly of actin filament structures and loss of cell adhesion. J Cell Biol. 1998;141(1):187–97.

16. Pinner S, Sahai E. PDK1 regulates cancer cell motility by antagonising inhibition of ROCK1 by RhoE. Nat Cell Biol. 2008;10(2):127–37.

17. Riento K, Ridley AJ. Rocks: multifunctional kinases in cell behaviour. Nat Rev Mol Cell Biol. 2003 Jun;4(6):446–56.

18. Feng J, Ito M, Kureishi Y, Ichikawa K, Amano M, Isaka N, et al. Rho-associated kinase of chicken gizzard smooth muscle. J Biol Chem. 1999;274(6):3744–52.

19. Shirao S, Kashiwagi S, Sato M, Miwa S, Nakao F, Kurokawa T, et al. Sphingosylphosphorylcholine is a novel messenger for Rho-kinase-mediated Ca2+ sensitization in the bovine cerebral artery: unimportant role for protein kinase C. Circ Res. 2002;91(2):112–9.

20. Yoneda A, Multhaupt HA, Couchman JR. The Rho kinases I and II regulate different aspects of myosin II activity. J Cell Biol. 2005;170(3):443–53.

21. Lowery DM, Clauser KR, Hjerrild M, Lim D, Alexander J, Kishi K, et al. Proteomic screen defines the Polo-box domain interactome and identifies Rock2 as a Plk1 substrate. Embo J. 2007;26(9):2262–73.

22. Leung T, Chen XQ, Manser E, Lim L. The p160 RhoA-binding kinase ROK alpha is a member of a kinase family and is involved in the reorganization of the cytoskeleton. Mol Cell Biol. 1996;16(10):5313–27.

23. Leung T, Manser E, Tan L, Lim L. A novel serine/threonine kinase binding the Ras-related RhoA GTPase which translocates the kinase to peripheral membranes. J Biol Chem. 1995;270(49):29051–4.

24. Matsui T, Amano M, Yamamoto T, Chihara K, Nakafuku M, Ito M, et al. Rho-associated kinase, a novel serine/threonine kinase, as a putative target for small GTP binding protein Rho. Embo J. 1996;15(9):2208–16.

25. Miyazaki K, Komatsu S, Ikebe M. Dynamics of RhoA and ROKalpha translocation in single living cells. Cell Biochem Biophys. 2006;45(3):243–54.

26. Kawabata S, Usukura J, Morone N, Ito M, Iwamatsu A, Kaibuchi K, et al. Interaction of Rho-kinase with myosin II at stress fibres. Genes to Cells. 2004;(2002):653–60.

27. Tanaka T, Nishimura D, Wu RC, Amano M, Iso T, Kedes L, et al. Nuclear Rho kinase, ROCK2, targets p300 acetyltransferase. J Biol Chem. 2006;281(22):15320–9.

28. Kosako H, Goto H, Yanagida M, Matsuzawa K, Fujita M, Tomono Y, et al. Specific accumulation of Rho-associated kinase at the cleavage furrow during cytokinesis: cleavage furrow-specific phosphorylation of intermediate filaments. Oncogene. 1999;18(17):2783–8.

29. Yokoyama T, Goto H, Izawa I, Mizutani H, Inagaki M. Aurora-B and Rho-kinase/ROCK, the two cleavage furrow kinases, independently regulate the progression of cytokinesis: possible existence of a novel cleavage furrow kinase phosphorylates ezrin/radixin/moesin (ERM). Genes Cells. 2005;10(2):127–37.

30. Ma Z, Kanai M, Kawamura K, Kaibuchi K, Ye K, Fukasawa K. Interaction between ROCK II and nucleophosmin/B23 in the regulation of centrosome duplication. Mol Cell Biol. 2006;26(23):9016–34.

31. Maekawa M, Ishizaki T, Boku S, Watanabe N, Fujita A, Iwamatsu A, et al. Signaling from Rho to the actin cytoskeleton through protein kinases ROCK and LIM-kinase. Science. 1999;285(5429):895–8.

32. Ohashi K, Nagata K, Maekawa M, Ishizaki T, Narumiya S, Mizuno K. Rho-associated kinase ROCK activates LIM-kinase 1 by phosphorylation at threonine 508 within the activation loop. J Biol Chem. 2000;275(5):3577–82.

33. Amano T, Tanabe K, Eto T, Narumiya S, Mizuno K. LIM-kinase 2 induces formation of stress fibres, focal adhesions and membrane blebs, dependent on its activation by Rho-associated kinase- catalysed phosphorylation at threonine-505. Biochem J. 2001;354(Pt 1):149–59.

34. Sumi T, Matsumoto K, Nakamura T. Specific activation of LIM kinase 2 via phosphorylation of threonine 505 by ROCK, a Rho-dependent protein kinase. J Biol Chem. 2001;276(1):670–6.

35. Edwards DC, Sanders LC, Bokoch GM, Gill GN. Activation of LIM-kinase by Pak1 couples Rac/Cdc42 GTPase signalling to actin cytoskeletal dynamics. Nat Cell Biol. 1999;1(5):253–9.

36. Dan C, Kelly A, Bernard O, Minden A. Cytoskeletal changes regulated by the PAK4 serine/threonine kinase are mediated by LIM kinase 1 and cofilin. The Journal of biological chemistry. 2001 Aug 24;276(34):32115–21.

37. Somlyo AP, Somlyo AV. Signal transduction by G-proteins, rho-kinase and protein phosphatase to smooth muscle and non-muscle myosin II. J Physiol. 2000;522 Pt 2:177–85.

38. Amano M, Ito M, Kimura K, Fukata Y, Chihara K, Nakano T, et al. Phosphorylation and activation of myosin by Rho-associated kinase (Rho- kinase). J Biol Chem. 1996;271(34):20246–9.

39. Iizuka K, Yoshii A, Samizo K, Tsukagoshi H, Ishizuka T, Dobashi K, et al. A major role for the rho-associated coiled coil forming protein kinase in G-protein-mediated Ca2+ sensitization through inhibition of myosin phosphatase in rabbit trachea. Br J Pharmacol. 1999;128(4):925–33.

40. Ito M, Nakano T, Erdodi F, Hartshorne DJ. Myosin phosphatase: structure, regulation and function. Mol. Cell. Biochem. 2004;259:197–209.

41. Feng J, Ito M, Ichikawa K, Isaka N, Nishikawa M, Hartshorne DJ, et al. Inhibitory phosphorylation site for Rho-associated kinase on smooth muscle myosin phosphatase. J Biol Chem. 1999;274(52):37385–90.

42. Velasco G, Armstrong C, Morrice N, Frame S, Cohen P. Phosphorylation of the regulatory subunit of smooth muscle protein phosphatase 1M at Thr850 induces its dissociation from myosin. FEBS Lett. 2002;527(1-3):101–4.

43. Terrak M, Kerff F, Langsetmo K, Tao T, Dominguez R. Structural basis of protein phosphatase 1 regulation. Nature. 2004;429(6993):780–4.

44. Kimura K, Ito M, Amano M, Chihara K, Fukata Y, Nakafuku M, et al. Regulation of myosin phosphatase by Rho and Rho-associated kinase (Rho- kinase). Science. 1996;273(5272):245–8.

45. Hagerty L, Weitzel DH, Chambers J, Fortner CN, Brush MH, Loiselle D, et al. ROCK1 phosphorylates and activates zipper-interacting protein kinase. J Biol Chem. 2007;282(7):4884–93.

46. Ishizaki T, Naito M, Fujisawa K, Maekawa M, Watanabe N, Saito Y, et al. p160ROCK, a Rho-associated coiled-coil forming protein kinase, works downstream of Rho and induces focal adhesions. FEBS Lett. 1997;404(2-3):118–24.

47. Chrzanowska-Wodnicka M, Burridge K. Rho-stimulated contractility drives the formation of stress fibers and focal adhesions. J Cell Biol. 1996;133(6):1403–15.

48. Ridley AJ, Hall A. The small GTP-binding protein rho regulates the assembly of focal adhesions and actin stress fibers in response to growth factors. Cell. 1992;70(3):389–99.

49. Byers HR, White GE, Fujiwara K. Organization and function of stress fibers in cells in vitro and in situ. A review. Cell Muscle Motil. 1984;5:83–137.

50. Pellegrin S, Mellor H. Actin stress fibres. J Cell Sci. 2007;120(Pt 20):3491–9.

51. Watanabe N, Kato T, Fujita A, Ishizaki T, Narumiya S. Cooperation between mDia1 and ROCK in Rho-induced actin reorganization. Nat Cell Biol. 1999;1(3):136–43.

52. Carlier MF, Pantaloni D. Control of actin assembly dynamics in cell motility. J Biol Chem. 2007;282(32):23005–9.

53. Itoh K, Yoshioka K, Akedo H, Uehata M, Ishizaki T, Narumiya S. An essential part for Rho-associated kinase in the transcellular invasion of tumor cells. Nature medicine. 1999 Feb;5(2):221–5.

54. Yamada KM, Cukierman E. Modeling tissue morphogenesis and cancer in 3D. Cell. 2007 Aug;130(4):601–10.

55. Friedl P, Wolf K. Tumour-cell invasion and migration: diversity and escape mechanisms. Nat Rev Cancer. 2003 May;3(5):362–74.

56. Sahai E, Marshall CJ. Differing modes of tumour cell invasion have distinct requirements for Rho/ROCK signalling and extracellular proteolysis. Nature cell biology. 2003 Aug;5(8):711–9.

57. Coleman ML, Sahai E a, Yeo M, Bosch M, Dewar A, Olson MF. Membrane blebbing during apoptosis results from caspase-mediated activation of ROCK I. Nature cell biology. 2001 Apr;3(4):339–45.

58. Yamazaki D, Kurisu S, Takenawa T. Regulation of cancer cell motility through actin reorganization. Cancer Sci. 2005 Jul;96(7):379–86.

59. Trinkaus JP. Surface activity and locomotion of Fundulus deep cells during blastula and gastrula stages. Dev Biol. 1973;30(1):69–103.

60. Wyckoff JB, Pinner SE, Gschmeissner S, Condeelis JS, Sahai E. ROCK- and myosin-dependent matrix deformation enables protease-independent tumor-cell invasion in vivo. Curr Biol. 2006 Aug;16(15):1515–23.

61. Baehrecke EH. How death shapes life during development. Nature reviews. Molecular cell biology. 2002 Oct;3(10):779–87.

62. Elliott MR, Ravichandran KS. Clearance of apoptotic cells: implications in health and disease. The Journal of cell biology. 2010 Jun;189(7):1059–70.

63. Kerr JF, Wyllie AH, Currie AR. Apoptosis: a basic biological phenomenon with wide-ranging implications in tissue kinetics. Br J Cancer. 1972;26(4):239–57.

64. Fulda S, Debatin K-M. Extrinsic versus intrinsic apoptosis pathways in anticancer chemotherapy. Oncogene. 2006 Aug 7;25(34):4798–811.

65. Saelens X, Festjens N, Vande Walle L, van Gurp M, van Loo G, Vandenabeele P. Toxic proteins released from mitochondria in cell death. Oncogene. 2004 Apr 12;23(16):2861–74.

66. Hengartner MO. The biochemistry of apoptosis. Nature. 2000 Oct 12;407(6805):770–6.

67. Cornelis J.F. VN. The history of Z-VAD-FMK, a tool for understanding the significance of caspase inhibition. Acta Histochemica. 2001;103(3):241–51.

68. Charras GT, Coughlin M, Mitchison TJ, Mahadevan L. Life and Times of a Cellular Bleb. Biophys. J. 2007;:biophysj.107.113605.

69. Charras GT, Yarrow JC, Horton MA, Mahadevan L, Mitchison TJ. Non-equilibration of hydrostatic pressure in blebbing cells. Nature. 2005;435(7040):365–9.

70. Charras GT, Hu CK, Coughlin M, Mitchison TJ. Reassembly of contractile actin cortex in cell blebs. J Cell Biol. 2006;175(3):477–90.

71. Croft DR, Coleman ML, Li S, Robertson D, Sullivan T, Stewart CL, et al. Actin-myosin-based contraction is responsible for apoptotic nuclear disintegration. The Journal of cell biology. 2005 Jan;168(2):245–55.

72. Orlando K a, Stone NL, Pittman RN. Rho kinase regulates fragmentation and phagocytosis of apoptotic cells. Experimental cell research. 2006 Jan;312(1):5–15.

73. Coleman ML, Sahai EA, Yeo M, Bosch M, Dewar A, Olson MF. Membrane blebbing during apoptosis results from caspase-mediated activation of ROCK I. Nat Cell Biol. 2001;3(4):339–45.

74. Sebbagh M, Renvoize C, Hamelin J, Riche N, Bertoglio J, Breard J. Caspase-3-mediated cleavage of ROCK I induces MLC phosphorylation and apoptotic membrane blebbing. Nat Cell Biol. 2001;3(4):346–52.

75. Croft DR, Coleman ML, Li S, Robertson D, Sullivan T, Stewart CL, et al. Actin-myosin-based contraction is responsible for apoptotic nuclear disintegration. J Cell Biol. 2005 Jan;168(2):245–55.

76. Sebbagh M, Renvoize C, Hamelin J, Riche N, Bertoglio J, Breard J, et al. Caspase-3-mediated cleavage of ROCK I induces MLC phosphorylation and apoptotic membrane blebbing. Nature cell biology. 2001 Apr;3(4):346–52.

77. Chang J, Xie M, Shah VR, Schneider MD, Entman ML, Wei L, et al. Activation of Rho-associated coiled-coil protein kinase 1 (ROCK-1) by caspase-3 cleavage plays an essential role in cardiac myocyte apoptosis. Proc Natl Acad Sci U S A. 2006;103(39):14495–500.

78. Sebbagh M, Hamelin J, Bertoglio J, Solary E, Bréard J. Direct cleavage of ROCK II by granzyme B induces target cell membrane blebbing in a caspase-independent manner. The Journal of experimental medicine. 2005 Feb 7;201(3):465–71.

79. Mochizuki H. Histochemical detection of apoptosis in Parkinson's disease. Journal of the Neurological Sciences. 1996 May;137(2):120–3.

80. Scott RS, McMahon EJ, Pop SM, Reap EA, Caricchio R, Cohen PL, et al. Phagocytosis and clearance of apoptotic cells is mediated by MER. Nature. 2001 May 10;411(6834):207–11.

81. Erwig L-P, Henson PM. Immunological consequences of apoptotic cell phagocytosis. The American journal of pathology. 2007;171(1):2–8.

82. Erwig L-P, McPhilips KA, Wynes MW, Ivetic A, Ridley AJ, Henson PM. Differential regulation of phagosome maturation in macrophages and dendritic cells mediated by Rho GTPases and ezrin-radixin-moesin (ERM) proteins. Proceedings of the National Academy of Sciences of the United States of America. 2006 Aug 22;103(34):12825–30.

83. Kinchen JM, Doukoumetzidis K, Almendinger J, Stergiou L, Tosello-Trampont A, Sifri CD, et al. A pathway for phagosome maturation during engulfment of apoptotic cells. Nature cell biology. 2008 May;10(5):556–66.

84. Kinchen JM, Ravichandran KS. Identification of two evolutionarily conserved genes regulating processing of engulfed apoptotic cells. Nature. 2010 Apr 1;464(7289):778–82.

85. Verhoven B, Schlegel RA, Williamson P. Mechanisms of phosphatidylserine exposure, a phagocyte recognition signal, on apoptotic T lymphocytes. The Journal of experimental medicine. 1995 Nov 1;182(5):1597–601.

86. Hanayama R, Tanaka M, Miwa K, Shinohara A, Iwamatsu A, Nagata S. Identification of a factor that links apoptotic cells to phagocytes. Nature. 2002 May 9;417(6885):182–7.

87. Dillon SR, Mancini M, Rosen A, Schlissel MS. Annexin V binds to viable B cells and colocalizes with a marker of lipid rafts upon B cell receptor activation. Journal of immunology (Baltimore, Md.□: 1950). 2000 Mar 1;164(3):1322–32.

88. van den Eijnde SM, van den Hoff MJ, Reutelingsperger CP, van Heerde WL, Henfling ME, Vermeij-Keers C, et al. Transient expression of phosphatidylserine at cell-cell contact areas is required for myotube formation. Journal of cell science. 2001 Oct;114(Pt 20):3631–42.

89. Fadeel B. Plasma membrane alterations during apoptosis: role in corpse clearance. Antioxidants & redox signaling. 2004 Apr;6(2):269–75.

90. Franz S, Herrmann K, Fuhrnrohr B, Sheriff A, Frey B, Gaipl US, et al. After shrinkage apoptotic cells expose internal membrane-derived epitopes on their plasma membranes. Cell Death Differ. 2006 Dec 15;14(4):733–42.

91. Orlando KA, Pittman RN. Rho kinase regulates phagocytosis, surface expression of GlcNAc, and Golgi fragmentation of apoptotic PC12 cells. Experimental cell research. 2006 Oct;312(17):3298–311.

92. Duvall E, Wyllie AH, Morris RG. Macrophage recognition of cells undergoing programmed cell death (apoptosis). Immunology. 1985 Oct;56(2):351–8.

93. Casiano CA, Ochs RL, Tan EM. Distinct cleavage products of nuclear proteins in apoptosis and necrosis revealed by autoantibody probes. Cell death and differentiation. 1998 Mar;5(2):183–90.

94. Gregory CD. CD14-dependent clearance of apoptotic cells: relevance to the immune system. Current opinion in immunology. 2000 Feb;12(1):27–34.

95. Ogden CA, DeCathelineau A, Hoffmann PR, Bratton D, Ghebrehiwet B, Fadok VA, et al. C1q and Mannose Binding Lectin Engagement of Cell Surface Calreticulin and Cd91 Initiates Macropinocytosis and Uptake of Apoptotic Cells. Journal of Experimental Medicine. 2001 Sep 17;194(6):781–96.

96. Schagat TL, Wofford JA, Wright JR. Surfactant protein A enhances alveolar macrophage phagocytosis of apoptotic neutrophils. Journal of immunology (Baltimore, Md.□: 1950). 2001 Mar 15;166(4):2727–33.

97. Erwig LP, Henson PM. Clearance of apoptotic cells by phagocytes. Cell death and differentiation. 2008;15(2):243–50.

98. Grimsley C. Cues for apoptotic cell engulfment: eat-me, don’t eat-me and come-get-me signals. Trends in Cell Biology. 2003 Dec;13(12):648–56.

99. Hoffmann PR, DeCathelineau AM, Ogden CA, Leverrier Y, Bratton DL, Daleke DL, et al. Phosphatidylserine (PS) induces PS receptor-mediated macropinocytosis and promotes clearance of apoptotic cells. The Journal of cell biology. 2001 Nov 12;155(4):649–59.

100. Meagher LC, Savill JS, Baker A, Fuller RW, Haslett C. Phagocytosis of apoptotic neutrophils does not induce macrophage release of thromboxane B2. Journal of leukocyte biology. 1992 Sep;52(3):269–73.

101. Stern M, Savill J, Haslett C. Human monocyte-derived macrophage phagocytosis of senescent eosinophils undergoing apoptosis. Mediation by alpha v beta 3/CD36/thrombospondin recognition mechanism and lack of phlogistic response. The American journal of pathology. 1996 Sep;149(3):911–21.

102. Voll RE, Herrmann M, Roth EA, Stach C, Kalden JR, Girkontaite I. Immunosuppressive effects of apoptotic cells. Nature. 1997;534(1988):0–1.

103. Poon IKH, Hulett MD, Parish CR. Molecular mechanisms of late apoptotic/necrotic cell clearance. Cell death and differentiation. 2010 Mar;17(3):381–97.

104. Overbeeke R, Steffens-Nakken H, Vermes I, Reutelingsperger C, Haanen C. Early features of apoptosis detected by four different flow cytometry assays. Apoptosis : an international journal on programmed cell death. 1998 Mar;3(2):115–21.

105. Savill J, Fadok V, Henson P, Haslett C. Phagocyte recognition of cells undergoing apoptosis. Immunology Today. 1993;14(3):131–6.

106. Whitacre CC. Sex differences in autoimmune disease. Nature immunology. 2001;2(9):777–80.

107. Gigante A, Gasperini ML, Afeltra A, Barbano B, Margiotta D, Cianci R, et al. Cytokines expression in SLE nephritis. European review for medical and pharmacological sciences. 2011 Jan;15(1):15–24.

108. Van Bruggen MC, Kramers C, Berden JH. Autoimmunity against nucleosomes and lupus nephritis. Annales de médecine interne. 1996 Jan;147(7):485–9.

109. Hanayama R, Tanaka M, Miyasaka K, Aozasa K, Koike M, Uchiyama Y, et al. Autoimmune disease and impaired uptake of apoptotic cells in MFG-E8-deficient mice. Science (New York, N.Y.). 2004 May;304(5674):1147–50.

110. Botto M, Dell'Agnola C, Bygrave AE, Thompson EM, Cook HT, Petry F, et al. Homozygous C1q deficiency causes glomerulonephritis associated with multiple apoptotic bodies. Nature Genetics. 1998 May;19(1):56–9.

111. Herrmann M, Voll RE, Zoller OM, Hagenhofer M, Ponner BB, Kalden JR. Impaired phagocytosis of apoptotic cell material by monocyte-derived macrophages from patients with systemic lupus erythematosus. Arthritis and rheumatism. 1998 Jul;41(7):1241–50.

112. Baumann I, Kolowos W, Voll RE, Manger B, Gaipl U, Neuhuber WL, et al. Impaired uptake of apoptotic cells into tingible body macrophages in germinal

centers of patients with systemic lupus erythematosus. Arthritis and rheumatism. 2002 Jan;46(1):191–201.

113. Gaipl US, Munoz LE, Grossmayer G, Lauber K, Franz S, Sarter K, et al. Clearance deficiency and systemic lupus erythematosus (SLE). Journal of autoimmunity. 2007;28(2-3):114–21.

114. Perniok A, Wedekind F, Herrmann M, Specker C, Schneider M. High levels of circulating early apoptic peripheral blood mononuclear cells in systemic lupus erythematosus. Lupus. 1998 Feb 1;7(2):113–8.

115. Bowness P, Davies KA, Norsworthy PJ, Athanassiou P, Taylor-Wiedeman J, Borysiewicz LK, et al. Hereditary C1q deficiency and systemic lupus erythematosus. QJM□: monthly journal of the Association of Physicians. 1994 Aug;87(8):455–64.

116. Radic MZ, Weigert M. Genetic and structural evidence for antigen selection of anti-DNA antibodies. Annual review of immunology. 1994 Jan;12:487–520.

117. Winkler TH, Fehr H, Kalden JR. Analysis of immunoglobulin variable region genes from human IgG anti-DNA hybridomas. European journal of immunology. 1992 Jul;22(7):1719–28.

118. Stuart LM, Takahashi K, Shi L, Savill J, Ezekowitz RAB. Mannose-binding lectin-deficient mice display defective apoptotic cell clearance but no autoimmune phenotype. Journal of immunology (Baltimore, Md.□: 1950). 2005 Mar 15;174(6):3220–6.

119. Erwig L-P, Henson PM. Immunological consequences of apoptotic cell phagocytosis. The American journal of pathology. 2007 Jul;171(1):2–8.

120. Nagata S, Hanayama R, Kawane K. Autoimmunity and the clearance of dead cells. Cell. 2010 Mar 5;140(5):619–30.

121. Orlando K a, Stone NL, Pittman RN. Rho kinase regulates fragmentation and phagocytosis of apoptotic cells. Experimental Cell Research. 2006 Jan;312(1):5–15.

122. Witasp E, Uthaisang W, Elenström-Magnusson C, Hanayama R, Tanaka M, Nagata S, et al. Bridge over troubled water: milk fat globule epidermal growth factor 8 promotes human monocyte-derived macrophage clearance of non-blebbing phosphatidylserine-positive target cells. Cell death and differentiation. 2007 May;14(5):1063–5.

123. Pace KE, Lee C, Stewart PL, Baum LG. Restricted receptor segregation into membrane microdomains occurs on human T cells during apoptosis induced by galectin-1. Journal of immunology (Baltimore, Md.□: 1950). 1999 Oct 1;163(7):3801–11.

124. Navratil JS, Watkins SC, Wisnieski JJ, Ahearn JM. The globular heads of C1q specifically recognize surface blebs of apoptotic vascular endothelial cells. Journal of immunology (Baltimore, Md.□: 1950). 2001 Mar 1;166(5):3231–9.

125. Franz S, Herrmann K, Fürnrohr BG, Führnrohr B, Sheriff a, Frey B, et al. After shrinkage apoptotic cells expose internal membrane-derived epitopes on their plasma membranes. Cell death and differentiation. 2007 Apr;14(4):733–42.

126. Casciola-Rosen L a, Anhalt G, Rosen A. Autoantigens targeted in systemic lupus erythematosus are clustered in two populations of surface structures on apoptotic keratinocytes. The Journal of experimental medicine. 1994 Apr;179(4):1317–30.

127. Schiller M, Bekeredjian-Ding I, Heyder P, Blank N, Ho AD, Lorenz H-m. Autoantigens are translocated into small apoptotic bodies during early stages of apoptosis. Cell death and differentiation. 2008 Jan;15(1):183–91.

128. Fransen JH, Hilbrands LB, Jacobs CW, Adema GJ, Berden JH, Van der Vlag J. Both early and late apoptotic blebs are taken up by DC and induce IL-6 production. Autoimmunity. 2009 May;42(4):325–7.

129. Fransen JH, Hilbrands LB, Ruben J, Stoffels M, Adema GJ, van der Vlag J, et al. Mouse dendritic cells matured by ingestion of apoptotic blebs induce T cells to produce interleukin-17. Arthritis and rheumatism. 2009 Aug;60(8):2304–13.

130. Frisoni L, McPhie L, Colonna L, Sriram U, Monestier M, Gallucci S, et al. Nuclear autoantigen translocation and autoantibody opsonization lead to increased dendritic cell phagocytosis and presentation of nuclear antigens: a novel pathogenic pathway for autoimmunity? Journal of immunology (Baltimore, Md.□: 1950). 2005 Aug 15;175(4):2692–701.

131. Suber T, Rosen A. Apoptotic cell blebs: repositories of autoantigens and contributors to immune context. Arthritis and rheumatism. 2009 Aug;60(8):2216–9.

132. Shimizu Y, Thumkeo D, Keel J, Ishizaki T, Oshima H, Oshima M, et al. ROCK-I regulates closure of the eyelids and ventral body wall by inducing assembly of actomyosin bundles. J Cell Biol. 2005;168(6):941–53.

133. Zhang Y-MM, Bo J, Taffet GE, Chang J, Shi J, Reddy AK, et al. Targeted deletion of ROCK1 protects the heart against pressure overload by inhibiting reactive fibrosis. Faseb J. 2006 May;20(7):916–25.

134. Rikitake Y, Oyama N, Wang CY, Noma K, Satoh M, Kim HH, et al. Decreased perivascular fibrosis but not cardiac hypertrophy in ROCK1+/- haploinsufficient mice. Circulation. 2005;112(19):2959–65.

135. Thumkeo D, Shimizu Y, Sakamoto S, Yamada S, Narumiya S. ROCK-I and ROCK-II cooperatively regulate closure of eyelid and ventral body wall in mouse embryo. Genes Cells. 2005;10(8):825–34.

136. Thumkeo D, Keel J, Ishizaki T, Hirose M, Nonomura K, Oshima H, et al. Targeted disruption of the mouse rho-associated kinase 2 gene results in intrauterine growth retardation and fetal death. Mol Cell Biol. 2003;23(14):5043–55.

137. Rashid-Doubell F, Tannetta D, Redman CW, Sargent IL, Boyd CA, Linton EA. Caveolin-1 and lipid rafts in confluent BeWo trophoblasts: evidence for Rock-1 association with caveolin-1. Placenta. 2007;28(2-3):139–51.

138. Uehata M, Ishizaki T, Satoh H, Ono T, Kawahara T, Morishita T, et al. Calcium sensitization of smooth muscle mediated by a Rho-associated protein kinase in hypertension. Nature. 1997;389(6654):990–4.

139. Chijiwa T, Mishima A, Hagiwara M, Sano M, Hayashi K, Inoue T, et al. Inhibition of forskolin-induced neurite outgrowth and protein phosphorylation by a newly synthesized selective inhibitor of cyclic AMP-dependent protein kinase, N-[2-(p-bromocinnamylamino)ethyl]-5-isoquinolinesulfonamide (H-89), of PC12D pheochromocytoma . J Biol Chem. 1990;265(9):5267–72.

140. Asano T, Ikegaki I, Satoh S, Suzuki Y, Shibuya M, Takayasu M, et al. Mechanism of action of a novel antivasospasm drug, HA1077. J Pharmacol Exp Ther. 1987;241(3):1033–40.

141. Arai M, Sasaki Y, Nozawa R. Inhibition by the protein kinase inhibitor HA1077 of the activation of NADPH oxidase in human neutrophils. Biochem Pharmacol. 1993;46(8):1487–90.

142. Hidaka H, Inagaki M, Kawamoto S, Sasaki Y. Isoquinolinesulfonamides, novel and potent inhibitors of cyclic nucleotide dependent protein kinase and protein kinase C. Biochemistry. 1984;23(21):5036–41.

143. Ikenoya M, Hidaka H, Hosoya T, Suzuki M, Yamamoto N, Sasaki Y. Inhibition of rho-kinase-induced myristoylated alanine-rich C kinase substrate (MARCKS) phosphorylation in human neuronal cells by H-1152, a novel and specific Rho-kinase inhibitor. J Neurochem. 2002;81(1):9–16.

144. Yarrow JC, Totsukawa G, Charras GT, Mitchison TJ. Screening for cell migration inhibitors via automated microscopy reveals a Rho-kinase inhibitor. Chem Biol. 2005;12(3):385–95.

145. Takami A, Iwakubo M, Okada Y, Kawata T, Odai H, Takahashi N, et al. Design and synthesis of Rho kinase inhibitors (I). Bioorg Med Chem. 2004;12(9):2115–37.

146. Huse M, Kuriyan J. The conformational plasticity of protein kinases. Cell. 2002;109(3):275–82.

147. Bain J, Plater L, Elliott M, Shpiro N, Hastie CJ, McLauchlan H, et al. The selectivity of protein kinase inhibitors: a further update. Biochem J. 2007;408(3):297–315.

148. Benitah SA, Valeron PF, van Aelst L, Marshall CJ, Lacal JC. Rho GTPases in human cancer: an unresolved link to upstream and downstream transcriptional regulation. Biochim Biophys Acta. 2004;1705(2):121–32.

149. Ellenbroek SIJ, Collard JG. Rho GTPases: functions and association with cancer. Clin Exp Metastasis. 2007 Jan;24(8):657–72.

150. Ma L, Teruya-Feldstein J, Weinberg RA. Tumour invasion and metastasis initiated by microRNA-10b in breast cancer. Nature. 2007;449(7163):682–8.

151. Kamai T, Tsujii T, Arai K, Takagi K, Asami H, Ito Y, et al. Significant association of Rho/ROCK pathway with invasion and metastasis of bladder cancer. Clin Cancer Res. 2003 Jul;9(7):2632–41.

152. Kamai T, Arai K, Sumi S, Tsujii T, Honda M, Yamanishi T, et al. The rho/rho-kinase pathway is involved in the progression of testicular germ cell tumour. BJU Int. 2002;89(4):449–53.

153. Kamai T, Yamanishi T, Shirataki H, Takagi K, Asami H, Ito Y, et al. Overexpression of RhoA, Rac1, and Cdc42 GTPases is associated with progression in testicular cancer. Clinical cancer research : an official journal of the American Association for Cancer Research. 2004 Jul;10(14):4799–805.

154. Samuel MS, Lopez JI, McGhee EJ, Croft DR, Strachan D, Timpson P, et al. Actomyosin-Mediated Cellular Tension Drives Increased Tissue Stiffness and β-Catenin Activation to Induce Epidermal Hyperplasia and Tumor Growth. Cancer cell. 2011 Jun 14;19(6):776–91.

155. Greenman C, Stephens P, Smith R, Dalgliesh GL, Hunter C, Bignell G, et al. Patterns of somatic mutation in human cancer genomes. Nature. 2007 Mar;446(7132):153–8.

156. Vishnubhotla R, Sun S, Huq J, Bulic M, Ramesh A, Guzman G, et al. ROCK-II mediates colon cancer invasion via regulation of MMP-2 and MMP-13 at the site of invadopodia as revealed by multiphoton imaging. Lab Invest. 2007 Nov;87(11):1149–58.

157. Croft DR, Olson MF. The Rho GTPase Effector ROCK Regulates Cyclin A, Cyclin D1, and p27Kip1 Levels by Distinct Mechanisms. Mol. Cell. Biol. 2006;26(12):4612–27.

158. Pirone DM, Liu WF, Ruiz SA, Gao L, Raghavan S, Lemmon CA, et al. An inhibitory role for FAK in regulating proliferation: a link between limited adhesion and RhoA-ROCK signaling. J. Cell Biol. 2006;174(2):277–88.

159. Meyer TN, Schwesinger C, Sampogna RV, Vaughn DA, Stuart RO, Steer DL, et al. Rho kinase acts at separate steps in ureteric bud and metanephric mesenchyme morphogenesis during kidney development. Differentiation. 2006;74(9-10):638–47.

160. McMullan R, Lax S, Robertson VH, Radford DJ, Broad S, Watt FM, et al. Keratinocyte Differentiation Is Regulated by the Rho and ROCK Signaling Pathway. Curr Biol. 2003;13(24):2185–9.

161. Watanabe K, Ueno M, Kamiya D, Nishiyama A, Matsumura M, Wataya T, et al. A ROCK inhibitor permits survival of dissociated human embryonic stem cells. Nat Biotech. 2007;25(6):681–6.

162. Kishore R, Qin G, Luedemann C, Bord E, Hanley A, Silver M, et al. The cytoskeletal protein ezrin regulates EC proliferation and angiogenesis via TNF-alpha-induced transcriptional repression of cyclin A. J Clin Invest. 2005;115(7):1785–96.

163. Sahai E, Ishizaki T, Narumiya S, Treisman R. Transformation mediated by RhoA requires activity of ROCK kinases. Curr Biol. 1999 Feb;9(3):136–45.

164. Uchida S, Watanabe G, Shimada Y, Maeda M, Kawabe A, Mori A, et al. The suppression of small GTPase rho signal transduction pathway inhibits angiogenesis in vitro and in vivo. Biochem Biophys Res Commun. 2000;269(2):633–40.

165. Nagatoya K, Moriyama T, Kawada N, Takeji M, Oseto S, Murozono T, et al. Y-27632 prevents tubulointerstitial fibrosis in mouse kidneys with unilateral ureteral obstruction. Kidney Int. 2002;61(5):1684–95.

166. Cechin SR, Dunkley PR, Rodnight R. Signal transduction mechanisms involved in the proliferation of C6 glioma cells induced by lysophosphatidic acid. Neurochem Res. 2005;30(5):603–11.

167. Nicole O, Goldshmidt A, Hamill CE, Sorensen SD, Sastre A, Lyuboslavsky P, et al. Activation of protease-activated receptor-1 triggers astrogliosis after brain injury. J Neurosci. 2005;25(17):4319–29.

168. Swant JD, Rendon BE, Symons M, Mitchell RA. Rho GTPase-dependent signaling is required for macrophage migration inhibitory factor-mediated expression of cyclin D1. J Biol Chem. 2005;280(24):23066–72.

169. Tura A, Grisanti S, Petermeier K, Henke-Fahle S. The Rho-Kinase Inhibitor H-1152P Suppresses the Wound-Healing Activities of Human Tenon's Capsule Fibroblasts In Vitro. Invest Ophthalmol Vis Sci. 2007;48(5):2152–61.

170. Nishimaki H, Kasai K, Kozaki K, Takeo T, Ikeda H, Saga S, et al. A role of activated Sonic hedgehog signaling for the cellular proliferation of oral squamous cell carcinoma cell line. Biochem Biophys Res Commun. 2004;314(2):313–20.

171. He H, Pannequin J, Tantiongco JP, Shulkes A, Baldwin GS. Glycine-extended gastrin stimulates cell proliferation and migration through a Rho- and ROCK-dependent pathway, not a Rac/Cdc42-dependent pathway. Am J Physiol Gastrointest Liver Physiol. 2005;289(3):G478–88.

172. Seibold S, Schurle D, Heinloth A, Wolf G, Wagner M, Galle J. Oxidized LDL induces proliferation and hypertrophy in human umbilical vein endothelial cells via regulation of p27Kip1 expression: role of RhoA. J Am Soc Nephrol. 2004;15(12):3026–34.

173. Kamiyama M, Utsunomiya K, Taniguchi K, Yokota T, Kurata H, Tajima N, et al. Contribution of Rho A and Rho kinase to platelet-derived growth factor-BB-induced proliferation of vascular smooth muscle cells. J Atheroscler Thromb. 2003;10(2):117–23.

174. Takeda N, Kondo M, Ito S, Ito Y, Shimokata K, Kume H. Role of RhoA inactivation in reduced cell proliferation of human airway smooth muscle by simvastatin. Am J Respir Cell Mol Biol. 2006;35(6):722–9.

175. Rees RW, Foxwell NA, Ralph DJ, Kell PD, Moncada S, Cellek S. Y-27632, a Rho-kinase inhibitor, inhibits proliferation and adrenergic contraction of prostatic smooth muscle cells. J Urol. 2003;170(6 Pt 1):2517–22.

176. Zhao Z, Rivkees SA. Rho-associated kinases play an essential role in cardiac morphogenesis and cardiomyocyte proliferation. Dev Dyn. 2003;226(1):24–32.

177. Porter KE, Turner NA, O'Regan DJ, Balmforth AJ, Ball SG. Simvastatin reduces human atrial myofibroblast proliferation independently of cholesterol lowering via inhibition of RhoA. Cardiovasc Res. 2004;61(4):745–55.

178. Dhawan J, Helfman DM. Modulation of acto-myosin contractility in skeletal muscle myoblasts uncouples growth arrest from differentiation. J Cell Sci. 2004;117(Pt 17):3735–48.

179. Mallat Z, Gojova A, Sauzeau V, Brun V, Silvestre JS, Esposito B, et al. Rho-associated protein kinase contributes to early atherosclerotic lesion formation in mice. Circ Res. 2003;93(9):884–8.

180. Vichalkovski A, Baltensperger K, Thomann D, Porzig H. Two different pathways link G-protein-coupled receptors with tyrosine kinases for the modulation of growth and survival in human hematopoietic progenitor cells. Cell Signal. 2005;17(4):447–59.

181. Wang G, Woods A, Sabari S, Pagnotta L, Stanton LA, Beier F. RhoA/ROCK signaling suppresses hypertrophic chondrocyte differentiation. J Biol Chem. 2004;279(13):13205–14.

182. Iwamoto H, Nakamuta M, Tada S, Sugimoto R, Enjoji M, Nawata H. A p160ROCK-specific inhibitor, Y-27632, attenuates rat hepatic stellate cell growth. J Hepatol. 2000;32(5):762–70.

183. Masamune A, Kikuta K, Satoh M, Satoh K, Shimosegawa T. Rho kinase inhibitors block activation of pancreatic stellate cells. Br J Pharmacol. 2003;140(7):1292–302.

184. Otis M, Gallo-Payet N. Differential involvement of cytoskeleton and rho-guanosine 5'-triphosphatases in growth-promoting effects of angiotensin II in rat adrenal glomerulosa cells. Endocrinology. 2006;147(11):5460–9.

185. Svoboda KK, Moessner P, Field T, Acevedo J. ROCK inhibitor (Y27632) increases apoptosis and disrupts the actin cortical mat in embryonic avian corneal epithelium. Dev Dyn. 2004;229(3):579–90.

186. Moore M, Marroquin BA, Gugliotta W, Tse R, White SR. Rho kinase inhibition initiates apoptosis in human airway epithelial cells. Am J Respir Cell Mol Biol. 2004;30(3):379–87.

187. Shibata R, Kai H, Seki Y, Kato S, Morimatsu M, Kaibuchi K, et al. Role of Rho-associated kinase in neointima formation after vascular injury. Circulation. 2001;103(2):284–9.

188. Shibata R, Kai H, Seki Y, Kusaba K, Takemiya K, Koga M, et al. Rho-kinase inhibition reduces neointima formation after vascular injury by enhancing Bax expression and apoptosis. J Cardiovasc Pharmacol. 2003;42 Suppl 1:S43–7.

189. Matsumoto Y, Uwatoku T, Oi K, Abe K, Hattori T, Morishige K, et al. Long-term inhibition of Rho-kinase suppresses neointimal formation after stent implantation in

porcine coronary arteries: involvement of multiple mechanisms. Arterioscler Thromb Vasc Biol. 2004;24(1):181–6.

190. Abe K, Shimokawa H, Morikawa K, Uwatoku T, Oi K, Matsumoto Y, et al. Long-Term Treatment With a Rho-Kinase Inhibitor Improves Monocrotaline-Induced Fatal Pulmonary Hypertension in Rats. Circ Res. 2004;94(3):385–93.

191. Furuyama T, Komori K, Shimokawa H, Matsumoto Y, Uwatoku T, Hirano K, et al. Long-term inhibition of Rho kinase suppresses intimal thickening in autologous vein grafts in rabbits. J Vasc Surg. 2006;43(6):1249–56.

192. Li X, Liu L, Tupper JC, Bannerman DD, Winn RK, Sebti SM, et al. Inhibition of protein geranylgeranylation and RhoA/RhoA kinase pathway induces apoptosis in human endothelial cells. J Biol Chem. 2002;277(18):15309–16.

193. Ikeda H, Nagashima K, Yanase M, Tomiya T, Arai M, Inoue Y, et al. Involvement of Rho/Rho kinase pathway in regulation of apoptosis in rat hepatic stellate cells. Am J Physiol Gastrointest Liver Physiol. 2003;285(5):G880–6.

194. Kobayashi M, Nishita M, Mishima T, Ohashi K, Mizuno K. MAPKAPK-2-mediated LIM-kinase activation is critical for VEGF-induced actin remodeling and cell migration. Embo J. 2006;25(4):713–26.

195. Nagashima T, Okazaki H, Yudoh K, Matsuno H, Minota S. Apoptosis of rheumatoid synovial cells by statins through the blocking of protein geranylgeranylation: a potential therapeutic approach to rheumatoid arthritis. Arthritis Rheum. 2006;54(2):579–86.

196. Song J, Li J, Lulla A, Evers BM, Chung DH. Protein kinase D protects against oxidative stress-induced intestinal epithelial cell injury via Rho/ROK/PKC-delta pathway activation. Am J Physiol Cell Physiol. 2006;290(6):C1469–76.

197. Zhong W-B, Wang C-Y, Chang T-C, Lee W-S. Lovastatin Induces Apoptosis of Anaplastic Thyroid Cancer Cells via Inhibition of Protein Geranylgeranylation and de Novo Protein Synthesis. Endocrinology. 2003;144(9):3852–9.

198. Rattan R, Giri S, Singh AK, Singh I. Rho / ROCK Pathway as a Target of Tumor Therapy. Journal of Neuroscience Research. 2006;83(2):243–55.

199. Burthem J, Rees-Unwin K, Mottram R, Adams J, Lucas GS, Spooncer E, et al. The rho-kinase inhibitors Y-27632 and fasudil act synergistically with imatinib to inhibit the expansion of ex vivo CD34(+) CML progenitor cells. Leukemia. 2007;21(8):1708–14.

200. De Sarno P, Shestopal SA, Zmijewska AA, Jope RS. Anti-apoptotic effects of muscarinic receptor activation are mediated by Rho kinase. Brain Research. 2005;1041(1):112–5.

201. Somlyo APAVP, Phelps C, Dipierro C, Eto M, Read P, Barrett M, et al. Rho kinase and matrix metalloproteinase inhibitors cooperate to inhibit angiogenesis and growth of human prostate cancer xenotransplants. Faseb J. 2003 Feb;17(2):223–34.

202. Sanz-Moreno V, Gadea G, Ahn J, Paterson H, Marra P, Pinner S, et al. Rac activation and inactivation control plasticity of tumor cell movement. Cell. 2008;135(3):510–23.

203. Clark EA, Golub TR, Lander ES, Hynes RO. Genomic analysis of metastasis reveals an essential role for RhoC. Nature. 2000;406(6795):532–5.

204. Hakem A, Sanchez-Sweatman O, You-Ten A, Duncan G, Wakeham A, Khokha R, et al. RhoC is dispensable for embryogenesis and tumor initiation but essential for metastasis. Genes & development. 2005 Sep 1;19(17):1974–9.

205. Ikoma T, Takahashi T, Nagano S, Li Y-M, Ohno Y, Ando K, et al. A definitive role of RhoC in metastasis of orthotopic lung cancer in mice. Clinical cancer research : an official journal of the American Association for Cancer Research. 2004 Feb 1;10(3):1192–200.

206. Ying H, Biroc SL, Li W-W, Alicke B, Xuan J-A, Pagila R, et al. The Rho kinase inhibitor fasudil inhibits tumor progression in human and rat tumor models. Molecular cancer therapeutics. 2006 Oct;5(9):2158–64.

207. Genda T, Sakamoto M, Ichida T, Asakura H, Kojiro M, Narumiya S, et al. Cell motility mediated by rho and Rho-associated protein kinase plays a critical role in intrahepatic metastasis of human hepatocellular carcinoma. Hepatology. 1999;30(4):1027–36.

208. Takamura M, Sakamoto M, Genda T, Ichida T, Asakura H, Hirohashi S. Inhibition of intrahepatic metastasis of human hepatocellular carcinoma by Rho-associated protein kinase inhibitor Y-27632. Hepatology. 2001;33(3):577–81.

209. Somlyo AV, Bradshaw D, Ramos S, Murphy C, Myers CE, Somlyo AP. Rho-kinase inhibitor retards migration and in vivo dissemination of human prostate cancer cells. Biochem Biophys Res Commun. 2000;269(3):652–9.

210. Nakajima M, Hayashi K, Egi Y, Katayama K-ichi, Amano Y, Uehata M, et al. Effect of Wf-536, a novel ROCK inhibitor, against metastasis of B16 melanoma. Cancer chemotherapy and pharmacology. 2003 Oct;52(4):319–24.

211. Croft DR, Sahai E, Mavria G, Li S, Tsai J, Lee WMF, et al. Conditional ROCK Activation In vivo Induces Tumor Cell Dissemination and Angiogenesis. Cancer Res. 2004 Dec;64(24):8994–9001.

212. Hidalgo-Carcedo C, Hooper S, Chaudhry SI, Williamson P, Harrington K, Leitinger B, et al. Collective cell migration requires suppression of actomyosin at cell-cell contacts mediated by DDR1 and the cell polarity regulators Par3 and Par6. Nature cell biology. 2011 Jan;13(1):49–58.

213. Lindsten T, Ross AJ, King A, Zong W-X, Rathmell JC, Shiels HA, et al. The Combined Functions of Proapoptotic Bcl-2 Family Members Bak and Bax Are Essential for Normal Development of Multiple Tissues. Molecular Cell. 2000 Dec;6(6):1389–99.

214. Rahman A, Isenberg DA. Systemic lupus erythematosus. The New England journal of medicine. 2008 Feb 28;358(9):929–39.

215. Hanayama R, Tanaka M, Miyasaka K, Aozasa K, Koike M, Uchiyama Y, et al. Autoimmune disease and impaired uptake of apoptotic cells in MFG-E8-deficient mice. Science (New York, N.Y.). 2004;304(5674):1147–50.

216. Bennett GD, Kay MM. Homeostatic removal of senescent murine erythrocytes by splenic macrophages. Experimental hematology. 1981 Mar;9(3):297–307.

217. Poulet FM, Penraat K, Collins N, Evans E, Thackaberry E, Manfra D, et al. Drug-induced hemolytic anemia and thrombocytopenia associated with alterations of cell membrane lipids and acanthocyte formation. Toxicologic pathology. 2010 Jan;38(6):907–22.

218. Gehrs BC, Friedberg RC. Autoimmune hemolytic anemia. American journal of hematology. 2002 Apr;69(4):258–71.

219. Kokori S. Autoimmune hemolytic anemia in patients with systemic lupus erythematosus. The American Journal of Medicine. 2000 Feb 15;108(3):198–204.

220. Gabet A-S, Coulon S, Fricot A, Vandekerckhove J, Chang Y, Ribeil J-A, et al. Caspase-activated ROCK-1 allows erythroblast terminal maturation independently of cytokine-induced Rho signaling. Cell death and differentiation. 2011 Apr;18(4):678–89.

221. Zermati Y, Garrido C, Amsellem S, Fishelson S, Bouscary D, Valensi F, et al. Caspase activation is required for terminal erythroid differentiation. The Journal of experimental medicine. 2001 Jan 15;193(2):247–54.

222. Brodsky I, Dennis LH, Kahn SB, Brady LW. Normal mouse erythropoiesis. I. The role of the spleen in mouse erythropoiesis. Cancer research. 1966 Feb;26(2):198–201.

223. Peter C, Wesselborg S, Lauber K. Molecular Suicide Notes□: Last Call from Apoptosing Cells. Internal Medicine. 2010;:78–80.

224. Muñoz LE, Peter C, Herrmann M, Wesselborg S, Lauber K. Scent of dying cells: the role of attraction signals in the clearance of apoptotic cells and its immunological consequences. Autoimmunity reviews. 2010 Apr;9(6):425–30.

225. Segundo C, Medina F, Rodríguez C, Martínez-Palencia R, Leyva-Cobián F, Brieva JA. Surface molecule loss and bleb formation by human germinal center B cells undergoing apoptosis: role of apoptotic blebs in monocyte chemotaxis. Blood. 1999 Aug 1;94(3):1012–20.

226. Smolewski P, Grabarek J, Halicka HD, Darzynkiewicz Z. Assay of caspase activation in situ combined with probing plasma membrane integrity to detect three distinct stages of apoptosis. Journal of immunological methods. 2002;265(1-2):111–21.

227. Hristov M, Erl W, Linder S, Weber PC. Apoptotic bodies from endothelial cells enhance the number and initiate the differentiation of human endothelial progenitor cells in vitro. Differentiation. 2004;104(9):2761–6.

228. Scaffidi P, Misteli T, Bianchi ME. Release of chromatin protein HMGB1 by necrotic cells triggers inflammation. Nature. 2002;418(6894):191–5.

229. Kothakota S, Azuma T, Reinhard C, Klippel A, Tang J, Chu K, et al. Caspase-3-generated fragment of gelsolin: effector of morphological change in apoptosis. Science. 1997 Oct;278(5336):294–8.

230. Dinubile MJ. Plasma gelsolin: in search of its raison d'etre. Focus on "Modifications of cellular responses to lysophosphatidic acid and platelet-activating factor by plasma gelsolin". American journal of physiology. Cell physiology. 2007 Apr;292(4):C1240–2.

231. Goetzl EJ, Lee H, Azuma T, Stossel TP, Turck CW, Karliner JS. Gelsolin binding and cellular presentation of lysophosphatidic acid. The Journal of biological chemistry. 2000 May;275(19):14573–8.

232. Osborn TM, Dahlgren C, Hartwig JH, Stossel TP. Modifications of cellular responses to lysophosphatidic acid and platelet-activating factor by plasma gelsolin. American journal of physiology. Cell physiology. 2007 Apr;292(4):C1323–30.

233. DiNubile MJ. Plasma gelsolin as a biomarker of inflammation. Arthritis Res Ther. 2008 Jan;10(6):124.

234. Christofidou-Solomidou M, Scherpereel A, Solomides CC, Muzykantov VR, Machtay M, Albelda SM, et al. Changes in plasma gelsolin concentration during acute oxidant lung injury in mice. Lung. 2002;180(2):91–104.

235. Dahl B, Schiodt FV, Ott P, Gvozdenovic R, Yin HL, Lee WM. Plasma gelsolin is reduced in trauma patients. Shock. 1999;12(2):102–4.

236. Ito H, Kambe H, Kimura Y, Nakamura H, Hayashi E, Kishimoto T, et al. Depression of plasma gelsolin level during acute liver injury. Gastroenterology. 1992;102(5):1686–92.

237. Smith DB, Janmey PA, Sherwood JA, Howard RJ, Lind SE. Decreased plasma gelsolin levels in patients with Plasmodium falciparum malaria: a consequence of hemolysis? Blood. 1988;72(1):214–8.

238. Christofidou-Solomidou M, Scherpereel A, Solomides CC, Christie JD, Stossel TP, Goelz S, et al. Recombinant plasma gelsolin diminishes the acute inflammatory response to hyperoxia in mice. J Investig Med. 2002;50(1):54–60.

239. Rothenbach PA, Dahl B, Schwartz JJ, O'Keefe GE, Yamamoto M, Lee WM, et al. Recombinant plasma gelsolin infusion attenuates burn-induced pulmonary microvascular dysfunction. J Appl Physiol. 2004 Jan;96(1):25–31.

240. Osborn TM, Dahlgren C, Hartwig JH, Stossel TP. Modifications of cellular responses to lysophosphatidic acid and platelet-activating factor by plasma gelsolin. American journal of physiology. Cell physiology. 2007 Apr;292(4):C1323–30.

241. Weigert A, Weis N, Brüne B. Regulation of macrophage function by sphingosine-1-phosphate. Immunobiology. 2009 Jan;214(9-10):748–60.

242. Lauber K, Bohn E, KrÃ¶ber SM, Xiao Y-jin, Blumenthal SG, Lindemann RK, et al. Apoptotic cells induce migration of phagocytes via caspase-3-mediated release of a lipid attraction signal. Cell. 2003;113(6):717–30.

243. Weigert A, Johann AM, von Knethen A, Schmidt H, Geisslinger G, Brüne B. Apoptotic cells promote macrophage survival by releasing the antiapoptotic mediator sphingosine-1-phosphate. Blood. 2006 Sep;108(5):1635–42.

244. Herr B, Zhou J, Werno C, Menrad H, Namgaladze D, Weigert A, et al. The supernatant of apoptotic cells causes transcriptional activation of hypoxia-inducible factor-1alpha in macrophages via sphingosine-1-phosphate and transforming growth factor-beta. Blood. 2009 Sep;114(10):2140–8.

245. Gu Y, Forostyan T, Sabbadini R, Rosenblatt J. Epithelial cell extrusion requires the sphingosine-1-phosphate receptor 2 pathway. The Journal of cell biology. 2011 May 16;193(4):667–76.

246. Witke W, Sharpe AH, Hartwig JH, Azuma T, Stossel TP, Kwiatkowski DJ. Hemostatic, inflammatory, and fibroblast responses are blunted in mice lacking gelsolin. Cell. 1995;81(1):41–51.

247. Leifeld L, Fink K, Debska G, Fielenbach M, Schmitz V, Sauerbruch T, et al. Anti-apoptotic function of gelsolin in fas antibody-induced liver failure in vivo. Am J Pathol. 2006 Mar;168(3):778–85.

248. Oikonomou N, Thanasopoulou A, Tzouvelekis A, Harokopos V, Paparountas T, Nikitopoulou I, et al. Gelsolin expression is necessary for the development of modelled pulmonary inflammation and fibrosis. Thorax. 2009;64(6):467–75.

249. Maniatis NA, Harokopos V, Thanassopoulou A, Oikonomou N, Mersinias V, Witke W, et al. A critical role for gelsolin in ventilator-induced lung injury. American journal of respiratory cell and molecular biology. 2009 Oct;41(4):426–32.

250. Sahai E, Marshall CJ. ROCK and Dia have opposing effects on adherens junctions downstream of Rho. Nat Cell Biol. 2002;4(6):408–15.

251. Narumiya S, Tanji M, Ishizaki T. Rho signaling, ROCK and mDia1, in transformation, metastasis and invasion. Cancer Metastasis Rev. 2009 Jun;28(1-2):65–76.

252. Nakajima M. Wf-536 prevents tumor metastasis by inhibiting both tumor motility and angiogenic actions. European Journal of Pharmacology. 2003 Jan;459(2-3):113–20.

253. Ogawa T, Tashiro H, Miyata Y, Ushitora Y, Fudaba Y, Kobayashi T, et al. Rho-associated kinase inhibitor reduces tumor recurrence after liver transplantation in a rat hepatoma model. Am J Transplant. 2007 Feb;7(2):347–55.

254. Xue F, Takahara T, Yata Y, Xia Q, Nonome K, Shinno E, et al. Blockade of Rho/Rho-associated coiled coil-forming kinase signaling can prevent progression of hepatocellular carcinoma in matrix metalloproteinase-dependent manner. Hepatol Res. 2008;38(8):810–7.

255. Abe H, Kamai T, Tsujii T, Nakamura F, Mashidori T, Mizuno T, et al. Possible role of the RhoC/ROCK pathway in progression of clear cell renal cell carcinoma. Biomed Res. 2008;29(3):155–61.

256. Kamai T, Yamanishi T, Shirataki H, Takagi K, Asami H, Ito Y, et al. Overexpression of RhoA, Rac1, and Cdc42 GTPases is associated with progression in testicular cancer. Clin Cancer Res. 2004 Jul;10(14):4799–805.

257. Greenman C, Stephens P, Smith R, Dalgliesh GL, Hunter C, Bignell G, et al. Patterns of somatic mutation in human cancer genomes. Nature. 2007 Mar;446(7132):153–8.

258. Olson MF, Sahai E. The actin cytoskeleton in cancer cell motility. Clin Exp Metastasis. 2008;

259. Doki Y, Shiozaki H, Tahara H, Inoue M, Oka H, Iihara K, et al. Correlation between E-cadherin expression and invasiveness in vitro in a human esophageal cancer cell line. Cancer Res. 1993 Jul;53(14):3421–6.

260. Wen W, Liu W, Yan J, Zhang M. Structure Basis and Unconventional Lipid Membrane Binding Properties of the PH-C1 Tandem of Rho Kinases. The Journal of biological chemistry. 2008 Sep;283(38):26263–73.

261. Brognard J, Zhang Y-W, Puto LA, Hunter T. Cancer-associated loss-of-function mutations implicate DAPK3 as a tumor-suppressing kinase. Cancer research. 2011 Apr 15;71(8):3152–61.

262. Bokoch GM. Caspase-mediated activation of PAK2 during apoptosis: proteolytic kinase activation as a general mechanism of apoptotic signal transduction? Cell Death Differ. 1998;5(8):637–45.

263. Tan I, Seow KT, Lim L, Leung T. Intermolecular and Intramolecular Interactions Regulate Catalytic Activity of Myotonic Dystrophy Kinase-Related Cdc42-Binding Kinase {alpha}. Mol. Cell. Biol. 2001;21(8):2767–78.

264. Lee EC, Yu D, Martinez de Velasco J, Tessarollo L, Swing DA, Court DL, et al. A highly efficient Escherichia coli-based chromosome engineering system adapted for recombinogenic targeting and subcloning of BAC DNA. Genomics. 2001 Apr 1;73(1):56–65.

265. Liu P, Jenkins NA, Copeland NG. A highly efficient recombineering-based method for generating conditional knockout mutations. Genome research. 2003 Mar;13(3):476–84.

266. George SHL, Gertsenstein M, Vintersten K, Korets-Smith E, Murphy J, Stevens ME, et al. Developmental and adult phenotyping directly from mutant embryonic stem cells. Proceedings of the National Academy of Sciences of the United States of America. 2007 Mar 13;104(11):4455–60.

267. Scott RW, Hooper S, Crighton D, Li A, König I, Munro J, et al. LIM kinases are required for invasive path generation by tumor and tumor-associated stromal cells. The Journal of cell biology. 2010 Oct;191(1):169–85.